The model of the fruit fly *Drosophila melanogaster* as a novel tool for characterization of human membrane transporters

Dissertation

der Mathematisch-Naturwissenschaftlichen Fakultät

der Eberhard Karls Universität Tübingen

zur Erlangung des Grades eines

Doktors der Naturwissenschaften

(Dr. rer. nat.)

vorgelegt von

Jing Yang

aus Anhui/China

Tübingen

2023

Gedruckt mit Genehmigung der Mathematisch-Naturwissenschaftlichen Fakultät der Eberhard Karls Universität Tübingen.

Tag der mündlichen Qualifikation:	30.05.2023
Dekan:	Prof. Dr. Thilo Stehle
1. Berichterstatter/-in:	PD Dr. Bernard Moussian
2. Berichterstatter/-in:	Prof. Dr. Matthias Schwab

TABLE OF CONTENTS

List of Abbreviations **1**

Abstract **4**

Zusammenfassung **6**

1. Introduction **8**

1.1 Membrane transporters **8**

1.2 Organic anion-transporting polypeptides **9**

1.2.1 General characteristics of OATPs 9

1.2.2 General properties and tissue distribution of OATP1B1, OATP2B1, and OATP1B3 11

1.2.3 Substrates and inhibitors of OATP1B1, OATP2B1, and OATP1B3 12

1.2.4 The physiological and pharmacological function of OATP1B1, OATPB21, and OATP1B3 14

1.2.5 OATP1B1, OATP2B1, and OATP1B3 polymorphism and drug disposition 15

1.3 Organic cation transporter 1 (OCT1) **20**

1.3.1 General properties and distribution of OCT1 20

1.3.2 Substrates and inhibitors of OCT1 21

1.3.3 Pharmacological and physiological function of OCT1 22

1.4 Multidrug-resistance protein 1（MDR1, ABCB1） **23**

1.5 Oatps in *D. melanogaster* compared with their human orthologs. **24**

1.6 *D. melanogaster* as a novel tool to research human membrane transporters **27**

1.6.1 The advantage of *D. melanogaster* as a model organism 27

1.6.2 Gene expression by GAL4/UAS system 28

1.6.3 The function of PhiC31 integrase in human transgenic fly 30

1.6.4 Generation of a membrane transporter test system in *D. melanogaster* 31

1.7 Aims of the present study **33**

2. Materials and methods **35**

2.1 Materials **35**

2.1.1 Chemicals 35
2.1.2 Buffers and solutions 36
2.1.3 Enzymes, reagents 37
2.1.4 Equipment 38
2.1.5 Primer for PCR 38
2.1.6 Primer for In-Fusion cloning 39
2.1.7 Primer for qRT-PCR 40
2.1.8 Primer for sequence test 41
2.2 Methods 41
2.2.1 Fly works 41
2.2.2 Generation of human transgenic fly 43
2.2.3 Immunofluorescence of embryos 47
2.2.4 Recombination 50
2.2.5 Extraction of single fly genomic DNA 51
2.2.6 Injection of fluorescent substrate 52
2.2.7 Transcription analyses by quantitative real-time polymerase chain reaction (qRT-PCR) 52
2.2.8 Feeding oatp RNAi larvae with MDBF 53
2.2.9 The drug test for human OCT1 transgenic flies 54
3. Results 55
3.1 Expression and function of hOATP1B1, hOATP2B1, and hOATP1B3 in fly embryos 55
3.1.1 Induction of hOATP1B1, hOATP2B1, and hOATP1B3 expression in transgenic embryos was measured by RT-qPCR 55
3.1.2 hOATP1B1 localization by antibody staining in embryos 56
3.1.3 hOATP2B1 localization by immuno-detection in embryos 59
3.1.4 hOATP1B3 localization by antibody staining in embryos 62
3.1.5 Distribution of hOATP1B1-, hOATP2B1-, and hOATP1B3-RFP in embryos and larvae 66
3.1.6 Evaluation of hOATP1B1, hOATP2B1, and hOATP1B3 function by injection of their fluorescent substrates into embryos 70
3.1.7 The function of *D. melanogaster* Oatps was evaluated by feeding MDBF into fly *oatp* RNAi larvae 89
3.2 Study of the expression and function of hOCT1 and hABCB1 in embryos 93
3.2.1 Generation of *hABCB1* expressing flies 93

3.2.2 Immune-detection of hABCB1 in embryos..... 94
3.2.3 Transcription of the *hABCB1* and *hOCT1* genes in transgenic embryos was measured by qRT-PCR..... 95
3.2.4 Analyses of the function of hOCT1 and hABCB1 in “humanized” transgenic fly embryos using EtBr..... 97
3.2.5 The function of hOCT1 and hABCB1 was studied in “humanized” hOCT1 and hABCB1 embryos using rhodamine 123 98
3.3 Functional analysis of hOCT1 in embryos by feeding cisplatin and cimetidine 99
3.3.1 The effect of cimetidine on the mortality of embryos expressing hOCT1 in different embryonic tissues produced by mothers fed with cisplatin 100
3.3.2 The effect of cisplatin and cimetidine on embryo hatchability expressing hOCT1 in the nervous system..... 103
3.3.3 Cimetidine rescued the toxicity of cisplatin in embryos expressing hOCT1 in the nervous system under the control of the pros-GAL4 driver..... 105
3.3.4 The expression pattern of pros-GAL4 in different stage embryos..... 108
4 Discussion 110
4.1 hOATP1B1, hOATP2B1, and hOATP1B3 function in fly embryos 110
4.1.1 Epitope damage might affect the immune-detection of human transporters in the fly embryo 110
4.1.2 hOATP1B1-, hOATP2B1-, and hOATP1B3-RFP fusion proteins did not localize to their target tissues..... 112
4.1.3 Fluorescent substrates were taken up into the lumen of salivary glands independently of hOATP1B1, hOATP2B1, and hOATP1B3..... 114
4.1.4 Fluorescent substrates were not taken up into the oenocytes by hOATP1B1, hOATP2B1, or hOATP1B3 115
4.1.5 Fluorescent substrates were taken up into the tracheae independently of hOATP1B1, hOATP2B1, or hOATP1B3 116
4.1.6 *Drosophila oatps* have redundant functions in the fly larvae..... 117
4.2 The function of hOCT1 and hABCB1 in fly embryos 118
4.3 Drug interaction assays in hOCT1 expressing embryos..... 119
5. References 122
6. Acknowledgements 137

List of Abbreviations

ABC	ATP-binding cassette
ARM	Armadillo
ASP	4-(4-(dimethylamino)styryl)-N-methylpyridinium iodide
BBB	Blood-brain barrier
BCRP	Breast cancer resistance protein
BSA	Bovine serum albumin
btl	breathless
cDNA	complementary DNA
CHO	Chinese hamster ovary
CLF	Cholyl-Lysyl-Fluorescein
CNS	Central nervous system
DBF	4,5- Dibromofluorescein
DDI	Drug-drug interaction
DHEAS	Dehydroepiandrosterone-3-sulfate
DMSO	Dimethylsulfoxide
DNA	Deoxyribonucleic acid
dNTP	2’-deoxy-nucleoside triphosphate
drm	drumstick
ECM	Extracellular matrix
EDTA	Ethylene diamine tetraacetic acid
EGTA	Ethylene glycol-bis (β-aminoethyl ether)-N,N,N',N'-tetraacetic acid
elav	embryonic lethal abnormal vision
en	engrailed
EtBr	Ethidium bromide
Et^+	Ethidium
fb	fat body
FBF	Formaldehyde-Based Fixation
fne	found in neurons

fkh	forkhead
GFP	Green fluorescent protein
GMCs	Ganglion mother cells
HEK	Human embryonic kidney
hh	hedgehog
HMF	Heat-Methanol Fixation
HUGO	Human Genome Organisation
IgG	Immunoglobulin G
Kb	kilobase
kDa	kilodalton
LB	Luria-Bertani broth
MATEs	Multidrug and toxin extrusions
MDBF	Mercury dibromofluorescein disodium salt
MDR	Multidrug resistance
mg	milligrams
ml	milliliter
mM	millimolar
mRNA	messenger RNA
MDR1	Multidrug-resistant protein 1
MRPs	Multidrug resistance-associated proteins
NBD	Nucleotide-binding domains
ng	nanogram
NRT	Neurotactin
nub	nubbin
OATs	Organic anion transporters
OATPs	Organic anion-transporting polypeptides
OCTs	Organic cation transporters
OCT1	Organic cation transporter 1
OCTNs	Organic cation and carnitine transporters
PBS	Phosphate-buffered saline
PBST	Phosphate-buffered saline with Triton
PBSTA	Phosphate buffered saline with Triton and BSA
PCR	Polymerase chain reaction

P-GP	P-glycoprotein
pros	prospero
RBPs	RNA-binding proteins
rbp9	*RNA binding protein 9*
RFP	Red fluorescent protein
RNA	Ribonucleic acid
RNAi	RNA interference
RT	Room temperature
RT-PCR	Reverse transcription polymerase chain reaction
Serp	Serpentine
SLC	Solute carrier
SNP	Single-nucleotide polymorphism
TAE	Tris-acetate-EDTA
TMD	Transmembrane domain
UV	Ultraviolet
μg	microgram
μl	microliter
°C	degree Celsius

Abstract

Numerous studies have demonstrated that membrane transporters are critical determinants for drug disposition, drug absorption, therapeutic efficacy, and adverse drug reactions. In the human genome, more than 400 membrane transporters have been annotated and been divided into two superfamilies: ATP-binding cassette (ABC) family and solute carrier (SLC) family. Many ABC and SLC transporters not only contribute to the influx of metabolites and drugs but are also involved in their efflux. *In vitro* and *in vivo*, various animal models including mice, rats, rabbits, monkeys, and different cell lines were used to study the relationship between clinical pharmacokinetic drug-drug interaction (DDI) and human transporters. However, these studies are usually expensive and time-consuming. Therefore, we planned to use the fruit fly *Drosophila melanogaster* as a rapid testing and low-cost animal model to study the function of human membrane transporters.

At first, I sought to study the function of the organic anion transporters hOATP1B1 (encoded by *SLCO1B1*), hOATP2B1 (*SLCO2B1*) and hOATP1B3 (*SLCO1B3*), which are clinically relevant uptake transporters in the sinusoidal membrane of human hepatocytes. For this purpose, I generated flies expressing these human uptake transporters in the salivary glands. They did not localize to the target tissue, but were instead found in excretory cells suggesting that they were eliminated because of potential cell toxic properties. Arguing that undetectable levels of hOATP1B1, hOATP2B1 and hOATP1B3 may nevertheless be localized correctly, I performed tracer transport assays by confocal microscopy. My results suggested that fluorescent substrates of hOATP1B1, hOATP2B1 and hOATP1B3 (Mercury dibromofluorescein disodium salt, MDBF; 4,5- Dibromofluorescein, DBF; Cholyl-Lysyl-Fluorescein, CLF) were transported to the lumen of the salivary glands of embryos independently of these human transporters. Further results failed to demonstrate that fly organic anion-transporting polypeptides (Oatps) may assist fluorescent substrate transfer across the cell membrane into the lumen of the salivary glands. Rather, my data suggested that dyes were transported by transcytosis to the lumen of this organ. Thus, contrary to our

expectation, the fruit fly is not a suitable model for pharmacological studies of OATPs.

In a second project, I established a test system for DDI involving hOCT1, a further clinically relevant uptake transporter in human hepatocytes. hOCT1 was expressed in various organs and tissues in embryos produced by females that were fed with the cytotoxin and hOCT1 substrate cisplatin. My results suggested that cisplatin was transported into embryos by hOCT1 and was embryonic lethal. Interestingly, cimetidine, another substrate of hOCT1, reduced the toxicity of cisplatin in embryos that expressed hOCT1 in the nervous system. Thus, this setup allows studying successfully DDI in *D. melanogaster* and may ultimately serve to identify and evaluate new hOCT1 interacting molecules in pharmaceutical experiments.

Zusammenfassung

Zahlreiche Studien haben gezeigt, dass Membrantransporter kritische Determinanten für die Arzneimitteldisposition, Arzneimittelabsorption, therapeutische Wirksamkeit und Nebenwirkungen von Arzneimitteln sind. Im menschlichen Genom wurden mehr als 400 Membrantransporter annotiert und in zwei Superfamilien unterteilt: die Familie der ATP-binding cassette (ABC) und die Familie der solute carrier (SLC). Viele ABC- und SLC-Transporter tragen nicht nur zum Einstrom chemischer Komponenten bei, sondern sind auch am Ausstrom von Metaboliten und Arzneimitteln beteiligt. In vitro und in vivo wurden verschiedene Tiermodelle, darunter Mäuse, Ratten, Kaninchen, Affen und verschiedene Zelllinien, verwendet, um die Beziehung zwischen klinischen pharmakokinetischen Arzneimittelinteraktionen (drug-drug interactions, DDI) und menschlichen Transportern zu untersuchen. Diese Studien sind jedoch in der Regel teuer und zeitaufwändig. Daher planten wir, die Fruchtfliege *Drosophila melanogaster* als schnelles Test- und kostengünstiges Tiermodell zu verwenden, um die Funktion menschlicher Membrantransporter zu untersuchen.

Zunächst wollte ich die Funktion der organischen Anionentransporter hOATP1B1, hOATP2B1 und hOATP1B3 untersuchen, die klinisch relevante Aufnahmetransporter in der Sinusoidalmembran menschlicher Hepatozyten sind. Zu diesem Zweck habe ich Fliegen generiert, die diese menschlichen Aufnahmetransporter in den Speicheldrüsen exprimieren. Sie lokalisierten sich nicht im Zielgewebe, sondern wurden stattdessen in Ausscheidungszellen gefunden, was darauf hindeutet, dass sie aufgrund potenzieller zelltoxischer Eigenschaften eliminiert wurden. Mit dem Argument, dass nicht nachweisbare Konzentrationen von hOATP1B1, hOATP2B1 und hOATP1B3 dennoch korrekt lokalisiert werden können, führte ich Tracer-Transport-Assays durch konfokale Mikroskopie durch. Meine Ergebnisse legen nahe, dass fluoreszierende Substrate von hOATP1B1, hOATP2B1 und hOATP1B3 (Mercury dibromofluorescein disodium salt, MDBF; 4,5- Dibromofluorescein, DBF; Cholyl-Lysyl-Fluorescein, CLF) unabhängig von diesen menschlichen Transportern in das Lumen der Speicheldrüsen von Embryonen transportiert werden. Weitere

Ergebnisse zeigten dass auch organische anionentransportierende Polypeptide (Oatps) der Fliege den Transfer fluoreszierender Substrate durch die Zellmembran in das Lumen der Speicheldrüsen nicht unterstützen können. Vielmehr deuten meine Daten darauf hin, dass die Farbstoffe durch Transzytose in das Lumen dieses Organs transportiert werden. Somit ist die Fruchtfliege entgegen unserer Erwartung kein geeignetes Modell für pharmakologische Untersuchungen von OATPs.

In einem zweiten Projekt habe ich ein Testsystem für DDI mit hOCT1, einem weiteren klinisch relevanten Aufnahmetransporter in menschlichen Hepatozyten, aufgebaut. hOCT1 wurde in verschiedenen Organen und Geweben in Embryonen exprimiert, die von Weibchen produziert wurden, die mit dem Zytotoxin und hOCT1-Substrat Cisplatin gefüttert wurden. Meine Ergebnisse legen nahe, dass Cisplatin durch hOCT1 in Embryonen transportiert wird und embryonal tödlich ist. Interessanterweise reduziert Cimetidin, ein weiteres Substrat von hOCT1, die Toxizität von Cisplatin in Embryonen, die hOCT1 im Nervensystem exprimieren. Somit ermöglicht dieser Aufbau die erfolgreiche Untersuchung von DDI in *Drosophila* und kann letztendlich dazu dienen, neue mit hOCT1 interagierende Moleküle in pharmazeutischen Experimenten zu identifizieren und zu bewerten.

1. Introduction

1.1 Membrane transporters

Membrane transporters are essential for the transport of various compounds across the plasma membrane, such as sugars, amino acids, nucleotides, vitamins, cofactors, and many drugs (Kell et al., 2011, Kell and Oliver, 2014). Therefore, regulating transport of small molecules across the membrane plays a vital role in maintaining cell homeostasis (Nigam, 2015). Moreover, membrane transporters are involved in processes affecting drug pharmacokinetics including absorption, distribution, and excretion of drugs, and may substantially contribute to drug failure, drug resistance, and adverse drug reactions (Giacomini et al., 2010, DeGorter et al., 2012).

About 2000 genes of the human genome encode for transport-related proteins (DeGorter et al., 2012, Hediger et al., 2013). Membrane transporters from two major superfamilies have been recognized as being important for drug pharmacokinetics: ABC family and SLC family. The human ABC family contains 48 members that are divided into seven subfamilies (ABCA to ABCG) depending on phylogenetic analysis and amino acid sequence (Dean et al., 2001). Membrane transporters from the ABCB, ABCC and ABCG subfamily are involved in drug pharmacokinetics and drug response, including drug resistance: MDR1 P-glycoprotein (P-GP/*ABCB1*), multidrug resistance-associated proteins (MRPs/*ABCC*s), and breast cancer resistance protein (BCRP/*ABCG2*) (Slot et al., 2011, Schinkel and Jonker, 2003). To date, 458 SLC transporters have been identified in the human genome (Pizzagalli et al., 2021), which are further grouped into 65 subfamilies including organic anion-transporting polypeptides, OATPs (encoded by *SLCO* genes), SLC22 transporter family (*SLC22*), and multidrug and toxin extrusions, MATEs (*SLC47As*). The SLC22 transporter family is divided into six subfamilies: organic anion transporter (OAT), OAT-like, OAT-related, organic cation transporter (OCT), organic cation/carnitine transporter (OCTN), and OCT/OCTN-related (Niemi, 2007, Nies et al., 2009, Chen et al.,

2010, Yamada et al., 2011, Hagenbuch and Stieger, 2013, Motohashi and Inui, 2013, Nigam, 2018).

In humans, SLC transporters and ABC transporters are widely expressed in various tissues, such as the heart, liver, kidney, brain, and intestine (Roth et al., 2012, Shitara et al., 2013). A multitude of genetic variants has been identified in transporter genes and several have of these have been shown to affect pharmacokinetics and response, including drug resistance (Bruhn and Cascorbi, 2014, Wolking et al., 2015, Fohner et al., 2017). For example, the nonsynonymous polymorphism in *SLCO1B1* (rs4149056) is associated with statin-induced myopathy, the missense polymorphism in *ABCG2* (rs2231142) with response to rosuvastatin, and an Asian-specific non-synonymous variant in *SLC22A8* (rs11568482) with a reduction of cefotaxime renal clearance (Yee et al., 2018).

1.2 Organic anion-transporting polypeptides

1.2.1 General characteristics of OATPs

Based on the nomenclature of the HUGO (Human Genome Organisation) Gene Nomenclature Committee, Organic anion transporting peptides (OATP for humans, Oatps for other species) are encoded by *SLC21/SLCO* genes (Hagenbuch and Meier, 2004). As membrane influx transporters, OATPs play an important role in regulating the cellular uptake of many endogenous compounds and clinical drugs (Niemi, 2007). According to the phylogenetic relationship and chronology of identification, 11 human OATP transporters have been divided into multiple families that are denoted in Arabic numerals. OATPs that share more than 40% amino acid sequence identity belong to the same family and are designated by Arabic numbering (Hagenbuch and Meier, 2004). Similarly, proteins with the same subfamily have more than 60% of amino acid sequence identity and are designated by letters. When there are individual gene products (proteins) within the same subfamily, additional Arabic numbers are designated. According to these rules, the human OATPs are classified into 11 members: OATP1A2, 1B1, 1B3, 1C1, 2A1, 2B1, 3A1, 4A1, 4C1, 5A1, and 6A1 (Hagenbuch and Meier, 2003, Mikkaichi et al., 2004) (Table 1).

Table 1 Human OATP transporters, their gene names and chromosomal localization. Modified from Kalliokoskii and Niemi (Kalliokoski and Niemi, 2009).

OATP	**Gene name**	**Gene locus**
OATP1A2	*SLCO1A2*	12p12
OATP1B1	*SLCO1B1*	12p12
OATP1B3	*SLCO1B3*	12p12
OATP1C1	*SLCO1C1*	12p12
OATP2A1	*SLCO2A1*	3q21
OATP2B1	*SLCO2B1*	11q13
OATP3A1	*SLCO3A1*	15q26
OATP4A1	*SLCO4A1*	20q13.1
OATP4C1	*SLCO4C1*	5q21
OATP5A1	*SLCO5A1*	8q13.1
OATP6A1	*SLCO6A1*	5q21

OATPs transporters contain a very similar 12-transmembrane domain (TMD) (Konig et al., 2006) (Fig 1). Their superfamily signature is D-XRW-(I, V)-GAWWX-G-(F, L)-L, at the extracellular border of TMD6, including 13 amino acids that are conserved between human OATPs and rodent Oatps. Between TMD 9 and 10, OATPs share a large extracellular loop that has 11 conserved cysteine residues that play an important role in OATP function (Hagenbuch and Meier, 2003).

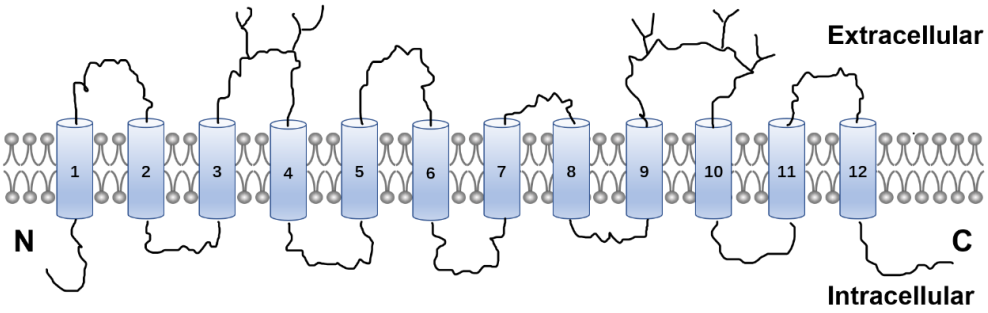

Figure 1. Schematic representation of OATPs protein structures. TMDs are numbered from 1 to 12. “Y” shapes represent potential glycosylation sites.

OATPs are expressed in different organs throughout the body and mediate the transport of a wide spectrum of amphipathic organic compounds, including cyclic nucleotides, organic dyes, bile acids, steroid hormones, prostaglandins, drugs, and other xenobiotics (Thakkar et al., 2015).

1.2.2 General properties and tissue distribution of OATP1B1, OATP2B1, and OATP1B3

OATP1B1, also known as OATP-C, OATP2, or LST-1, is mostly expressed in the sinusoidal membrane of human hepatocytes (König et al., 2000). However, the OATP1B1 mRNA has been observed in other cell types, like intestinal enterocytes (Glaeser et al., 2007). OATP1B1 is encoded by the *SLCO1B1* gene and consists of 691-amino acid. Its molecular mass is 84 kDa, reduced to 58 kDa after deglycosylation (Niemi et al., 2011). OATP1B1 has 12 TMDs that are highly conserved, which play an important role in transport function (Fan et al., 2020).

OATP2B1 (previously named OATP-B), is abundantly expressed in various tissues, for example, the liver, intestine, placenta, skin, and heart (Kullak-Ublick et al., 2001, Kobayashi et al., 2003, Grube et al., 2006). It is localized in multiple cell types of different organs, such as in the sinusoidal membrane of hepatocytes, capillary endothelial cells of the brain, endocrine cells of the colon, and small arteries and veins of the heart (Grube et al., 2006, Kleberg et al., 2012, Gao et al., 2015). Depending on the type of cells, OATP2B1 molecular mass is 84 kDa, reduced to 58 kDa after deglycosylation (Matsumoto et al., 2015).

OATP1B3 (previously OATP8, LST-2) shares 80% amino acid sequence identity with OATP1B1. Similar to OATP1B1, OATP1B3 is mainly expressed in the sinusoidal membrane of human hepatocytes, and its mRNA has been detected in the intestines (Glaeser et al., 2007, Shitara, 2011). Interestingly, OATP1B3 is also localized in breast and primary colon tumors as well as pancreatic cancer cells. Interestingly, a cancer-specific isoform of OATP1B3 has been identified in colon tumors (Thakkar et al., 2013, Nagy et al., 2015).

The distribution of OATP1B1, OATP2B1 and OATP1B3 in different tissues of the human body is shown in Table 2.

Table 2 The tissue distributions of human OATP transporters.

Transporter	Tissue distribution	Reference
OATP1B1	Liver, intestine	König et al. 2000
OATP2B1	Liver, intestine, placenta, heart, skin, brain, colon	Tamai et al. 2000; Kobayashi et al. 2003; Grube et al. 2006
OATP1B3	Liver, intestine	Glaeser H et al. 2007

1.2.3 Substrates and inhibitors of OATP1B1, OATP2B1, and OATP1B3

As human transporters, OATPs are expressed in various organs, which mediate the transport of many drugs, endogenous and exogenous amphipathic compounds. A number of research data show that OATP substrates generally

are anionic amphipathic molecules (molecular weight > 450) that bind the protein under normal physiological conditions (Hagenbuch and Meier, 2004).

A series of drug substrates of OATP1B1 was identified, such as atrasentan (Smeijer et al., 2022), bosentan (Treiber et al., 2007), cerivastatin (Shitara et al., 2003), fluvastatin (Kopplow et al., 2005), pitavastatin (Hirano et al., 2004), and rosuvastatin (Schneck et al., 2004). Endogenous substrates of OATP1B1, for example unconjugated and conjugated bilirubin, thyroid hormones, eicosanoids, dehydroepiandrosterone-3-sulfate (DHEAS), and $E_2$17βG, have been found by OATP1B1-expressing cell lines (Briz et al., 2003, Briz et al., 2006, Suga et al., 2017). Both drug and endogenous substrates of OATP1B3 often overlap with those of OATP1B1, whose endogenous substrates include bilirubin, thyroid hormones, and eicosanoids. By contrast, CCK-8 is basically transported only by OATP1B3 (Kalliokoski and Niemi, 2009, DeGorter et al., 2012). Common drug substrates of OATP1B3 and OATP1B1 are atrasentan, bosentan, cerivastatin, fluvastatin, and pitavastatin. By contrast, digoxin, docetaxel, and paclitaxel are only transported by OATP1B3 in hepatic cells (Kullak-Ublick et al., 2001, Smith et al., 2005). OATP2B1 has been detected in various tissues, playing an important role in transporting diverse kinds of substrates in these tissues. Opposed to OATP1B1 and OATP1B3, OATP2B1 has rather a narrow substrate range, including endogenous compounds like DHEAS, estrone-3-sulfate, and vasoactive intestinal peptide (Kullak-Ublick et al., 2001) and drugs such as atorvastatin, benzylpenicillin, bosentan, fexofenadine, fluvastatin, glibenclamide, and pravastatin (Grube et al., 2006, Kalliokoski and Niemi, 2009).

Large chemical compounds such as the atorvastatin, bromocriptine, carfilzomib, dronedarone, glyburide, hyperforin, lapatinib, paclitaxel, nelfinavir, ritonavir, simeprevir, sirolimus, and telmisartan strongly inhibit the function of OATP1B1 (Kalliokoski and Niemi, 2009, Kotsampasakou et al., 2015). Moreover, inhibitors of OATP1B1 are usually substrate-dependent. Similarly, OATP1B3 also has a broad number of inhibitors including cyclosporine, azithromycin, erythromycin, rifampicin, glibenclamide, nateglinide, roxithromycin, and tolbutamide, which might interact with OATP1B3 substrates (Kalliokoski and Niemi, 2009, Meyer Zu Schwabedissen et al., 2014). Grapefruit juice was found one of the earliest

inhibitors for OATP2B1 inducing a significant decrease in the activity of OATP2B1 *in vitro* (Kirby and Unadkat, 2007). To date, many drugs and natural products have been identified to inhibit OATP2B1 activity *in vitro* such as afatinib, atazanavir, cyclosporine, eltrombopag, glyburide, hesperetin, hesperidin, phloridzin, rifamycin (Klatt et al., 2013, Shirasaka et al., 2013, Unger et al., 2020).

1.2.4 The physiological and pharmacological function of OATP1B1, OATPB21, and OATP1B3

The function of a transporter *in vivo* is usually studied by two methods. One is detecting the interaction of two drugs simultaneously administered as the potential inhibitor and substrate. Another one is comparing the pharmacokinetic parameters of homozygous individuals with the impaired function of the respective transporter variant. OATPs control the uptake of their substrates, which is the rate-limiting process of substrate clearance by the liver (Niemi et al., 2011). OATP1B1 plays a role in the uptake and clearance of various therapeutic drugs due to its high expression in human hepatocytes, when compared to OATP2B1 and OATP1B3 (Hirano et al., 2004, Karlgren et al., 2012). As some drugs can be taken up by several transporters in human hepatocytes, it is important to study each OATP isoform during this process for predicting drug-drug interactions. HEK293 cells expressing OATP1B1 or OATP1B3 were used as an *in vitro* model (Uchiyama et al., 2019). In hepatocellular carcinoma, compared with normal liver cells, the liver-specific transporters OATP1B1 and OATP1B3 are down-regulated at the mRNA and protein levels (Monks et al., 2007). Rotor syndrome is a rare benign hereditary conjugated bilirubinemia associated with inactive OATP1B1 and OATP1B3 variants (van de Steeg et al., 2012). The Rotor syndrome phenotype of *Slco1a/1b*$^{-/-}$ mice can be rescued by expressing human OATP1B1 or OATP1B3. Similarly, Oatp2b1-knockout mice have been used to study the pharmacological effects of OATP2B1 substrates such as fexofenadine and rosuvastatin tested (Medwid et al., 2019).

1.2.5 OATP1B1, OATP2B1, and OATP1B3 polymorphism and drug disposition

More than 40 non-synonymous variants have been described in the OATP1B1 coding gene. The most common ones are c.521T > C (p.Val174Ala) and c.388A > G (p.Asn130Asp) with the haplotypes designated as OATP1B1*1A (c.388A-c.521T), *1B (c.388G-c.521T), *5 (c.388A-c.521C) and *15 (c.388G-c.521C) (Nishizato et al., 2003, Nozawa et al., 2005, Chae et al., 2017). The c.521T > C variant has been shown to lower transport activities *in vitro* by using several OATP1B1 substrates, such as pravastatin, rosuvastatin, atorvastatin, cerivastatin, and rifampicin (Nozawa et al., 2005). Detailed analysis of the c.388A > G variant was needed to explain its effects on the pharmacokinetics *in vitro* and humans, and results were controversial, with some studies reporting reduced transport activity, some increased transport activity and many unchanged activity thus suggesting a substrate-dependent effect of this variant (Niemi et al. 2011).

Tirona (Tirona et al., 2001) reported on the identification and functional characterization of OATP1B1 genetic polymorphisms, and 16 alleles of OATP1B1 have been defined whose frequencies were markedly different in larger populations. For example, the above mentioned c.388A > G (p.Asn130Asp) single-nucleotide polymorphism (SNP) has a quite common frequency in Europeans (about 40%), Sub-Saharan Africans, and East Asians (about 80%), while the c.521T > C (p.Val174Ala) SNP has the lowest frequency in Sub-Saharan Africans (about 2%) but a relatively higher frequency in Europeans and Asians (10% - 20%) (Pasanen et al., 2008). The OATP1B1*1B haplotype, which varies commonly in Sub-Saharan Africans (allele frequency 77%), is less frequent in Europeans (26%). The *15 haplotype has a frequency of approximately 15% - 20% in Europeans, 10% - 15% in Asians, 2% in Sub-Saharan Africans, whereas the OATP1B1*5 was found in North Africa, the Middle East, and Europe (2%, 5%, 2.5%, respectively) (Pasanen et al., 2006, Pasanen et al., 2008).

Compared to the rich genetic variations in OATP1B1, there are fewer variations that have been found in the *SLCO2B1* gene including c.1457C > T (p.Ser486Phe), c.1175C > T (p.Thr392Asn), c.601G > A (p.Val201Met), and c.935G > A

(p.Arg312Gln) (Kinzi et al., 2021). The c.1457C >T variant has been described firstly in the *SLCO2B1* gene with reduced activity in an *in vitro* study (Tamai, 2012). It has a relatively lower frequency in Caucasians but is common in Asian and African populations (Kim et al., 2013).The c.601G > A variant was associated with reduced activity in the uptake of rosuvastatin *in vitro* (Medwid et al., 2021). This variant is less frequent in the African–American population (3%) (Niemi, 2007). Mougey (Mougey et al., 2011) has described a markedly lower montelukast concentration in individuals heterozygous for the c.935G > A variant. However, based on the controversial results as to whether OATP2B1 transports montelukast in vitro, further studies are necessary to clarify why the *SLCO2B1* variant c.935 G > A variant associated with altered montelukast pharmacokinetics (Chu et al., 2012). The c.1175C > T variant shows reduced estrone-3-sulfate uptake in HEK293 cells expressing the variant (Nozawa et al., 2002).

Similarly to OATP1B1, several nonsynonymous variations have been identified in the *SLCO1B3* gene encoding OATP1B3. According to a study with genomic DNA from diverse ethnic backgrounds, Schwarz (Schwarz et al., 2011) identified and functionally characterized 14 SNPs, including six non-synonymous polymorphisms in the coding region of OATP1B3: c.334T > G (p.Ser112Ala), 439A >G (p.Thr147Ala), c.699G > A (p.Met233Lle), 767G > C (p.Gly256Ala), 1559A > C (p.His520Pro), and 1679T > C (p.Val560Ala).

Two of the common OATP1B3 variants are the c.334T > G and the c.699G > A associated with altered transport activity *in vitro* and *in vivo*. They were found to be associated with the pharmacokinetics of the immunosuppressant mycophenolic acid in renal transplant patients that had markedly higher mycophenolic acid glucuronide amounts because of reduced hepatic uptake (Picard et al., 2010). Other studies show that c.334T > G and c.699 G> A variants affect the OATP1B3 substrate glucuronide metabolite of the immunosuppressant mycophenolic acid (Miura et al., 2008).

Nonsynonymous sequence variations in the genes encoding OATP1B1, OATP2B1, and OATP1B3 are summarized in Table 3.

Table 3 The summary of nonsynonymous sequence variations in the genes encoding OATP1B1, OATP2B1, and OATP1B3. Modified from Niemi (Niemi, 2007) and Gong and Kim (Gong and Kim, 2013).

Nucleotide change	Rs number	Exon	Amino acid change	In vitro function	*Europeans/ European–Americans	*Sub-Saharan Africans/African-Americans	*Chinese	*Japanese
OATP1B1								
c.217T>C	rs56101265	2	p.F73L	Decreased	0-2	0	Unknown	Unknown
c.245T>C	rs56061388	3	p.V82A	Decreased	0-2	0	Unknown	Unknown
c.388A>G	rs2306283	4	p.N130D	Decreased or unchanged	30-46	72-81	62-84	63-77
c.452A>G	rs2306282	4	p.N151S		0	0	0-4	1
c.463C>A	rs11045819	4	p.P155T	Unchanged	13-23	2-6	0-1	0
c.467A>G	rs72559745	4	p.E156G	Decreased	0-2	0	Unknown	Unknown
c.521T>C	rs4149056	5	p.V174A	Decreased	8-20	1-2	9-16	10-16
c.578T>G	rs72559746	5	p.L193R	Decreased	< 0.3	Unknown	Unknown	Unknown
c.1007C>G	rs72559747	8	p.P336R	Unchanged	Unknown	Unknown	1	Unknown
c.1058T>C	rs55901008	8	p.I353T	Decreased	0-2	0	Unknown	Unknown
c.1294A>G	rs56387224	9	p.N432D		0-1	0	Unknown	Unknown
c.1385A>G	rs72559748	10	p.D462G	Unchanged	0-1	0	Unknown	Unknown

c.1463G>C	rs59502379	10	p.G488A	Decreased	0	9	Unknown	Unknown
c.1929A>C	rs34671512	14	p.L643F	Unchanged	4	13	Unknown	Unknown
c.1964A>G	rs56199088	14	p.D655G	Decreased	0-2	0	Unknown	Unknown
c.2000A>G	rs55737008	14	p.E667G	Unchanged	0-2	34	Unknown	Unknown
OATP2B1								
c.601G>A	rs35199625	6	p.V201M		Unknown	*3*	Unknown	Unknown
c.935G>A	rs12422149	8	p.R312Q		2-11	7-15	21-39	35-40
c.1175C>T	rs1621378	10	p.T392I	Decreased	0	Unknown	Unknown	69
c.1457C>T	rs2306168	11	p.S486F		0-6	10-41	25-16	31-36
OATP1B3								
c.334T>G	rs4149117	4	p.S112A	Unchanged	78-89	35-41	68-83	64-68
c.699G>A	rs7311358	7	p.M233I	Decreased or unchanged	71-79	34-42	68-84	70-71
c.1564G>T	rs72559743	12	p.G522C	Decreased	0-2	0	0	Unknown
c.1679T>C	rs12299012		p.V560A	Decreased	Unknown	21	Unknown	Unknown

* Frequency is the range of values from different populations.

1.3 Organic cation transporter 1 (OCT1)

1.3.1 General properties and distribution of OCT1

OCT1 is a member of the SLC22 family that contains more than 20 members, which constitute six subfamilies: OCTs, OCTNs, OCT/OCTN-related, OATs, OAT-like, and OAT-related (Lai et al., 2018, Nigam, 2018). Rat Oct1, encoded by the *Slc22a1* gene, was isolated from the kidney and cloned as the first member of the SLC family in 1994 (Gründemann et al., 1994). In 1997, human OCT1 was identified and cloned, which is encoded by the *SLC22A1* gene (Gorboulev et al., 1997). The human OCT1 protein consists of 554 amino acids that were predicted to include 12 α-helical transmembrane domains, a large extracellular loop between the region of TMD1 and 2 with three putative N-linked glycosylation sites and a large intracellular loop between the region of TMD6 and 7 containing a conserved signature for phosphorylation (Fig. 2) (Jonker and Schinkel, 2004, Koepsell et al., 2007).

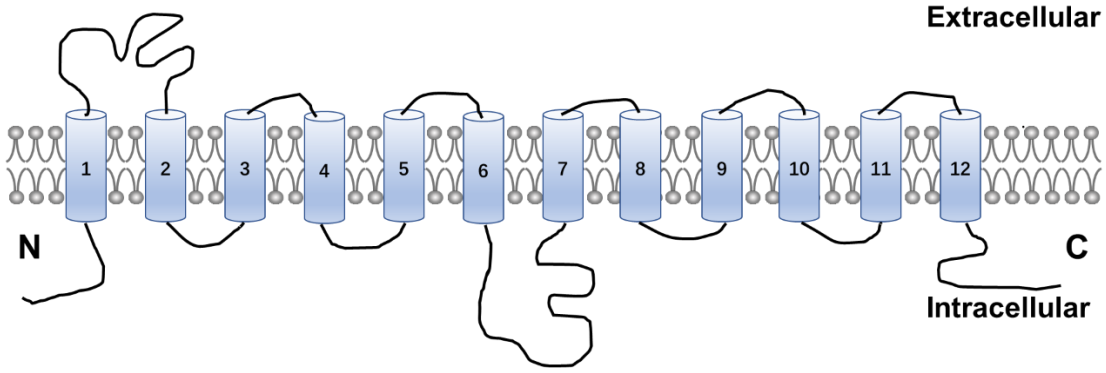

Figure 2. Predicted scheme of OCT1 protein structure. OCT1 is considered to include 12 transmembrane domains with a large glycosylated extracellular loop and a large phosphorylated intracellular loop.

The human OCT1 transporter is mainly located in the sinusoidal membrane of hepatocytes. Similar to the OATP1B1, it is a liver-specific transporter (Koepsell et al.,

2007, Nies et al., 2009, Lozano et al., 2013). It is also expressed in the luminal membranes of proximal and distal tubules of the kidney (Tzvetkov et al., 2009b). Apart from this, *SLC22A1* transcripts have been found in a large range of tissue including the spleen, skin, uterus, heart, intestine, whole blood, thymus, brain, pancreas, lung, mammary gland, muscles, testis, bone marrow, and ovary, yet at levels at least 1000fold lower than in liver (Jung et al., 2008, Nies et al., 2009). However, Oct1 is mainly located in the hepatocytes, kidneys, and small intestine in the rat and mouse (Lips et al., 2007).

1.3.2 Substrates and inhibitors of OCT1

The substrates of OCT1 are relatively small hydrophilic molecules with a relative molecular mass lesser than 500 and a variety of different molecular structures, such as weak basic uncharged compounds and monovalent and divalent organic cations (Jonker and Schinkel, 2004, Koepsell et al., 2007). As prototype substrates of OCT1, chemical compounds such as tetraethylammonium, 1-methyl-4-phenylpyridinium, and 4-(4-(dimethylamino)styryl)-N-methylpyridinium are commonly used to assess the transport capacity of OCT1 (Arimany-Nardi et al., 2015). Besides, a huge number of endogenous compounds has been recognized as OCT1 substrates with different affinities, for example, acetylcholine, adrenaline, agmatine, choline, corticosterone, dopamine, histamine, noradrenaline, polyamines, progesterone, putrescine, and, serotonin, spermidine, thiamine, and tyramine (Breidert et al., 1998, Gründemann et al., 1999, Hayer-Zillgen et al., 2002, Koepsell et al., 2007, Funk, 2008, Sala-Rabanal et al., 2013, Boxberger et al., 2014, Chen et al., 2014, Koepsell, 2015, Seitz et al., 2015, Andreev et al., 2016).

Many chemical compounds inhibit the function of OCT1, such as atropine as a muscarinic drug, verapamil as a Ca^{2+} channel blocker, ritonavir as an antiviral drug, varenicline as an anti-nicotine addiction, and levodopa as an anti-Parkinson disease drug (Ahlin et al., 2008, Becker et al., 2011, Hendrickx et al., 2013, Koepsell, 2015, Seitz et al., 2015, Andreev et al., 2016).

1.3.3 Pharmacological and physiological function of OCT1

OCT1 is involved in various aspects of pharmacology, pathophysiology, and general physiology. In the liver, OCT1 is mainly involved in the delivery of a variety of endogenous compounds and therapeutic drugs into the hepatocytes from sinusoidal blood (Jonker and Schinkel, 2004, Umehara et al., 2007, Jung et al., 2008). OCT1 has been identified to transport thiamine into hepatocytes. In *Oct1*$^{-/-}$ mice, the accumulation of the thiamine metabolites thiamine monophosphate and thiamine pyrophosphate in the liver was significantly reduced compared with wild-type mice, while phosphorylation of AMPK was increased indicating that Oct1 might play a role in hepatic steatosis through modulation of the levels of thiamine by the MPK pathway in mice (Chen et al., 2014). Metformin, as a widely used antidiabetic drug, is also transported by OCT1 in the liver. A report (Wang et al., 2003) showed that compared with *Oct1*$^{-/-}$ mice, metformin caused the levels of blood lactate to be significantly increased in wild-type mice, demonstrating that Oct1 may be involved in lactic acidosis induced by metformin in the liver. Another substrate of OCT1 is the cytostatic agent cisplatin, which showed a higher accumulation in OCT1-transfected cells than in control vector transfected cells (Yonezawa et al., 2006, Zhang et al., 2006) indicating a role of cisplatin in hepatic uptake of cisplatin.

OCT2 localizes to the luminal membrane of proximal tubule epithelial cells in the human kidney, whereas the localization of hOCT1 in these structures is not clear, yet. One study showed that it localizes to the apical side of proximal and distal tubules in human kidneys (Tzvetkov et al., 2009a).

Accumulating pieces of evidence have indicated that OCT1 may also assist transfer of endogenous substrates and drugs across the blood-brain barrier (BBB) (Lin et al., 2010). A report showed that N-Methyl-4-phenyl-1,2,3,6-tetrahydropyridine cannot be transported across the BBB in *Oct1*$^{-/-}$ mice (Lin et al., 2010).

In some cancer entities such as hepatocellular carcinoma, the function and expression of OCT1 might be downregulated (Heise et al., 2012, Schaeffeler et al., 2011). A

published report (Stefanko et al., 2017) has demonstrated that compared to the healthy controls, expression of *OCT1* mRNA was significantly reduced in acute myeloid leukemia patients.

1.4 Multidrug-resistance protein 1（MDR1, ABCB1）

ABCB1 (also called P-glycoprotein/ MDR1), as an efflux transporter, belongs to the ABCB transporter subfamily of the ABC transporter family. It has been the first discovered human ABC transporter by Juliano and Ling and associated with multidrug resistance of tumor cells (Juliano and Ling, 1976, Scherrmann, 2005). Human ABCB1 is encoded by the *ABCB1* gene, while in rodents there are two orthologs: *Abcb1a* and *Abcb1b*, which share over 80% amino acid identity with each other (Dewanjee et al., 2017). ABCB1 is a membrane glycoprotein with 170-kDa containing two nucleotide-binding domains (NBD) that consist of three conserved domains involved in ATP hydrolysis, and two TMDs each composed of 6 transmembrane helices involved in substrate binding and transport (Fig. 3) (Ambudkar et al., 2006, Weng and Tsai, 2021).

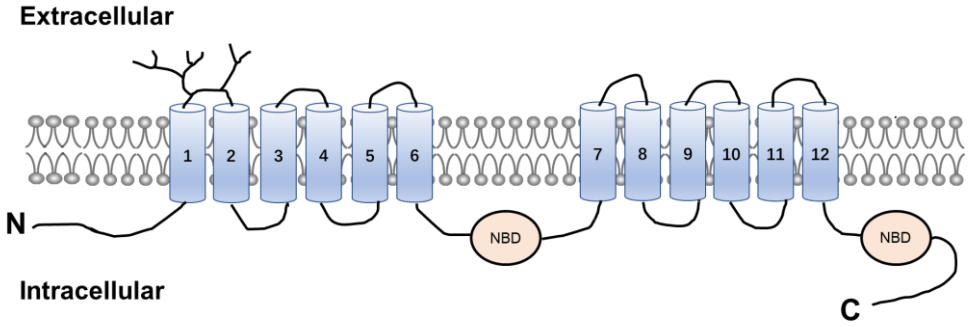

Figure 3. Predicted schematic of ABCB1 protein structure. ABCB1 consists of two NBDs and 2 TMDs that contain a total of 12 transmembrane helices.

ABCB1 is highly expressed in various organs, such as the intestine, liver, kidney, brain, testis, and placenta, and also in specific tissue barriers including the blood-brain, the blood-testis, and the fetal-maternal barriers (Cascorbi, 2011). In cancer cells, ABCB1

is suggested to be also expressed in the mitochondrial and nuclear membranes to assist anticancer drugs efflux to the cytosol (Solazzo et al., 2006, Su et al., 2012).

ABCB1 transports substrate by ATP hydrolysis creating energy (Litman et al., 1997). A large range of substrates has been identified: e.g., the anticancer drugs daunorubicin, doxorubicin, epirubicin, etoposide, irinotecan, methotrexate, teniposide, vincristine, imatinib; antihistamines fexofenadine, ranitidine, terfenadine; neuroleptics phenothiazine, trifluoperazine; antiarrhythmics amiodarone, lidocaine, propafenone, and quinidine. It also has a wide range of inhibitors, which might inhibit the function by changing the expression of ABCB1 or binding a site by reversible or irreversible competition (Liu, 2019).

In the brain, ABCB1 is mainly expressed on the luminal side of the brain capillary endothelial cells (Cordón-Cardo et al., 1989, Pardridge, 1997). Since most of the substrates of ABCB1 are hydrophobic that may enter the brain capillary endothelial cells, it plays an important role in assisting the translocation of endogenous and exogenous compounds back into blood thus protecting the brain parenchyma. Some reports have demonstrated that compared with wild-type mice, penetration of P-GP substrates into the brain was increased to 5- to 10-fold in *Abcb1a/1b*$^{-/-}$mice (Pardridge, 1997, Schnepf and Zolk, 2013, de Gooijer et al., 2021). In the kidney, ABCB1 is expressed in the mesangium, proximal tubules, and the collecting duct to transport substrates from the blood into urine. A report showed that ABCB1 shuffled drugs across the apical membrane of proximal tubule cells in the wild-type mice, but not in *Abcb1a/1b*$^{-/-}$mice (Tsuruoka et al., 2001).

1.5 Oatps in *D. melanogaster* compared with their human orthologs

In the fruit fly, 603 genes are encoding putative transporter proteins with 347 members of the SLC family divided into 42 subfamilies (Wang et al., 2018, Höglund et al., 2011). There are eight genes (*Oatp26F, Oatp30B, Oatp33Ea, Oatp33Eb, Oatp58Da, Oatp58Db, Oatp58Dc, and Oatp74D*) encoding Oatp proteins.

Oatp26F (CG31634) is highly expressed in the midline glia during embryogenesis in *D. melanogaster* (Fulkerson and Estes, 2011). The midline glia is a special cell type of the central nervous system (CNS) of embryos in *D. melanogaster* (Jacobs, 2000), which are involved in contacting surrounding tissues such as the axons of lateral neurons during embryogenesis (Jacobs, 2000, Crews, 2010). Oatp26F (CG31634) is homologous to the human transporters OATP4A1, OATP4C1, OATP6A1, and OATP5A1.

Oatp30B (CG3811) is expressed in the nervous system and has a KAZAL (Kazal type protease inhibitor domain) domain, indicating that it is probably involved in solute transport during remodeling of the extracellular matrix (ECM) by the KAZAL type serine protease inhibitor domain (Meyer et al., 2014). Oatp30B (CG3811) is homologous to the human transporters OATP4A1, OATP4C1, OATP6A1, OATP5A1, and OATP3A1.

Oatp33Eb (CG6417) shows homology with human OATP1B7, OATP2A1, OATP2B1, and OATP3A1. Oatp33Eb (CG6417) is in tumors and can specifically induce cachexia. When this gene was silenced in the tumor, cachectic symptoms were recovered (Santabárbara-Ruiz and Léopold, 2021).

Oatp33Ea (CG5427), Oatp58Da (CG30277), Oatp58Db (CG3382), Oatp58Dc (CG3380), and Oatp74D (CG7571) are homologous to the human OATP1A2, OATP1C1, OATP1B1, OATP1B3, OATP1B7, OATP2A1, OATP2B1, and OATP3A1. The six *oatp* genes *30B*, *33Ea*, *33Eb*, *58Db*, *58Dc*, and *74D* are expressed in the Malpighian tubules. In immunocytochemical experiments, it was shown that Oatp30B (CG3811), Oatp58Db (CG3382), and Oatp58Dc (CG3380) were detected at the basolateral membrane of the principal cells of Malpighian tubules, Oatp33Ea (CG5427) and Oatp74D (CG7571) were localized in the intracellular organelles, while Oatp33Eb (CG6417) was found at the boundaries between stellate and principal cells (Torrie et al., 2004). Silencing of *Oatp58Db (CG3382)* and *Oatp58Dc (CG3380)* gene expression causes a significant decrease in ouabain and methotrexate excretion by Malpighian tubules.

Oatp58Dc (CG3380) and *Oatp74D (CG7571)* are also highly expressed in the glial cells in *D. melanogaster* (Seabrooke and O'Donnell, 2013). Reduction of *Oatp58Dc (CG3380)* function in perineal Gila cells enhanced the penetration of the tracer fluorescein across the BBB. This indicated that Oatp58Dc contributed to excluding fluorescein at the BBB level to regulate fluorescein outflow from the brain (Seabrooke and O'Donnell, 2013).

The major homologues of the fly oatps in humans have the following characteristics. OATP1A2 is detected in the endothelial cells of the BBB, the kidney, the liver, the intestine, the lung, and testes in humans. It has a large range of substrates including endogenous compounds, various drugs, and toxins (van der Deure et al., 2010, Taub et al., 2011, Gao et al., 2015). It may therefore be involved in the reabsorption of drugs in the kidney, drug absorption in the intestine, and assisting substrate transport across the BBB (Sugiura et al., 2006, Glaeser et al., 2007, Saidijam et al., 2018). In humans, OATP1C1 has been mainly detected in endothelial cells of the BBB, the testis, and the ciliary body (Mayerl et al., 2014). It has a high affinity to thyroid hormones, so it might contribute to the transport of thyroid hormones into the brain and testis (Liedauer et al., 2009). OATP1B7 is highly expressed in the liver of humans and probably plays an important role in the hepatocellular handling of its substrates (Malagnino et al., 2018). As a prostaglandin transporter, the human OATP2A1 is widely expressed in various tissues including the brain, kidney, heart, liver, lung, prostate, ovary, muscle, and spleen (Kraft et al., 2010) indicating that it is involved in many physiological and pathophysiological processes (Nakanishi and Tamai, 2017). In humans, OATP3A1 is detected in different organs such as the heart, the brain, the lung, the spleen, and the testis (Huber et al., 2007). It might play a role in the transport of the thyroid hormone to the brain (Huber et al., 2007). OATP4A1 is expressed in a wide range of organs, such as the kidney, the brain, the heart, the placenta, the lung, the liver, skeletal muscled, and the pancreas. It is also expressed in cancer cells mediating E3S uptake into cells (Hagenbuch, 2007, Gilligan et al., 2017). OATP4C1 is predominantly expressed in the basolateral membrane of proximal tubule cells in humans,

transporting some drugs such as digoxin, methotrexate, and sitagliptin from the blood to the kidney (Sato et al., 2017). In humans, OATP5A1 has been detected in the brain, the heart, the skeletal muscle, and ovaries, and also in various tumors, including bone tumors, small cell lung cancer cells, colon tumors, and hepatic tumor cells (Liedauer et al., 2009, Kindla et al., 2011, Olszewski-Hamilton et al., 2011, Wlcek et al., 2011). It plays a role in cell differentiation and cell migration processes (Sebastian et al., 2013). OATP6A1 mRNA levels are found in the testis (Roth et al., 2012).

1.6 *D. melanogaster* as a novel tool to research human membrane transporters

1.6.1 The advantage of *D. melanogaster* as a model organism

More than a century ago, *D. melanogaster* has become a model organism for genetic research (Ugur et al., 2016). It has many characteristics that make it a model organism. Compared to rodents, the fruit fly has a rapid life cycle. At 25 degrees, they only need about 10 days to complete a generation production (Pandey and Nichols, 2011). From the embryo developing to the larva, the pupa, and the adult, four stages have their specific advantages for research. Moreover, in the embryos and larvae stage, transparent bodies are easy to observe and dissect. The fly whole genome has been sequenced and annotated. They have four pairs of chromosomes and encode over 14,000 genes. About 40% homologs were identified between fly and mammal at the nucleotide level or protein sequence, whereas about 80% - 90% in conserved functional domains. It has been indicated that approximately 65% of human disease-related genes have functional orthologs in the fly (Chien et al., 2002, Yamamoto et al., 2014). The fly has tissues similar to the functions of the equivalent human tissue (Chintapalli et al., 2007).

There are various genetic tools that have been developed for fruit fly research, for example, P-elements to induce mutagenesis or insert exogenous genes into the fly genome (Spradling and Rubin, 1982). In addition, the UAS/GAL4 system allows the

expression of exogenous genes (Brand and Perrimon, 1993). Because balancer chromosomes block the genetic recombination during meiosis, transgenic fly stocks can be maintained.

Due to maintenance and propagation cost less, it is possible to generate some different strains at the same time. The most convenient is no ethical limitations in the fly, so flies expressing human membrane transporters can be created to research the human transporter related functions and diseases.

1.6.2 Gene expression by GAL4/UAS system

Gal4 encodes a transcription activator, which was identified in the yeast *Saccharomyces cerevisiae* (Laughon and Gesteland, 1984). The GAL4 protein is banded specifically to the Upstream Activation Sequence (UAS) to activate the transcription of the gene downstream on the UAS site (Giniger et al., 1985). In 1988, Fisher et. al. achieved firstly expression of a reporter gene under UAS control based on stimulation by GAL4 expression in fruit fly larvae (Fischer et al., 1988). They also demonstrated that the GAL4 expression in fruit flies alone did not affect the animal. Brand and Perrimon published in 1993 their collection of GAL4 lines, which allow temporally and spatially specific expression of a target gene in many different cell types and tissues (Brand and Perrimon, 1993).

A common GAL4/UAS system has two lines, the GAL4 line (or driver) and the UAS line (responder). The GAL4 line expresses the GAL4 protein at a certain stage and tissue, which is determined by the promoter, coupled to the GAL4 gene. In the UAS line, the target gene locates downstream to numerous tandem arrays of UAS elements. Without the GAL4 protein, the target gene in the UAS line remains silent. When the UAS line is mated with the GAL4 line, the expression of the target gene is activated in the offspring. More importantly, the target gene expression is limited in where and when the GAL4 is expressed (Fig. 4).

The GAL4/UAS system is very flexible and powerful. The expression levels can be regulated directly by changing the incubation temperature (Duffy, 2002). This system is not only used in gene expression studies but also to knock down the target gene at a certain time and in specific tissues when the target gene in the UAS line produces a hairpin structure, which can block gene expression due to RNA interference (Dietzl et al., 2007).

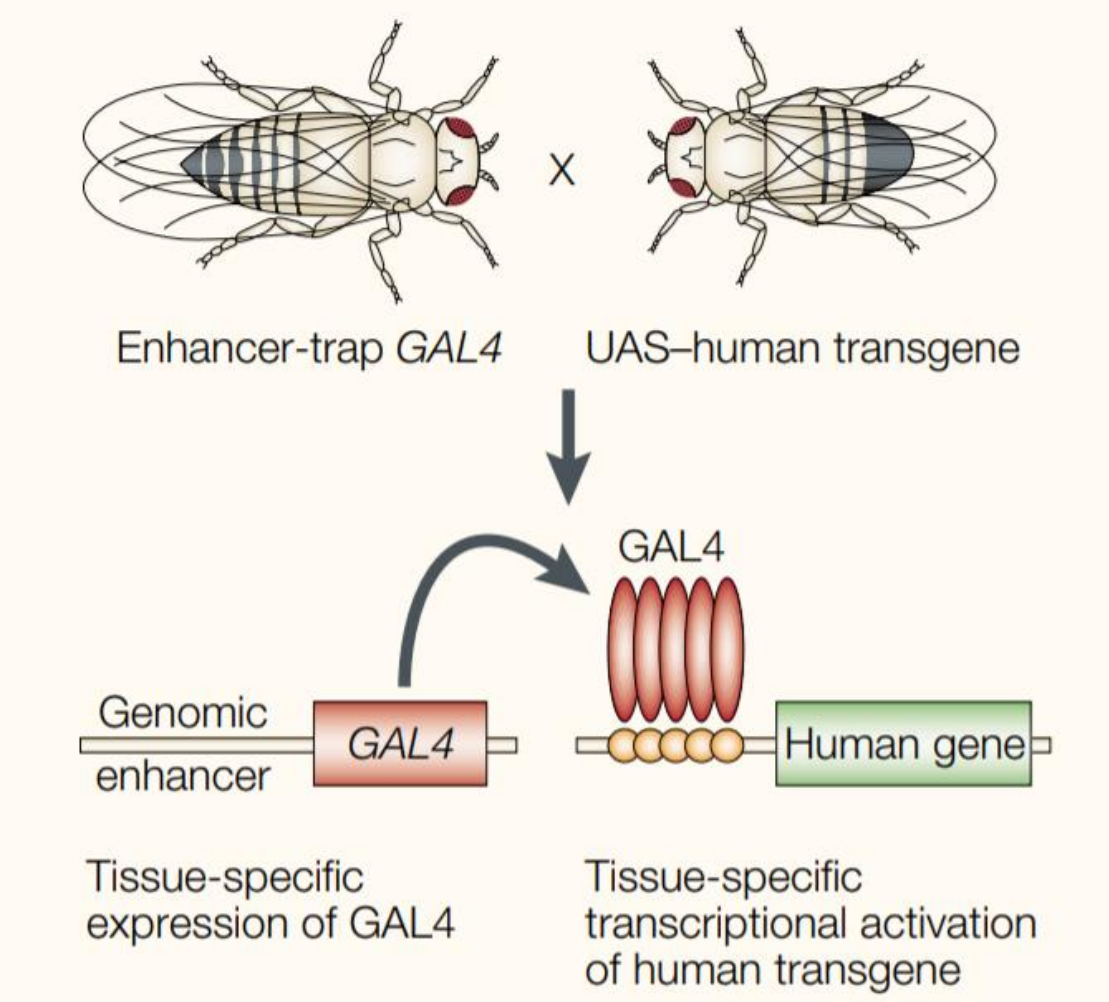

Figure 4. Mechanisms of the GAL4/UAS system inducing temporal and regional expression of certain target genes (Picture from Muqit and Feany) (Muqit and Feany, 2002).

1.6.3 The function of PhiC31 integrase in human transgenic fly

The traditional method to generate transgenic flies is based on P-element transposon transgenesis, which was first introduced in the early 1980s (Spradling and Rubin, 1982). P-elements are transposons that were discovered in fruit flies. Autonomous P-elements encode a functional transposase. The transposase cuts the P-element from the original site and reintegrates it into a random site of the genome. Non-autonomous P-elements have lost their transposase gene. But they are still able to move themselves to a new position in the genome when transposases are present in the cell (Castro and Carareto, 2004). In the P-element mediated germline transformation, the target gene is carried by a non-autonomous P-element, and integrated into a plasmid vector. The vector is introduced by microinjection into the pre-blastoderm of fruit fly embryos. A “helper-plasmid”, which is the transposase donor and itself unable to integrate into the genome, must be co-injected (Spradling and Rubin, 1982). The integration event can be detected through a visible marker gene, which is designed to co-integrate with the target gene. A commonly used marker is the *white mini* gene, which determines the red-eye phenotype in otherwise white-eyed flies (Klemenz et al., 1987). The major limitation of the P-element mediated germline transformation is that the P-elements randomly integrate into the genome. The expression level of transgenes in different locations is thus influenced by position effects and cannot be compared to each other.

The *Streptomyces* phage PhiC31 encodes an integrase that catalyzes recombination between a bacterial attachment site *attB* and a phage attachment site *attP* (Lutz et al., 2004). In PhiC31 integrase mediated transformation, an attP site must be first placed into the fruit fly genome at a certain albeit random location as the recipient site. The transgene is first integrated into a pUASTB plasmid and flanked by an attB site. The pUASTB-vector is injected this time in fly embryos that express integrase mRNA (Bischof et al., 2007). The target gene will insert into the genome at the attP site with high efficacy (Fish et al., 2007, Groth et al., 2004) (Fig. 5).

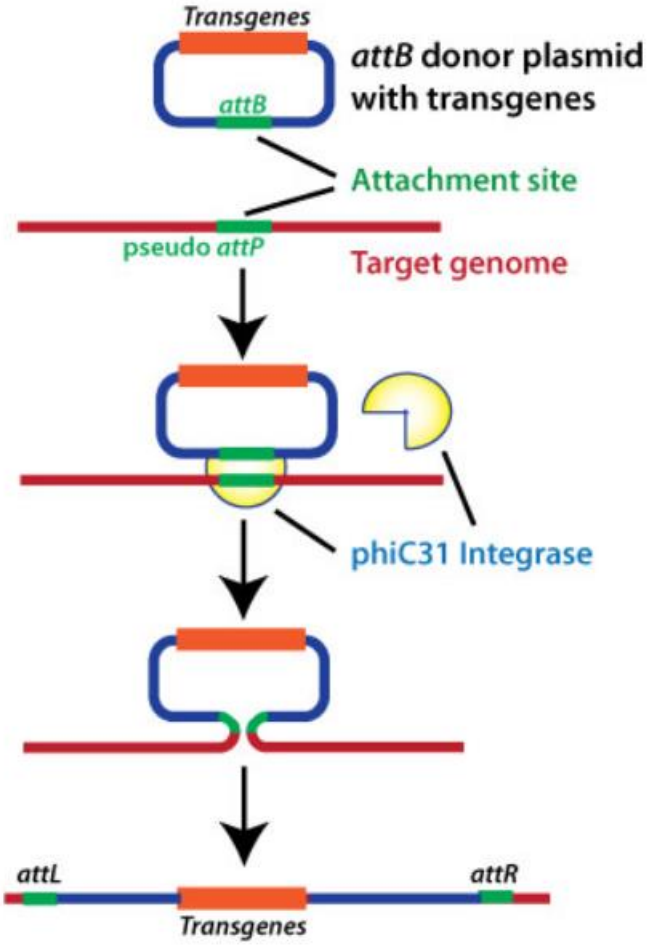

Figure 5. Schema of PhiC31 integrase mediated site-specific transgenesis. (Picture from https://www.biocat.com/genomics/gene-integration/phic31-integrase-vector-system-one-step-gene-addition-technology).

1.6.4 Generation of a membrane transporter test system in *D. melanogaster*

As previously proposed by Yiwen Wang (Wang et al., 2018) the fruit fly could be used as a novel tool to implement membrane transporter testing in drug development. The concerned membrane transporter as well as its clinically relevant genetic variants will be transformed into different fly strains and expressed in certain organs or tissues at defined embryonic stages. Transporter-specific fluorescent substrates will be introduced into the transparent fly embryos. The dynamic distribution of these tracers can be observed and analyzed to monitor the properties of these transporters. The

functional change between reference genotypes and genetic variants can also be elucidated in this way. To reveal the interaction of investigational drugs with the transporters, the fluorescent tracers will be given simultaneously with the drug through injection. Drugs that interact with a transporter will inhibit the transport of the tracer, and affect the tracer accumulation in the target tissue (Fig. 6).

A prerequisite is that the cells of the test organ must be polar and form a lumen. This situation allows testing both uptake and efflux transporters. For uptake transporters, the transporters localized in the basal membrane will take up the fluorescent tracer provided by injection into the embryos. For efflux transporters, the transporters positioned in the apical membrane will transport the tracer into the organ lumen (Fig. 6). Second, the organ should originally not take up or efflux the fluorescent tracer without exogenous human transporters. Third, the organ should not have any important function at the embryonic stages. This limits side effects on embryonic development caused by the expression of exogenous genes and accumulation of injected substances. Fourth, the organ must have a proper size for easy observation. Fifth, the organ must complete development and be morphologically stable at a relatively early stage during embryonic development. It should give enough time to perform injection and analysis by microscopy. The tracheae and salivary glands have in principle a similar morphology. They are big organs and are formed by a monolayer of epithelial cells. These cells are polarized with one side facing a lumen, and the other side facing the hemolymph (the insect blood). They are not essential during embryonic stages. Furthermore, appropriate GAL4-lines specific for these two organs already exist, such as btl-GAL4 for the tracheae (Klämbt et al., 1992), and fkh-GAL4 for salivary glands.

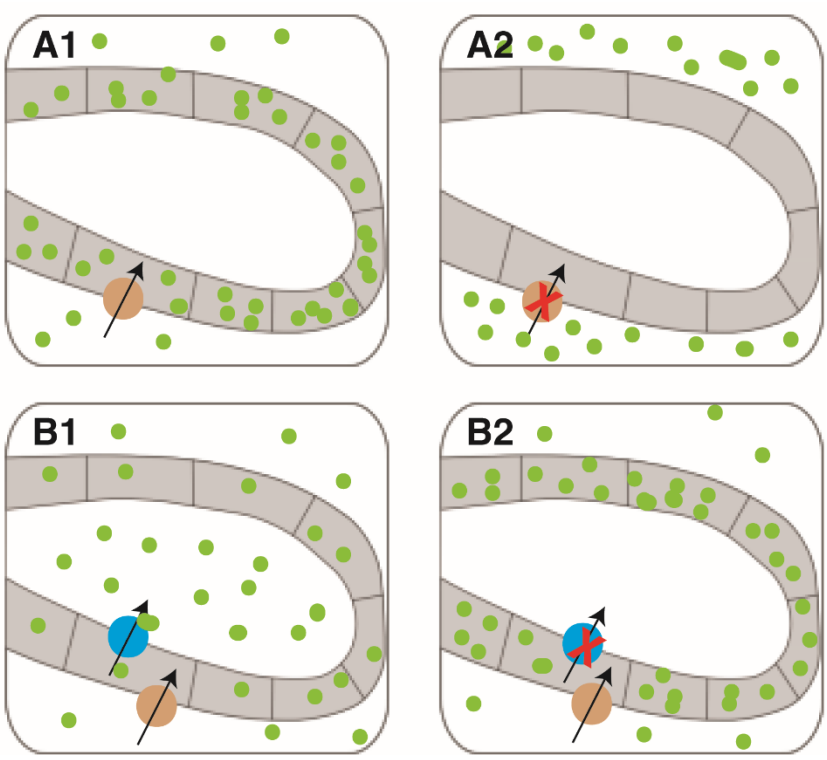

Figure 6. The human membrane transporter-mediated uptake and efflux of fluorescence tracer in a polarized fly organ. A1: Uptake transporters (grey circle) expressed in the basal membrane take up the tracer (green dotes) provided by injection; A2: Simultaneous injection of the tracer and an investigational drug inhibiting accumulation of the tracer in the cell; B1: An efflux transporter (blue circle) localized in the apical membrane transports the tracer into the lumen of this organ; B2: Simultaneous injection of the tracer and an investigational drug inhibiting the accumulation of the tracer in the lumen.

1.7 Aims of the present study

Based on the easy propagation, low costs of maintenance and lack of ethical limitations in preforming research with flies, *D. melanogaster* might serve as a novel preclinical model for human membrane transporter testing. It was therefore the primary aim of this thesis to elucidate the use of the fruit fly as a tool to study clinically relevant human membrane transporters.

The following specific questions should be addressed:

1. Analysis of the functions of the clinically relevant human organic anion uptake transporters

hOATP1B1, hOATP2B1 and hOATP1B3 expressed in the salivary glands of fly embryos

2. Analysis of the function of clinically relevant human organic cation transporter hOCT1 together with efflux transporter ABCB1 expressed in the salivary glands of fly embryos
3. Establishment of a drug testing system based on hOCT1 to monitor function of hOCT1 inhibitors in vivo.

2. Materials and methods

2.1 Materials

2.1.1 Chemicals

Table 4 List of chemicals

Material	Supplier
Agar	Sigma Aldrich
Agarose	Sigma Aldrich
Amphiline	Sigma Aldrich
ASP	Sigma Aldrich
BSA	Merck
CLF	Corning Incorporated
Cimetidine	Sigma Aldrich
Cisplatin	Sigma Aldrich
Decynium 22	Sigma Aldrich
DMSO	Honeywell Fluka
DBF	Sigma Aldrich
EDTA	Sigma Aldrich
EGTA	Sigma Aldrich
EtBr	Sigma Aldrich
Ethanol	Merck
Formaldehyde	Sigma Aldrich
Glacial acetic acid	Sigma Aldrich
Heptane	Sigma Aldrich
KCl	Sigma Aldrich
KH_2PO_4	Sigma Aldrich
MDBF	Sigma Aldrich
Methanol	Merck
$MgCl_2$	Sigma Aldrich
NaCl	Sigma Aldrich
Na_2HPO_4	Sigma Aldrich

NaOH	Sigma Aldrich
Nipagin	Sigma Aldrich
Prazosin	Sigma Aldrich
Triton	Carl Roth
Tryptone	Honeywell Fluka
Yeast extract	SERVA
Oil 10S, Voltalef	VWR
ß-Mercaptoethanol	SERVA

2.1.2 Buffers and solutions

Table 5 List of buffers and solutions

Buffer	**Ingredients**
PBS (10x)	NaCl 40 g
	KCl 1 g
	Na_2HPO_4 8.9 g
	KH_2PO_4 1.2 g
	NaOH add to reach pH 7.4
	ddH_2O up to 500 ml
PBST	PBS (1x) 50 ml
	Triton 50 µl
PBSTA	PBS (1x) 50 ml
	Triton 50 µl
	BSA 0.5 g
TAE (x50)	Glacial acetic acid 57.1 ml
	EDTA (0.5 M, pH 8) 100 ml
	Millipore H_2O up to 1000 ml
Squishing Buffer	Tris- HCL (pH 8) 10 mM
	EDTA 1 mM
	NaCl 25 mM
	ddH_2O

2.1.3 Enzymes, reagents

Table 6 List of enzymes and reagents

Material	Supplier
EcoRI	Fermentas
Kod polymerase	Sigma Aldrich
Proteinase K	Thermo Fisher
Taq polymerase	Qiagen
pUAST-attB	DGRC
1kb DNA ladder	Fermentas
100 kb DNA ladder	Fermentas
Stellar cells	Clontech
cDNA Synthesis kit	Roche
In-Fusion HD cloning kit	Takara
KOD Hot Start DNA polymerase kit	Sigma Aldrich
Micro spin S400 HR columns	GE Healthcare
QIAprep Spin Miniprep kit	Qiagen
RNase-Free DNase set	Qiagen
RNeasy mini kit	Qiagen
SYBR Green kit	Roche
Taq DNA polymerase kit	Qiagen
Plasmid Mini Kit	Sigma Aldrich

2.1.4 Equipment

Table 7 List of equipment

Equipment	Manufacturer
AccuBlock digital dry bath	LaborNet
Eppendorf Femtojet (microinjection machine)	Eppendorf
FiveGo Portable pH meter	Mettler Toledo
KE Puller-horizontal (peptite puller)	Laborbedarf
Leica EZ4HD (Binocular)	Leica
Light Cycler (Real time PCR machine)	Roche
Mastercycler pro PCR System	Eppendorf
MIKRO 120 centrifuge	Hettich
Milli-Q water Q-Pod	Merck
Mini Centrifuge MiniSpin	Eppendorf
Nanodrop ND-1000	PEQLAB
Nikon AZ100	Nikon

2.1.5 Primer for PCR

Table 8 List of primer

Primer	Forward	Reverse
pUAST-attB	ACCAGCAACCAAGTAAA	TGTGGTGTGACATAAT

2.1.6 Primer for In-Fusion cloning

Table 9 List of primer

Primer	Forward	Reverse
hOATP1B1	TGAATAGGGAATTGGGAATTATGGACCAAAATCAACATTTGAA	CGCAGATCTGTTAACGAATTCTACAGGAACAGGTGGTGGC
RFP (hOATP1B1)	ACATTGTTAAATGGTGCGCTCCTCCAAG	AGCGCACCATTTAACAATGTGTTTCACTATCTGCC
hOATP2B1	TGAATAGGGAATTGGGAATTGCAGTCATGGGACCCAGG	CGCAGATCTGTTAACGAATTCTACAGGAACAGGTGGTGGC
RFP (hOATP2B1)	CCGAGTGTGAATGGTGCGCTCCTCCAAG	AGCGCACCATTCACACTCGGGAATCCTCTGG
hOATP1B3	TGAATAGGGAATTGGGAATTATGGACCAACATCAACATTTGA	CGCAGATCTGTTAACGAATTCTACAGGAACAGGTGGTGGC
RFP (hOATP1B3)	TGCCAACTAAATGGTGCGCTCCTCCAAG	AGCGCACCATTTAGTTGGCAGCAGCATTGT
hABCB1	AGGGAATTGGGAATTATGGATCTTGAAGGGGACCGC	ATCTGTTAACGAATTTCACTGGCGCTTTGTTCCAGC

2.1.7 Primer for qRT-PCR

Table 10 List of primer

Primer	Forward	Reverse
hOATP1B1	ACTGATTCTCGATGGGTTGG	TATTTGGAGTTTGGGGCAAG
hOATP2B1	GAAAACCTGGCTGTTGTCCA	CCATTGGACGGCTTTAACCC
hOATP1B3	ATATGCTTCGTGGCATAGGG	AAAGCCAATGACTGGACCAA
hOCT1	TAATGGACCACATCGCTCAA	AGCCCCTGTAGAGCACAGA
hABCB1-1	CAGAGGGGATGGTCAGTGTT	CGTGGTGGCAAACAATACAG
hABCB1-2	CAAGAAGCCCTGGACAAAGC	ATGCTCCTTGACTCTGCCAT
OATP26F	GTTCAACTCAGCCTGACCAG	ATGTGCCTCGGAAACCCTT
OATP30B	AGGAACGGGTAGATAGTGCG	AACTACACCAATTGCGCCTG
OATP33EA	GGTCCTTGCTGTCGATCAAC	TACCTCGACGACAACACCAA
OATP33EB	GTGAATGACGGTCTTTGGCA	ATAGTCCGGCGGTGATAGGT
OATP58DA	TTATCCCGCTCCTGATTCGT	TCGCTGGATGGGTATAGGGT
OATP58DB	TAGCAGGACCCAGCATACG	AAAGAGCTGGGGACTACACG
OATP58DC	AAGACTCAACAAAGCCGGAG	GACCCTATGCCGCTTGAATG
OATP74D	CAGGCCATTCTTCAGGTGTC	GTCAAGCCTTCACACCACTG

2.1.8 Primer for sequence test

Table 11 List of primer

Primer	Sequence
hOATP1B1	GCTCTGATTGATACAACG
hOATP2B1	GAAAACCTGGCTGTTGTCCA
hOATP1B3	TCCTAAGGACTCTCGTTGGGT
hABCB1-1	CAGGGTTCTTCATGAATCTGG
hABCB1-2	GGCCATCAGTCCTGTTCTTGG
hABCB1-3	TAATGCTGACGTCATCGCTGG
hABCB1-4	ATAAATGGAGGCCTGCAACC
hABCB1-5	CCCATCATTGCAATAGCAGG
hABCB1-6	GGCAAGTCAGTTCATTTGCTCC
hABCB1-7	AGCGACTGAATGTTCAGTGG

2.2 Methods

2.2.1 Fly works

2.2.1.1 Cultivation of fly stocks

Flies were cultivated in vials with standard fly yeast-cornmeal-molasses food (0.8% agar, 1.8% dried yeast, 1.0% soybean meal, 2.2% molasses, 8.0% malt extract, 8.0% corn meal, 0.63% propionic acid) at 25˚C. The transgenic stocks UAS-hOCT1, UAS-hOATP1B1, UAS-hOATP2B1, UAS-hOATP1B3 were previously generated by our laboratory. The transgenic stocks UAS-hABCB1, UAS-hOATP1B1-RFP, UAS-hOATP2B1-RFP, UAS-hOATP1B3-RFP were generated by me. The stock UAS-hOCT1 was recombined with UAS-GFP; UAS-hOATP1B1, UAS-hOATP1B3 were recombined with UAS-CD8-RFP; UAS-hOATP2B1 was recombined with UAS-RFPnls; UAS-hOCT1 was recombined with UAS-hABCB1. All fly strains used in this research are listed in Table 12.

Table 12 List of fly stocks

Gene/strain	Chromosome	Origin
Wild-type	-	Lab stock
UAS-hOCT1	3	Lab stock
UAS-hABCB1	3	Lab stock
UAS-hOATP1B1	3	Lab stock
UAS-hOATP2B1	3	Lab stock
UAS-hOATP1B3	3	Lab stock
UAS-GFP	3	Lab stock
UAS-CD8-RFP	3	Lab stock
UAS- RFPnls	3	Lab stock
UAS-hOCT1; UAS-GFP	3	Lab stock
UAS-hOATP1B1; UAS-CD8-RFP	3	Lab stock
UAS-hOATP2B1; UAS- RFPnls	3	Lab stock
UAS-hOATP1B3; UAS-CD8-RFP	3	Lab stock
UAS-hOATP1B1-RFP	3	Lab stock
UAS-hOATP2B1-RFP	3	Lab stock
UAS-hOATP1B3-RFP	3	Lab stock
fkh-GAL4	3	Lab stock
bo-GAL4	3	Lab stock
cut-GAL4	3	Lab stock
nub-GAL4	3	Lab stock
FB-GAL4	3	Lab stock
L370-GAL4	3	Lab stock
drm-GAL4	3	Lab stock
en-GAL4	3	Lab stock
hh-GAL4	3	Lab stock
elav-GAL4	3	Lab stock
pros-GAL4	3	Lab stock
R24	3	Lab stock
tub-GAL4	3	Lab stock
Oatp26F[a] RNAi	2	VDRC

Oatp26F^{b} RNAi	3	VDRC
Oatp30B RNAi	2	VDRC
Oatp33Ea^{a} RNAi	2	VDRC
Oatp33Ea^{b} RNAi	2	VDRC
Oatp33Eb^{a} RNAi	2	VDRC
Oatp33Eb^{b} RNAi	3	VDRC
Oatp58Da^{a} RNAi	2	VDRC
Oatp58Da^{b} RNAi	3	VDRC
Oatp58Db RNAi	2	VDRC
Oatp58Dc^{a} RNAi	2	VDRC
Oatp58Dc^{b} RNAi	3	VDRC
Oatp74D RNAi	1	VDRC

2.2.1.2 Preparation of Amp-LB medium

To prepare Amp-LB medium, 10 g NaCl, 5 g yeast extract, and 10 g tryptone were dissolved in 950 ml deionized water. The medium was adjusted to pH 7.0 with 3 M NaOH and filled up with additional water to a total of 1 L, autoclaved for 2 hours. After cooling down to 55°C, 1 ml ampicillin solution (50 mg/ml in water) was added to the medium and the medium was stored at room temperature.

2.2.1.3 Preparation of Amp-LB agar plates

After preparing 1 L Amp-LB medium, 15 g agar was added and autoclaved. It was cooled down to 55°C and 1 ml ampicillin was added to the medium. The mixed solution was transferred onto Petri dishes on the clean bench. After waiting until the agar became hard, the dish was inverted, packed, and stored at 4°C.

2.2.2 Generation of human transgenic fly

2.2.2.1 KOD PCR

The plasmid was extracted using a Plasmid Mini Kit. According to the guides of the manufacturer of the KOD Hot Start DNA Polymerase Kit, about 50 ng plasmid DNA or 200 ng of genomic DNA was used as a template.

Table 13 Reaction mixtures for KOD PCR (Total Volume 50 µl)

Reagent	Volume
H2O	32.6 µl
10x Buffer	5 µl
4 mM dNTP	5 µl
MgCl2	2 µl
DNA Template	1 ul
Primer Mix	4 µl
KOD Polymerase	0.4 µl

Table 14 Features of KOD PCR

Effect / Reaction	Temperature	Time	Cycles
Denaturation	94°C	2 min	-
Amplification	94°C - 65°C - 72°C	30 s – 30 s – 60 s	25-35
Melting Curve	72°C	2 min	-
Cooling	4°C	-	-

2.2.2.2 Analysis of KOD PCR products by gel electrophoresis

The 0.8% agarose gel was prepared for DNA electrophoresis by adding 0.8 g agarose to 100 ml 1 x TBE buffer in the conical flask. To melt agarose, the conical flask was boiled in the microwave. After the agarose cooled down to about 60°C, 5 µl Ethidium Bromide (EtBr) was added into the agarose solution. This solution was poured into the mold and stocked at 4°C. 4 µl loading buffer was mixed with 10 µl KOD PCR product, then 8 µl mix was added into the pockets of the gel. A 1 kb-ladder was used as the DNA size reference. After the gel electrophoresis was run for about 30 min at 100 V/ 0.1 A, the DNA band was detected under UV light.

2.2.2.3 In-Fusion cloning

The concentration of the KOD PCR fragment was measured by Nanodrop ND-1000, then was diluted to 100 ng/µl. After mixing all reaction components for the In-fusion reaction, the solution was incubated for 15 min at 50°C, then placed on ice for stopping the reaction. The cloning reactions were stored at -20°C.

Table 15 Reaction mixtures for In-Fusion cloning (Total Volume 10 µl)

Reagent	**Volume**
5X In-Fusion HD Enzyme Premix	2.0 µl
KOD PCR product	0.8 µl
Vector pUAST-*attB*	1.2 µl
dH2O	6.0 µl

2.2.2.4 Transformation into Stellar Competent Cells

After thawing Stellar Competent Cells on ice, 5 µl In-Fusion reaction mixture was added to 50 µl competent Cells. At first, these mixed components were placed on ice 30 s, then they were heat-shocked at 42°C for 45 s. These mixed components were left on ice for 2 min. SOC medium was warmed to 37°C and added to mixed components to bring the final volume to 500 µl. The medium mixture was incubated for 1 h at 37°C with shaking at 200 rpm. 100 µl of SOC medium mixture was spread on a separate LB plate including 100 µg/ml of ampicillin. The experimental plate was incubated overnight at 37°C. On the next day, at least 20 individual isolated colonies

were picked from the experimental plate to a new LB plate and these colonies were incubated overnight at 37°C.

2.2.2.5 Selection of the interesting colonies

The interesting colonies were selected by PCR and gel electrophoresis. Colonies were used as a DNA template. Each colony was touched by a pipette tip and added to the PCR mixture. After the gel electrophoresis of the fragment was run for about 30 min at 100 V/ 0.1 A, the DNA band was detected under UV light.

Table 16 Reaction mixtures for PCR (total volume 25 µl)

Reagent	Volume
H2O	8.5 µl
1 X Red Taq Mixture	12.5 µl
Colony	-
Primer Mix	4 µl

Table 17 Features of PCR

Effect / Reaction	Temperature	Time	Cycles
Denaturation	94°C	2 min	-
Amplification	94°C - 58°C - 72°C	30 s – 40 s – 50 s	25
Melting Curve	72°C	5 min	-
Cooling	4°C	-	-

2.2.2.6 Sequencing

The selected colonies were cultured in liquid LB medium overnight at 37°C with shaking at 200 rpm. On the next day, the plasmid was extracted by Plasmid Mini Kit. The EZ seq service of Macrogen Europe (Netherlands) assisted in the sequencing of interesting genes. Each reaction mixture contained 200 - 500 ng plasmid and 5 µl primer (10 mM).

2.2.2.7 Micro-injection

For each injection, 100 to 200 embryos were collected 30 - 60 min after egg laying. After dechorionation, embryos were ordered on a fresh apple juice agar plate. The posterior poles of the embryos were arranged to point toward the same direction and

in the same dorsal-ventral orientation. 10 µl heptane glue was brushed on the coverslip. After evaporation of heptane, embryos were gently transferred to the coverslip and stuck to the glue stripe. To reduce the internal pressure of embryos, the cover slide was put in a dry chamber for about 5 min (humidity < 10%). Then about 50 µl 10S Voltalef oil was covered on the embryos to prevent dehydration.

The injection equipment of Eppendorf Femtojet (Eppendorf, Germany) was used to inject embryos. The needles of microinjection were made of borosilicate glass capillaries (Kwik-fill MIB 100-4) (World Precision Instrument, Inc. USA) and were pulled on a KE Puller (Helmut Saur Laborbedarf, Germany) manually. The ideal needle should have some features including a short taper, a thin tip with no discontinuity or step. The needles were filled with 4 µl plasmid using an Eppendorf GELoader tip (Eppendorf, Germany). The needle tip was opened by carefully and repeatedly hitting the slide.

The injection was observed under bright field optics (20 X objective). The needle tip was gently inserted into the posterior fifth of the embryo close to the germline nuclei. A drop of the mixture solution was injected into embryos by pushing the pressure button. If the injection was successful, a small cloud of dye or turbidity was detected in the embryos.

After injection, embryos were kept at room temperature (25°C) until they became adults, called G0 adults. They were collected and separated by sex. Each G0 male was crossed with 3 virgin females and each G0 female (virgin) was crossed with 2 males.

2.2.3 Immunofluorescence of embryos

2.2.3.1 Collection and dechorionation of embryos

3 - 5 days old female and male flies were used to set up the cage with an attached apple juice plate with a small amount of fresh yeast. Apple juice plates were changed every day. After 3 days, flies had adapted to life in a cage and could produce enough eggs. To collect enough embryos of stages 15 - 16, the new apple juice plate was

changed before collection after about 16 h.

To dechorionated embryos, they were gently transferred to a wire mesh basket from the apple juice plate by a soft short brush. Embryos were rinsed in tap water to remove yeast. Eggs were soaked in 3% sodium hypochlorite solution for about 3 min at room temperature. After dechorionation, embryos become transparent and floated on the surface of the solution. Embryos were rinsed in tap water several times. These embryos may easily dehydrate, so they should be fixed immediately.

2.2.3.2 Formaldehyde-Based fixation procedures

For preparation of the fixative buffer, 750 µl heptane and 750 µl 3.7% formaldehyde were mixed in a 1.5 ml Eppendorf tube. The solution was shaken vigorously for about 30 s. Embryos were gently transferred to this fixative buffer with a paint brush. Embryos were incubated at room temperature for 30 min with gently shaking. Embryos localized between the formaldehyde and the heptane phase. The formaldehyde solution in the lower layer was removed and 750 µl of methanol was added. The mixture solution was vigorously shaken for 15 s. Embryos stayed at in the methanol phase and sank to the bottom of the Eppendorf tube. Heptane was removed from the upper solution and 750 µl of methanol was added. Embryos were washed using methanol three times to remove heptane thoroughly. Embryos can be stored in methanol at −20°C for months.

2.2.3.3 Heat-Methanol fixation

20 ml salt solution (0.4% NaCl, 0.003% Triton X-100) was added into a 100 ml beaker and heated to boiling in the microwave. A wire mesh basket with embryos was put to the boiling solution and incubated for 10 s. Then, embryos were quickly put into cold salt solution for 10 s. Embryos were transferred to mixture solution with 750 µl of methanol and 750 µl of heptane. This solution was quickly shaken for 15 s. Embryos fell to the bottom of the Eppendorf tube. The mixture solution was removed and the embryos were washed using methanol three times.

2.2.3.4 Staining

After fixation, embryos were washed with 1 ml PBST for 10 min at room temperature,

wash was repeated three times. Then 1000 µl PBST containing 5% BSA was used to block unspecific antibody binding sites for 60 min at room temperature. The primary antibody was diluted to a suitable concentration by blocking buffer. Embryos were incubated in the primary antibody overnight at 4°C. On the next day, the primary antibody solution was removed, and embryos were washed with 1ml PBST for 10 min at room temperature, this was repeated three times. The secondary antibody was prepared using the blocking buffer. 500 µl of the secondary antibody solution was added to the embryos and incubated for 60 min at room temperature with shaking. Embryos were washed again using PBST for 10 min at room temperature, this was repeated three times. Mowiol was dropped on the slide. Then embryos were transferred into the Mowiol of the slide by a trimmed yellow pipet. After embryos were mixed with Mowiol, a coverslip was put onto the sample.

After solidification of Mowiol, embryos were observed by confocal microscopy. The primary and secondary antibodies are listed in table 18.

Table 18 List of antibodies

Antigen	Host species	Company	Dilution
Anti-OATP1B1	rabbit	Thermo Fisher Scientific (MA3-934)	1:500
Anti-OATP2B1	rabbit	abcam (ab222094)	1:500
Anti-OATP1B3	rabbit	Sigma-Aldrich (HPA004943)	1:500
Polyclonal hOATP1B3 antiserum SKT	rabbit	Peptide Specialty Laboratories, Heidelberg (Konig et al., 2000)	1:500
Anti-ABCB1	mouse	Sigma-Aldrich (C219)	1:50
Anti-ABCB1	rabbit	Sigma-Aldrich (HPA002199)	1:100
Anti-**rabbit IgG, Alexa Fluor 568** conjugated	goat	Invitrogen (A-11011)	1:500
Anti-mouse IgG, Alexa Fluor 568 conjugated	goat	Invitrogen (A-11004)	1:500

2.2.4 Recombination

In the following, I used the recombination of the UAS-hOATP1B1 insertion with the UAS-CD8-FRP insertion as an example to explain the process of recombination. The other recombination of this project was performed following the same scheme.

At first, hOATP1B1 transgenic virgins (UAS-hOATP1B1) were crossed with UAS-CD8-RFP males; this cross was called G0. In the next generation, appropriate virgins were

crossed with R24, a chromosome 3 balance stock by w; TM3, Ser, Sb, e / TM6, Tb, e, as males; this cross was called G1. G1 virgins had one chromosome with UAS-hOATP1B1, and one with UAS-CD8-RFP. In the G1 female gametes, these chromosomes may recombine during meiosis generating chromosomes with UAS-hOATP1B1 and UAS-CD8-RFP. To select files containing the chromosome of recombination, 20 single males were crossed with each three R24 (virgins) in the next generation called G2. After these flies were mated, 20 males were tested by PCR for the presence of both insertions. This is the case if the PCR results showed two bands, one with the size of *hOATP1B1,* another with the size of *RFP*. The schema of the procedure of the recombination crosses is shown in Fig. 7.

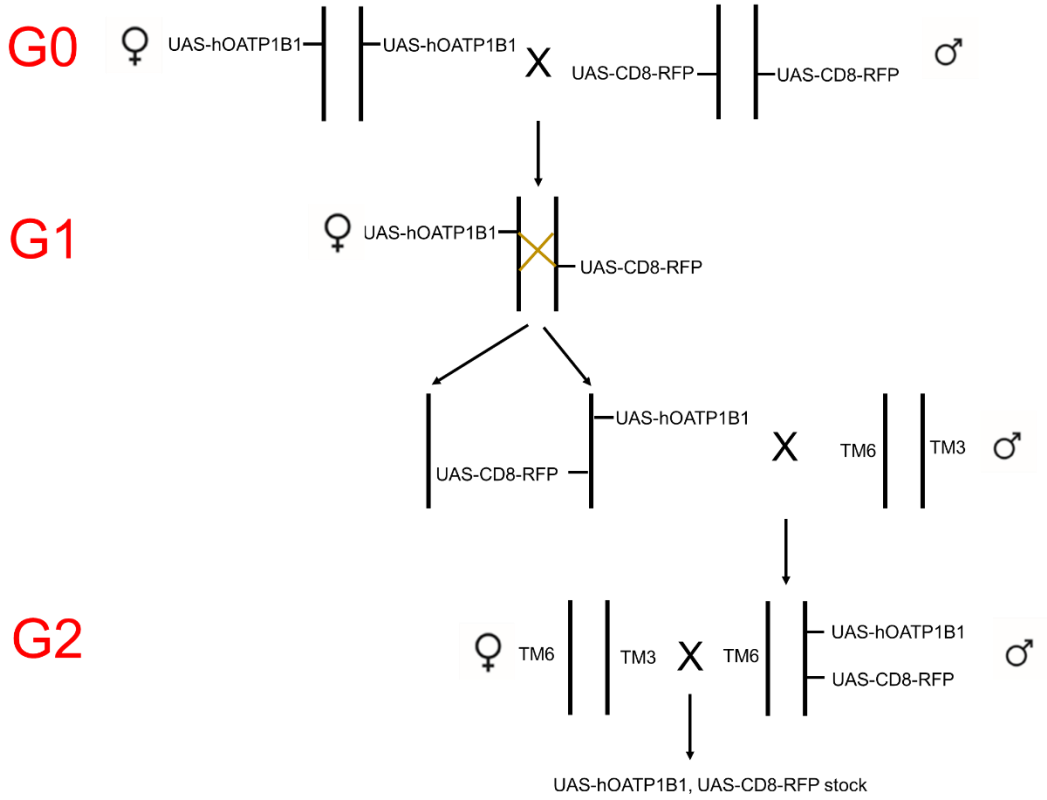

Figure 7. Scheme of the procedure of the recombination between UAS-CD8-RFP and UAS-hOATP1B1.

2.2.5 Extraction of single fly genomic DNA

2 µl Proteinase K (20 mg/ml) was added into 200 ml of squishing buffer. Single fly was

put into the 1.5 ml Eppendorf tube with 200 ml squishing buffer. They were crushed using the tip of a pipette and incubated at room temperature for 30 min. They were heat-shocked at 95°C for 3 min. the Eppendorf tubes were centrifuged at 10000 rpm for 5 min. Supernatants were kept containing genomic DNA.

2.2.6 Injection of fluorescent substrate

The injection of fluorescent substrates is very similar to the plasmid micro-injection experiments. However, some differences should be noticed. For injection of fluorescent substrates, collected embryos were at stages 15 - 16. After dechorionation, embryos were lined on a fresh apple juice agar plate, anterior to posterior, and one lateral side facing up. Injected liquid produced a bead with a diameter of about 20 - 25 µm. After injection, embryos were kept in the dark at room temperature for about 4 - 5 h. Then embryos were observed by confocal microscopy.

2.2.7 Transcription analyses by quantitative real-time polymerase chain reaction (qRT-PCR)

2.2.7.1 RNA extraction

In this project, when the embryos were used as samples, about 50 - 70 embryos at the stages 15 - 16 were collected as one sample. If the larvae were used as samples, about 20 - 30 larvae at the first instar were collected as one sample. In every experiment, three samples were collected from different plates. Total RNA was isolated according to the guide of RNeasy Kit. RNA was stored at -70°C until used for reverse transcription into cDNA.

2.2.7.2 Reverse transcription of RNA into cDNA

The concentration of each RNA extract was measured in the spectrophotometer (Nanodrop) at a wavelength of 260 nm. The formula $V_{RNA} = 500\ ng / C_{RNA}^{ng/µl}$ (V_{RNA} means RNA volume, C_{RNA} means RNA concentration) was used to calculate V_{RNA}. Depending on the V_{RNA}, DEPC water was added to bring the total volume to 10.5 µl as the RNA solution for cDNA synthesis.

According to the instructions of the cDNA Synthesis kit (Roche Switzerland), the reaction mixture solution needs to be prepared as shown in table 19. 10.5 µl RNA solution was added into the 9.5 µl reaction mixture solution and mixed. The reaction was incubated at 37°C for 1h for cDNA synthesis. The cDNA was stored at -20°C.

Table 19 Reagents of the reaction mixture solution for cDNA synthesis

Reagent	**Volume**
10X buffer	2 µl
RNase inhibitor	2.5 µl
dNTP mix	2 µl
Reverse transcriptase	1 µl
Oligo dT primer (10 µM)	2 µl

2.2.7.3 qRT-PCR

The SYBR Green Kit was used for qRT-PCR experiments. 2 µl of mixed primers were added to 13 µl of Master BYBR Green solution as reaction mixture solution. cDNA was diluted to 125 ng/µl. Then, 5 µl cDNA was added to the reaction mixture solution as a sample for qRT-PCR. The *RpS20* gene of the fly was used as a reference gene. The qRT-PCR program of the Light Cycler Nano machine is described in table 20.

Table 20 Features of qRT-PCR

Program	Temperature	Time	Cycles
Hold	95°C	10 min	1
Amplification	95°C - 60°C - 72°C	20s – 20s – 20s	45
Melting	65°C - 95°C	60s – 1s	1

2.2.8 Feeding oatp RNAi larvae with MDBF

2.2.8.1 Recipe of fly and larvae food

ddH_2O was mixed with dry yeast to generate fresh yeast for flies. 75 mg MDBF powder was dissolved in 10 ml ddH_2O to generate the MDBF solution of a concentration of 10 mM. The MDBF solution was mixed with dry yeast to generate experimental food for larvae.

2.2.8.2 Feed flies and larvae for experimental food and observe accumulation of MDBF in oatp RNAi larvae

3 - 5 days old female and male flies were used to set up the cage on apple juice plates with a small amount of fresh yeast and kept at 25˚C. Apple juice plates were changed every day. After 3 days, flies had adapted to life in a cage and could produce enough eggs. To ensure all larvae were at the same development stages 17 (after tracheae gas filling) embryos were collected. After embryos hatched, they were transferred into new apple juice plates with a small amount of experimental food. After larvae were fed 14 h, they were transferred onto the slide to detected accumulation of MDBF under the fluorescence microscope.

2.2.9 The drug test for human OCT1 transgenic flies

2.2.9.1 Recipe of fly food

7 mg cisplatin powder was dissolved in 7 ml sterile saline (0.9% NaCl) to generate the cisplatin solution of a concentration of 1 mg/ml. The lower concentration cimetidine mixture solution containing 1 mg/ml of cisplatin and 20 mg/ml cimetidine was prepared. The higher concentration cimetidine mixture solution containing 1 mg/ml of cisplatin and 100 mg/ml cimetidine was prepared. Similarly, the lower concentration metformin mixture solution containing 1 mg/ml of cisplatin and 20 mg/ml metformin was prepared. The higher concentration metformin mixture solution containing 1 mg/ml of cisplatin and 100 mg/ml metformin was prepared. These five drugs containing mixture solutions were mixed with dry yeast to generate experimental food.

2.2.9.2 Feed flies for experimental food and test hatchability of embryos

40 adult female and 20 male flies, 3 - 5 days old, were kept at 25˚C in egg-laying cages on apple juice plates for 7 days. A small drop of yeast was placed with drugs on the plates. Plates were changed every day. After the flies were fed with yeast containing drugs for 24 h, 50 embryos were collected from apple plates and numbers of hatching embryos were recorded for 6 days. Moreover, the pupal rate and fly eclosion rate of the eggs hatched were recorded in the first three days.

3. Results

3.1 Expression and function of hOATP1B1, hOATP2B1, and hOATP1B3 in fly embryos

3.1.1 Induction of hOATP1B1, hOATP2B1, and hOATP1B3 expression in transgenic embryos was measured by RT-qPCR

To test successful introduction of *hOATP1B1*, *hOATP2B1*, and *hOATP1B3* into flies, their transcription levels were verified by qPCR. Stage 16 - 17 embryos expressing these genes in the salivary glands (fkh-GAL4, UAS-hOATP1B1*,* fkh-GAL4, UAS-hOATP2B1*,* fkh-GAL4, UAS-hOATP1B3) were prepared for qPCR. The expression levels of *hOATP1B1*, *hOATP2B1*, and *hOATP1B3* were significantly higher in *hOATP1B1, hOATP2B1*, and *hOATP1B3* transgenic embryos than their background levels in wild-type Dijon embryos (Fig. 8). These results indicated that the human genes *hOATP1B1*, *hOATP2B1*, and *hOATP1B3* have been successfully transferred into and expressed in *D. melanogaster*.

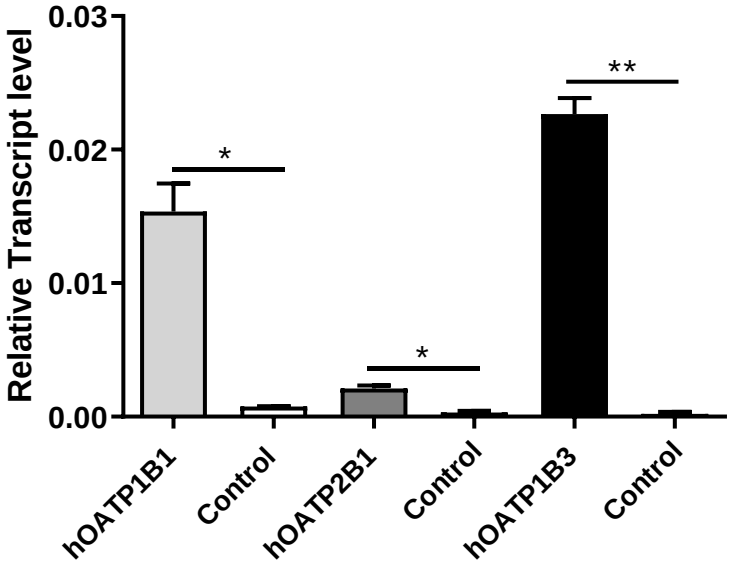

Figure 8. Gene transcription levels were measured in “humanized” embryos by qRT-PCR. Compared to the wild-type Dijon embryos, expression of *hOATP1B1*, *hOATP2B1*, and

hOATP1B3 genes in respective embryos (fkh-GAL4, UAS-hOATP1B1, fkh-GAL4, UAS-hOATP2B1, fkh-GAL4, UAS-hOATP1B3) was significantly higher (* $p < 0.05$, ** $p < 0.01$) than in control embryos. Data shown are mean ±SEM and represent two independent experiments.

3.1.2 hOATP1B1 localization by antibody staining in embryos

To verify the localization and distribution of hOATP1B1 in the "humanized" hOATP1B1 embryos, an antibody directed against hOATP1B1 (anti-hOATP1B1) was used to detect the transporter in embryos expressing hOATP1B1 in different tissues (UAS-hOATP1B1 driven by fkh-GAL4, bo-GAL4, or btl-GAL4). Stage 16 - 17 embryos were used for immunofluorescence. Embryos were fixed with formaldehyde (3.7%) or heat treatment for staining, and then observed by confocal microscopy. We engineered the "humanized" hOATP1B1 expressing flies to also express RFP in the same tissue in embryos in order to identify the tissue by the red fluorescent signal (see Materials & Methods 2.2.4).

Immunofluorescence localization of human hOATP1B1 was unsuccessful in the salivary glands of embryos expressing hOATP1B1 in the salivary glands (fkh-GAL4, UAS-hOATP1B1) fixed with formaldehyde or by heat treatment (Fig. 9 A1, A4). As a negative control, in wild-type Dijon embryos incubated with the anti-hOATP1B1 antibody no signal was detected (Fig. 9 A2, A5). A localization of hOATP1B1 in the membrane of oenocytes cells was identified in respective embryos (bo-GAL4, UAS-hOATP1B1) only when they were fixed with formaldehyde (Fig. 9 B1) but not by heat treatment (Fig. 9 B4). No signal was detected after anti-hOATP1B1 staining in wild-type Dijon embryos fixed with formaldehyde or by heat treatment (Fig. 9 B2, B5). A positive signal was found in the tracheae of respective embryos (btl-GAL4, UAS-hOATP1B1) fixed with formaldehyde or by heat treatment (Fig. 9 C1, C4). However, a signal was also detected in the tracheae of wild-type Dijon embryos (Fig. 9 C2, C5). In principle, because of immunofluorescence localization in oenocytes of respective embryos fixed with formaldehyde, I concluded that the anti-hOATP1B1 antibody successfully recognized the transporter expressed in fruit fly embryos. Further

experiments are needed to explore why hOATP1B1 expressed in the salivary glands cannot be detected by this antibody.

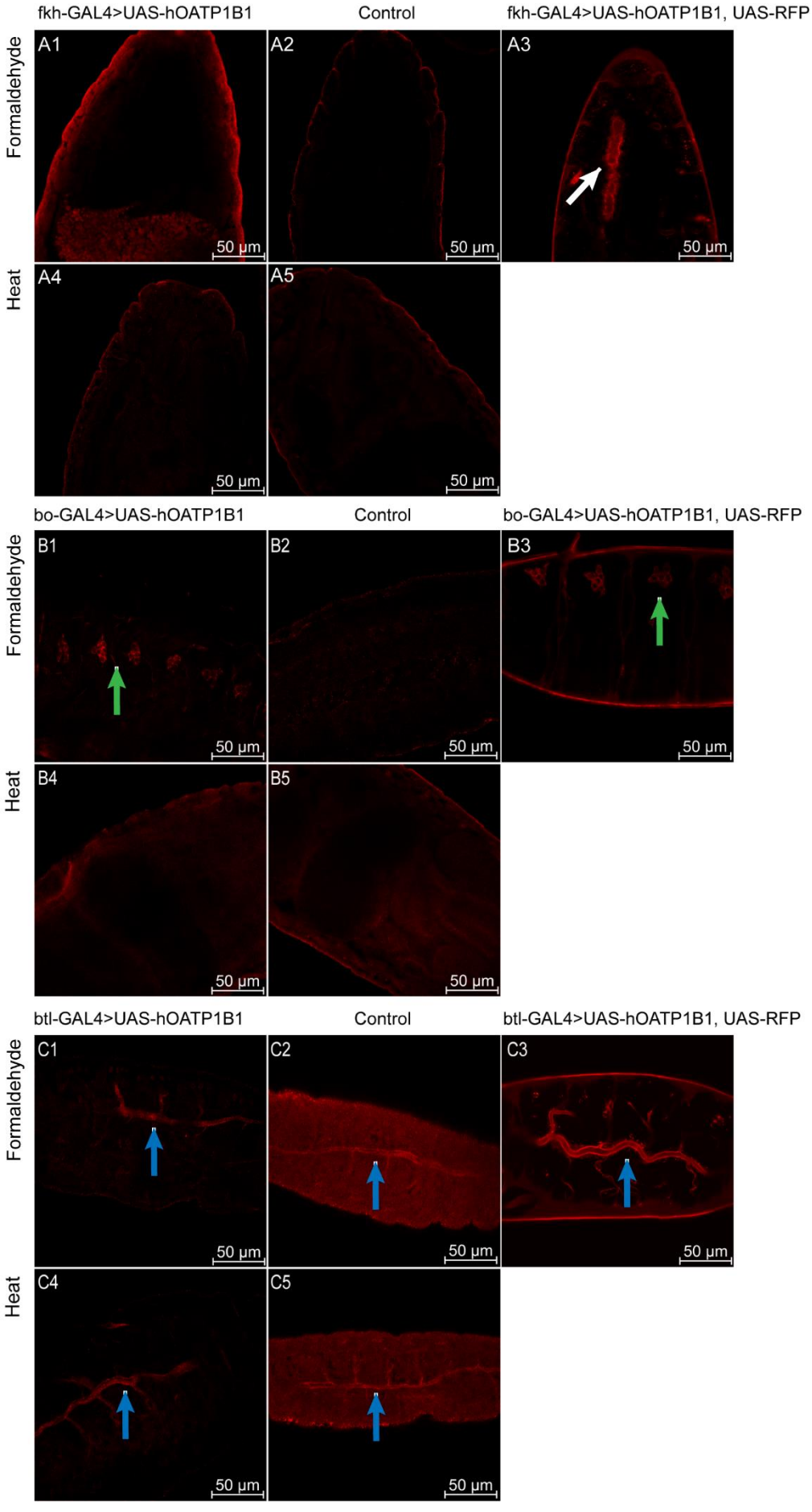
fkh-GAL4>UAS-hOATP1B1
Control
fkh-GAL4>UAS-hOATP1B1, UAS-RFP
Formaldehyde
Heat
A1
A2
A3
A4
A5
50 µm
bo-GAL4>UAS-hOATP1B1
Control
bo-GAL4>UAS-hOATP1B1, UAS-RFP
B1
B2
B3
B4
B5
btl-GAL4>UAS-hOATP1B1
Control
btl-GAL4>UAS-hOATP1B1, UAS-RFP
C1
C2
C3
C4
C5

Figure 9. Localization of hOATP1B1 protein in *D. melanogaster* embryos. After formaldehyde and heat fixation, hOATP1B1 was not detected by antibody staining in the salivary glands of stage 16 embryos that expressed hOATP1B1 under the control of a salivary gland-specific GAL4 driver (fkh-GAL4; UAS-hOATP1B1; A1, A4). The staining of wild-type Dijon embryos is shown as the negative control (A2, A5). After formaldehyde fixation and staining with the anti-hOATP1B1 antibody, a signal was observed in the oenocytes of respective embryos (bo-GAL4; UAS-hOATP1B1; B1). No signal was detected after heat fixation (B4). Wild-type Dijon embryos were used as a negative control for hOATP1B1 antibody staining (B2, B5). The hOATP1B1 protein was localized in the tracheae of btl-GAL4; UAS-hOATP1B1 and wild-type Dijon embryos after formaldehyde or heat fixation (C1, C4, C2, C5). Targeted expression of RFP in the salivary glands, oenocytes, and tracheae allowed identifying this tissue by fluorescence microscopy (A3, B3, C3). The salivary glands, oenocytes, and tracheae are indicated by a white arrow, green arrow, and blue arrow, respectively. Scale bar = 50 µm.

3.1.3 hOATP2B1 localization by immuno-detection in embryos

To verify the localization and distribution of hOATP2B1 in hOATP2B1 transgenic embryos, an antibody directed against hOATP2B1 (anti-hOATP2B1) was applied to detect the transporter in embryos expressing hOATP2B1 in different tissues (UAS-hOATP2B1 driven by fkh-GAL4, bo-GAL4, or btl-GAL4). For immune-detection, stage 16 - 17 embryos were fixed with formaldehyde (3.7%) or heat treatment, and subsequently observed by confocal microscopy. We recombined the hOATP2B1 insertion with UAS-CD8-RFPnls, so that the target tissue could be easily detected by its red fluorescence (see Materials & Methods 2.2.4).

Immunofluorescence localization of human hOATP2B1 was observed in the salivary glands of embryos expressing hOATP2B1 (fkh-GAL4, UAS-hOATP2B1) that were fixed with formaldehyde or by heat treatment (Fig. 10 A1, A4). As a negative control, in wild-type Dijon embryos incubated with the anti-hOATP2B1 antibody a signal was only detected by heat treatment (Fig. 10 A2, A5). Thus, fixation by heat treatment did not allow reliable detection. A localization of hOATP2B1 in the membrane of oenocytes

cells was identified in respective embryos (bo-GAL4, UAS-hOATP2B1) when they were fixed by either protocol (Fig. 10 B1, B4). After anti-hOATP2B1 staining, there was no signal observed in wild-type Dijon embryos fixed with formaldehyde or by heat treatment (Fig. 10 B2, B5). The hOATP2B1 protein was found in the tracheae of respective embryos (btl-GAL4, UAS-hOATP2B1; Fig. 10 C1, C4), but was not found in wild-type Dijon embryos (Fig. 10 C2, C5) fixed with formaldehyde or by heat treatment. In general, because of immunofluorescence localization in oenocytes and tracheae of respective embryos fixed with formaldehyde, I considered that the *hOATP2B1* gene was successfully expressed in fruit fly embryos. Further experiments need to be performed to explore the function of hOATP2B1 in these embryos.

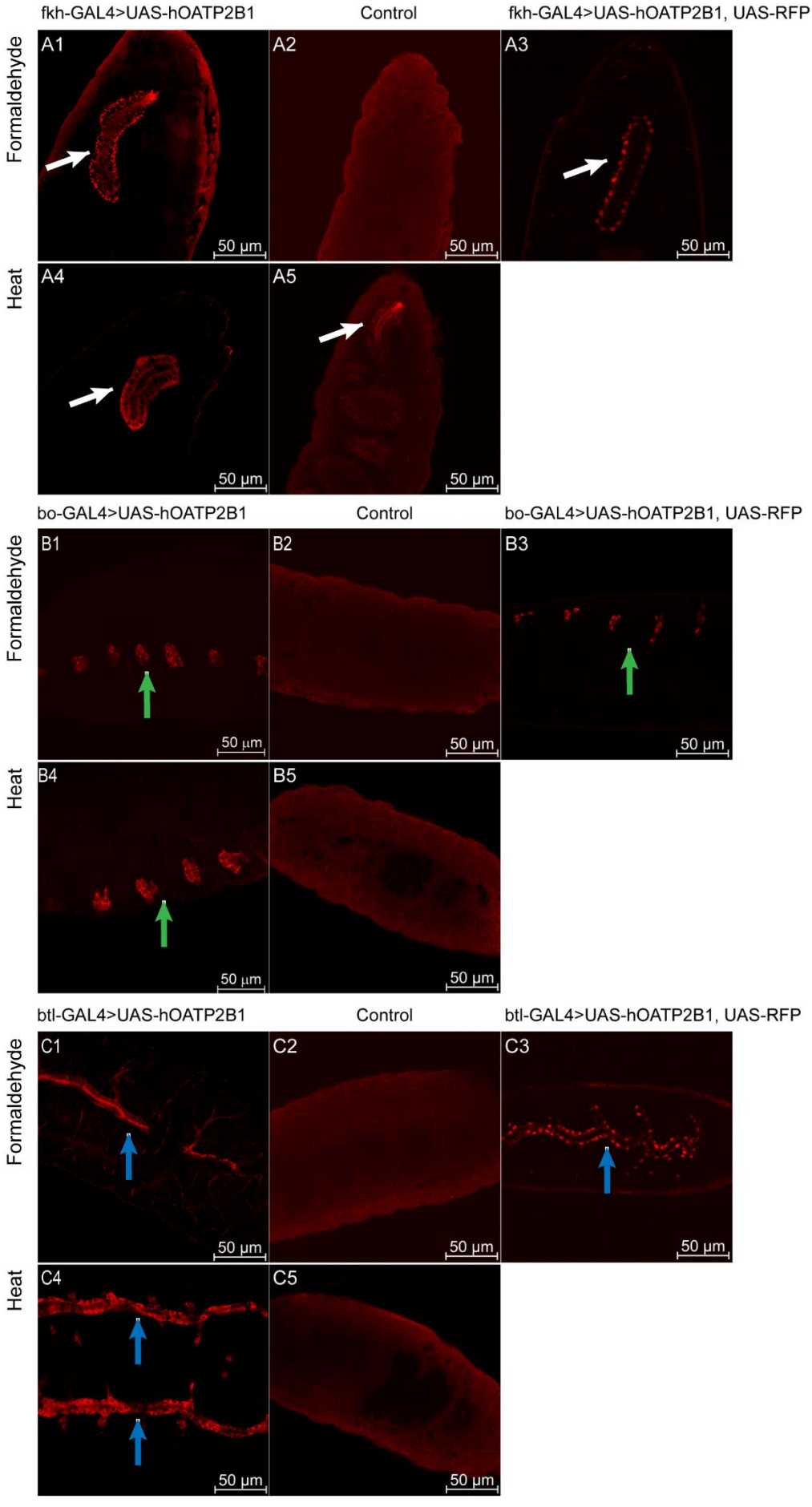
fkh-GAL4>UAS-hOATP2B1
Control
fkh-GAL4>UAS-hOATP2B1, UAS-RFP
Formaldehyde
Heat
A1
A2
A3
A4
A5
bo-GAL4>UAS-hOATP2B1
Control
bo-GAL4>UAS-hOATP2B1, UAS-RFP
B1
B2
B3
B4
B5
btl-GAL4>UAS-hOATP2B1
Control
btl-GAL4>UAS-hOATP2B1, UAS-RFP
C1
C2
C3
C4
C5
50 µm

Figure 10. Localization of hOATP2B1 protein in the *D. melanogaster* embryo**.** After formaldehyde or heat treatment fixation and staining with the anti-hOATP2B1 antibody, a signal was observed in the salivary gland of respective embryos (fkh-GAL4; UAS-hOATP2B1; A1, A4). But the signal was only detected in wild-type Dijon embryos by heat treatment (A2, A5). hOATP2B1 was detected by antibody staining in the oenocytes and tracheae that express hOATP2B1 under the control of an oenocytes-specific GAL4 driver (bo-GAL4; UAS-hOATP2B1; B1, B4) and tracheae-specific GAL4 driver (btl-GAL4; UAS-hOATP2B1; C1, C4) and fixed with formaldehyde or by heat fixation. The staining of wild-type Dijon embryos is shown as the negative control (B2, B5, C2, C5). Targeted expression of RFP in the salivary glands, oenocytes, and tracheae allowed identifying this tissue by fluorescence microscopy (A3, B3, C3). The salivary glands, oenocytes, and tracheae are indicated by a white arrow, green arrow, and blue arrow, respectively. Scale bar = 50 µm.

3.1.4 hOATP1B3 localization by antibody staining in embryos

The hOATP1B3 antibody was used to detect the localization and distribution of hOATP1B3 in different tissues (UAS-hOATP1B3 driven by fkh-GAL4, bo-GAL4, or btl-GAL4) of “humanized” hOATP1B3 embryos. The protocol of staining was the same as for the hOATP1B1 antibody staining. The hOATP1B3 insertion was recombined with the UAS-*RFP* insertion to express RFP in the same tissue in the embryos so that the target tissues could be easily recognized by their red fluorescence (see Materials & Methods 2.2.4).

A signal was detected in the neuronal system of respective embryos (fkh-GAL4, UAS-hOATP1B3; bo-GAL4, UAS-hOATP1B3; btl-GAL4, UAS-hOATP1B3) fixed with formaldehyde or by heat treatment (Fig. 11 A1, A4, B1, B4, C1, C4). Similarly, a signal was also detected in the neuronal system of wild-type Dijon embryos (Fig. 11 A2, A5, B2, B5, C2, C5). Because the hOATP1B3 antibody signal was only detected in the neuronal system, I concluded that the hOATP1B3 antibody did not successfully recognize the transporter expressed in fruit fly embryos. Therefore, I used the SKT hOATP1B3 antibody as an alternative antibody for detection.

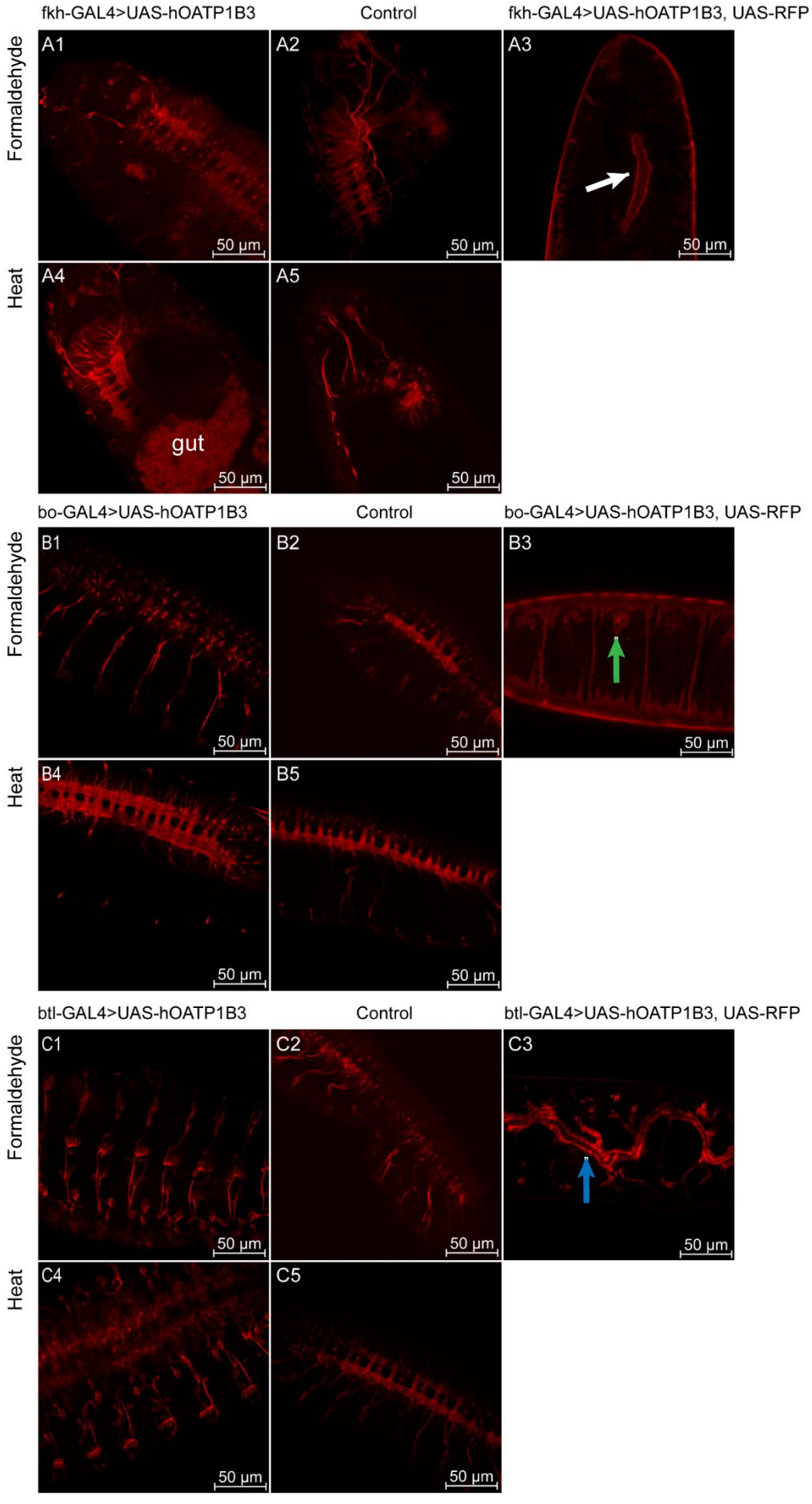
fkh-GAL4>UAS-hOATP1B3
Control
fkh-GAL4>UAS-hOATP1B3, UAS-RFP
Formaldehyde
Heat
A1
A2
A3
A4
A5
gut
50 µm
bo-GAL4>UAS-hOATP1B3
Control
bo-GAL4>UAS-hOATP1B3, UAS-RFP
B1
B2
B3
B4
B5
btl-GAL4>UAS-hOATP1B3
Control
btl-GAL4>UAS-hOATP1B3, UAS-RFP
C1
C2
C3
C4
C5

Figure 11. The hOATP1B3 (OATP1B3, HPA004943, Sigma) antibody did not show localization of the protein in the *D. melanogaster* embryos. The hOATP1B3 was detected by antibody staining in the neuronal system that expresses hOATP1B3 under the control of a salivary gland-specific GAL4 driver (fkh-GAL4; UAS-hOATP1B3; A1, A4), oenocytes-specific GAL4 driver (bo-GAL4; UAS-hOATP1B3; B1, B4), and tracheae-specific GAL4 driver (btl-GAL4; UAS-HOATP1B3; C1, C4), and fixed with formaldehyde or by heat fixation. The staining of wild-type Dijon embryos was also observed signal in the neuron system (A2, A5, B2, B5, C2, C5). Targeted expression of RFP in the salivary glands, oenocytes, and tracheae allowed identifying this tissue by fluorescence microscopy (A3, B3, C3). The salivary glands, oenocytes, and tracheae are indicated by a white arrow, green arrow, and blue arrow, respectively. Scale bar = 50 µm.

Immunofluorescence staining was observed in the salivary glands and tracheae of respective embryos (fkh-GAL4, UAS-hOATP1B3; btl-GAL4, UAS-hOATP1B3) fixed with formaldehyde or by heat treatment (Fig. 12 A1, A4, C1, C4). In the negative control, wild-type Dijon embryos incubated with the anti-hOATP1B3 SKT antibody, a signal was detected in the salivary glands and tracheae (Fig. 12 A2, A5, C2, C5). The hOATP1B3 protein was not found in the oenocytes of respective embryos (bo-GAL4, UAS-hOATP1B3; Fig. 12 B1, B4); a signal was absent in wild-type Dijon embryos (Fig. 12 B2, B5) fixed with formaldehyde or by heat treatment. According to these results, I concluded that both hOATP1B3 antibodies were unspecific. Therefore, I generated flies expressing hOATP1B3 fused to RFP in order to detect hOATP1B3 protein in embryos in the next step (see Result 3.1.5).

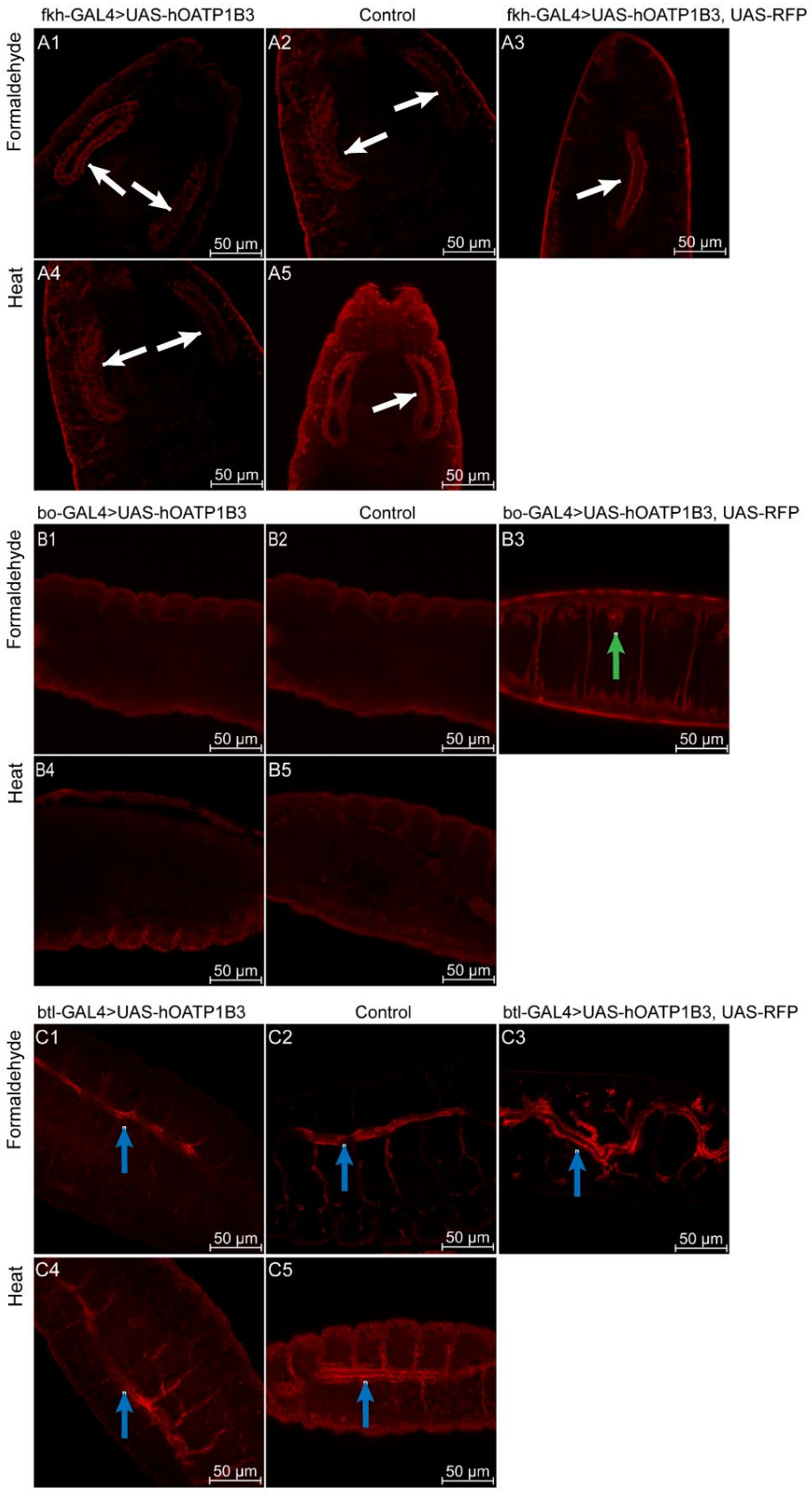
fkh-GAL4>UAS-hOATP1B3
Control
fkh-GAL4>UAS-hOATP1B3, UAS-RFP
Formaldehyde
Heat
A1
A2
A3
A4
A5
bo-GAL4>UAS-hOATP1B3
Control
bo-GAL4>UAS-hOATP1B3, UAS-RFP
B1
B2
B3
B4
B5
btl-GAL4>UAS-hOATP1B3
Control
btl-GAL4>UAS-hOATP1B3, UAS-RFP
C1
C2
C3
C4
C5
50 µm

Figure 12. Immunodetection of hOATP1B3 (SKT antiserum, OATP1B3) did not show localization of the protein in the *D. melanogaster* embryos. After formaldehyde or heat treatment fixation and staining with the anti-hOATP1B3 antibody, a signal was observed in the salivary glands and tracheae of respective embryos (fkh-GAL4; UAS-hOATP1B3; A1, A4; btl-GAL4; UAS-hOATP1B3; C1, C4), but the signal was also detected in wild-type Dijon embryos (A2, A5, C2, C5). No signal was detected after anti-hOATP1B3 staining in the oenocytes of embryos in hOATP1B3-flies (bo-GAL4; UAS-hOATP1B3; B1, B4) or in wild-type Dijon embryos (B2, B5) fixed with formaldehyde or by heat treatment. Targeted expression of RFP allowed identifying these tissues by fluorescence microscopy (A3, B3, C3). The salivary glands, oenocytes, and tracheae are indicated by a white arrow, green arrow, and blue arrow, respectively. Scale bar = 50 µm.

3.1.5 Distribution of hOATP1B1-, hOATP2B1-, and hOATP1B3-RFP in embryos and larvae

3.1.5.1 hOATP1B1-, hOATP2B1-, and hOATP1B3-RFP in the salivary glands

As the detection of hOATP1B1 and hOATP1B3 in the salivary glands of embryos expressing the respective genes was unsuccessful, I decided to generate flies expressing the hOATP1B1, hOATP2B1, or hOATP1B3 transporters fused to the red fluorescence protein RFP for tissue- and cell-specific localization. Therefore, I generated transgenic fly lines harboring UAS-transposons with the coding sequences of hOATP1B1, hOATP2B1, or hOATP1B3 fused to the coding sequence of RFP to further assess the distribution of human transporters in embryos and larvae (see Materials & Methods 2.2.2). Stage 17 embryos and first instar larvae were used for microscopic observation (Fig. 13 A1, A3, B1, B3, C1, C3, D1, D3). No signal was observed in the salivary glands of embryos expressing the hOATP1B1-, hOATP2B1-, or hOATP1B3-RFP fusion protein in the salivary glands (fkh-GAL4, UAS-hOATP1B1-RFP; fkh-GAL4, UAS-hOATP2B1-RFP; fkh-GAL4, UAS-hOATP1B3-RFP) (Fig. 13 B2, C2, D2). As a control, CD8-RFP (fkh-GAL4, UAS-CD8-RFP) was detected in salivary glands of embryos (Fig. 13 A2). Unexpectedly, the hOATP1B1-, hOATP2B1-, or

hOATP1B3-RFP fusion protein was found in the nervous system, the heart, and the anal pads of respective larvae (fkh-GAL4, UAS-hOATP1B1-RFP; fkh-GAL4, UAS-hOATP2B1-RFP; fkh-GAL4, UAS-hOATP1B3-RFP) (Fig. 13 B4, C4, D4). RFP was only detected in the salivary glands of control embryos (fkh-GAL4, UAS-CD8-RFP) (Fig. 13 A4).

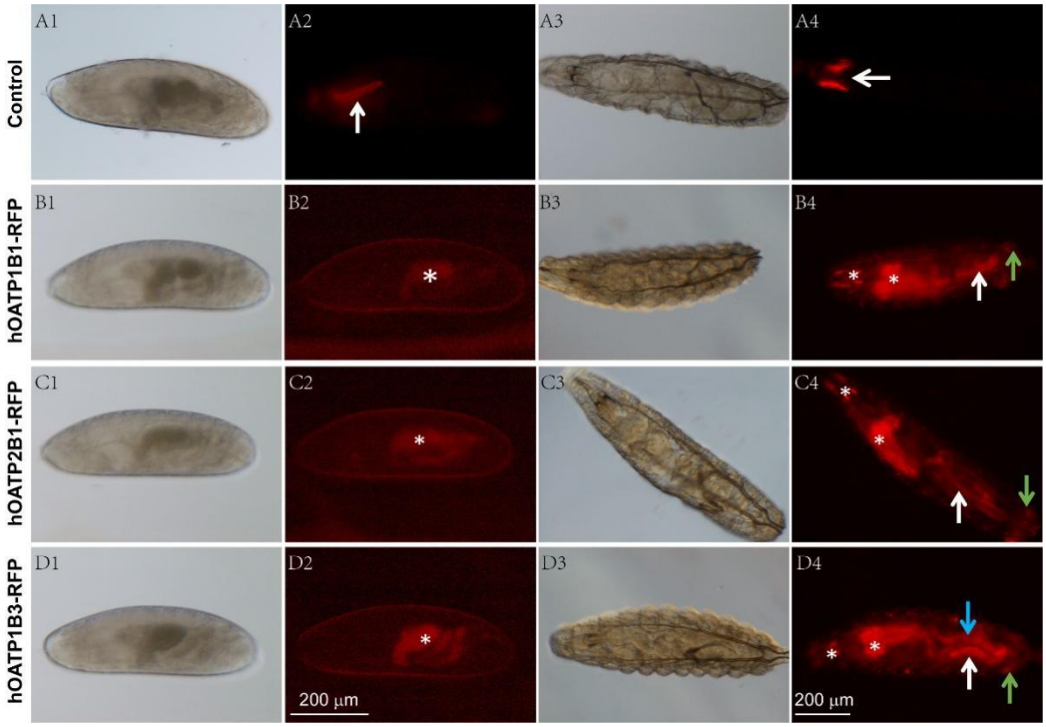

Figure 13. The hOATP1B1, hOATP2B1, and hOATP1B3 RFP fusion proteins were not detected in the salivary glands of *D. melanogaster* embryos and larvae. The white light of microscopy was used to observe tissues morphology to identify the stage of embryos and larvae (A1, A3, B1, B3, C1, C3, D1, D3). No signal was observed in the salivary glands of respective embryos (fkh-GAL4, UAS-hOATP1B1-RFP; fkh-GAL4, UAS-hOATP2B1-RFP; fkh-GAL4, UAS-hOATP1B3-RFP; B2, C2, D2). The RFP signal was detected in control embryos (fkh-GAL4, UAS-CD8-RFP; A2). The white star indicates the position of the gut, which showed autofluorescence (B2, C2, D2). The exposure time for hOATP1B1, hOATP2B1, or hOATP1B3-RFP detection was 3 s, and 600 ms for RFP detection in control embryos. The hOATP1B1, hOATP2B1, or hOATP1B3-RFP fusion protein was not detected in the salivary glands, but in

the nervous system, the heart, and the anal pads of first stage larvae (fkh-GAL4, UAS-hOATP1B1-RFP; fkh-GAL4, UAS-hOATP2B1-RFP; fkh-GAL4, UAS-hOATP1B3-RFP; B4, C4, D4). In control larvae (fkh-GAL4, UAS-CD8-RFP; A4), a signal was detected in the salivary glands. The white arrow indicates the location of the salivary glands (A2, A4). The white star, white arrow, green arrow, and blue arrow indicate the positions of the neuronal system, heart, anal pads, and gut (B4, C4, D4), respectively. The exposure time for hOATP1B1, hOATP2B1, or hOATP1B3-RFP detection was 6 s and 400 ms for the detection in control animals. Scale bar = 200 µm.

3.1.5.2 hOATP1B1-, hOATP2B1-, and hOATP1B3-RFP in the tracheal system

Lack of signal in the salivary glands of embryos and larvae expressing the hOATP1B1-, hOATP2B1-, or hOATP1B3-RFP fusion protein may be a tissue-specific problem. To test this hypothesis, I tried to detect the hOATP1B1-, hOATP2B1-, or hOATP1B3-RFP signal in the tracheae of embryos and larvae using the tracheae-specific GAL4 driver btl-GAL4 to induce expression. The position of the tracheae of stage 17 embryos and first stage larvae was identified by bright-field microscopy (Fig. 14 A1, A3, B1, B3, C1, C3, D1, D3). In these experiments, the human hOATP1B1-, hOATP2B1-, and hOATP1B3-RFP proteins were not observed in the tracheae of respective embryos (btl-GAL4, UAS-hOATP1B1-RFP; btl-GAL4, UAS-hOATP2B1-RFP; btl-GAL4, UAS-hOATP1B3-RFP) (Fig. 14 B2, C2, D2). As a control, CD8-RFP (btl-GAL4, UAS-CD8-RFP) was detected in the tracheae of embryos (Fig. 14 A2). The hOATP1B1-, hOATP2B1-, or hOATP1B3-RFP fusion proteins were observed in the nervous system, the heart, and the anal pads of respective larvae (btl-GAL4, UAS-hOATP1B1-RFP; btl-GAL4, UAS-hOATP2B1-RFP; btl-GAL4, UAS-hOATP1B3-RFP) (Fig. 14 B4, C4, D4), but not in the tracheae. In control embryos (btl-GAL4, UAS-CD8-RFP), the tracheal expression of CD8-RFP was observed (Fig. 14 A4).

These results suggested that like their RFP-tagged versions, hOATP1B1, hOATP2B1, and hOATP1B3 did not localize to the salivary glands of respective embryos. These results confirmed the lack of immunodetection of these transporters in the salivary glands in my initial antibody staining experiments.

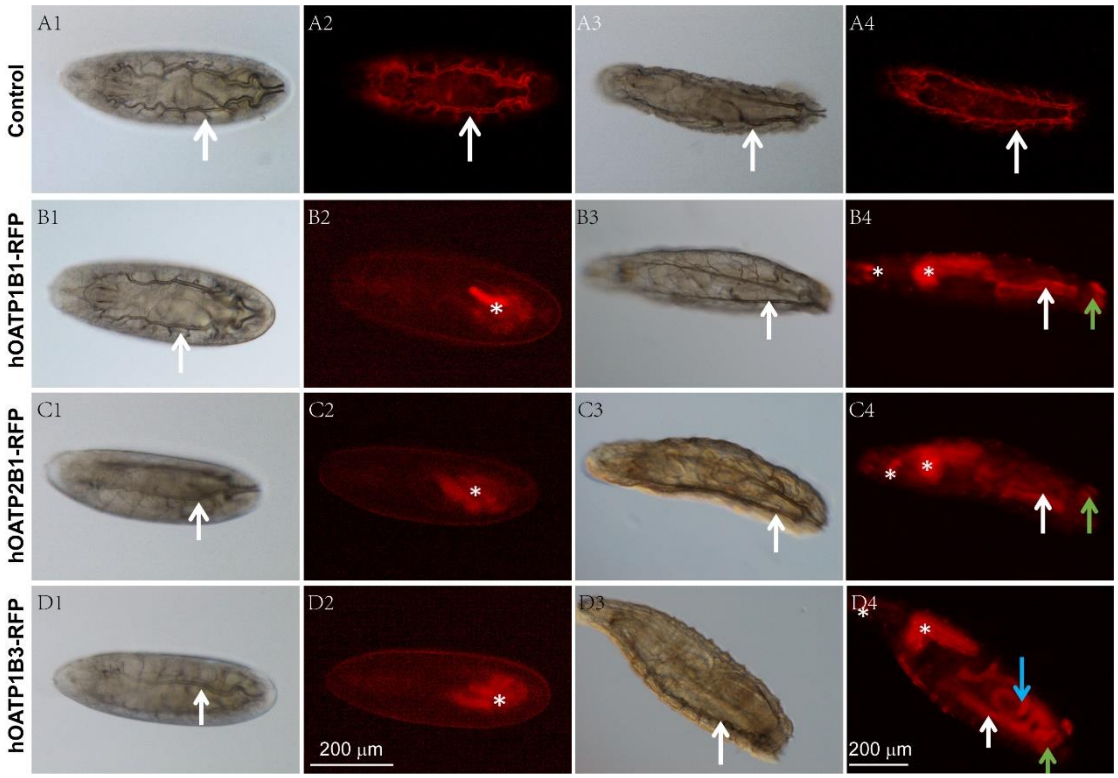

Figure 14. The hOATP1B1-, hOATP2B1-, or hOATP1B3-RFP fusion protein was not found in the tracheae of *D. melanogaster* embryos and larvae. The white arrow indicates the position of the tracheae in embryos and larvae by bright-field microscopy (A1, A3, B1, B3, C1, C3, D1, D3). The hOATP1B1-, hOATP2B1-, or hOATP1B3-RFP proteins were not detected in the tracheal system when expressed under the control of a tracheae-specific GAL4 driver (btl-GAL4, UAS-hOATP1B1-RFP; btl-GAL4, UAS-hOATP2B1-RFP; btl-GAL4, UAS-hOATP1B3-RFP; B2, C2, D2). The white star indicates the position of the gut, which shows autofluorescence. In control embryos (btl-GAL4, UAS-CD8-RFP) a red signal was observed in the tracheae, indicated by a white arrow (A2). Exposure time was 3 s for hOATP1B1-, hOATP2B1-, or hOATP1B3-RFP detection, and 600 ms detection of CD8-RFP in control embryos. In the control larvae (btl-GAL4, UAS-CD8-RFP), the white arrow points to tracheal expression (A4). Some signal was detected in the nervous system, the heart, the anal pads, and the gut of larvae expressing hOATP1B1-, hOATP2B1-, or hOATP1B3-RFP, indicated by a white star, white arrow, green arrow, and blue arrow, respectively (btl-GAL4, UAS-hOATP1B1-RFP; btl-GAL4, UAS-hOATP2B1-RFP; btl-GAL4, UAS-hOATP1B3-RFP; B4, C4, D4). The exposure time was 6 s for hOATP1B1-, hOATP2B1-, or hOATP1B3-RFP, and 400

ms for the CD8-RFP control. Scale bar = 200 µm.

3.1.6 Evaluation of hOATP1B1, hOATP2B1, and hOATP1B3 function by injection of their fluorescent substrates into embryos

3.1.6.1 Fluorescent substrates were taken up into the lumen of salivary glands and tracheae independently of hOATP1B1, hOATP2B1, or hOATP1B3

To investigate the function of hOATP1B1, hOATP2B1, and hOATP1B3 in salivary glands and tracheae system, MDBF, DBF, and CLF which are fluorescent hOATP1B1, hOATP2B1, and hOATP1B3 substrates were injected into embryos expressing hOATP1B1, hOATP2B1, and hOATP1B3 in their salivary glands (fkh-GAL4; UAS-hOATP1B1, UAS-CD8-RFP; UAS-hOATP2B1, UAS-CD8-RFPnls; UAS-hOATP1B3, UAS-CD8-RFP) and tracheae (btl-GAL4; UAS-hOATP1B1, UAS-CD8-RFP; UAS-hOATP2B1, UAS-CD8-RFPnls; UAS-hOATP1B3, UAS-CD8-RFP). Stage 15 - 16 embryos were used for injection; their salivary glands and tracheae were visualized through RFP (Fig. 15 A2, A5, B2, B5, C2, C5; Fig. 17 A2, A5, B2, B5, C2, C5; Fig. 18 A2, A5, B2, B5, C2, C5; Fig. 20 A2, A5, B2, B5, C2, C5) or RFPnls co-expression (Fig. 16 A2, A5, B2, B5, C2, C5; Fig. 19 A2, A5, B2, B5, C2, C5). Four hours after injection, salivary glands and tracheae were observed by confocal microscopy. The MDBF signal was observed in the salivary gland (Fig. 15 A1, A3; Fig. 16 A1, A3; Fig. 17 A1, A3) and tracheal lumen (Fig. 18 A1, A3; Fig. 19 A1, A3; Fig. 20 A1, A3). In negative control embryos (fkh-GAL4; UAS-CD8-RFP; fkh-GAL4; UAS-CD8-RFPnls; btl-GAL4; UAS-CD8-RFP; btl-GAL4; UAS-CD8-RFPnls) injected with MDBF, a signal was detected in the salivary glands (Fig. 15 A4, A6; Fig. 16 A4, A6; Fig. 17 A4, A6) and tracheal lumen (Fig. 18 A4, A6; Fig. 19 A4, A6; Fig. 20 A4, A6). Similarly, a DBF signal and a CLF signal were detected in the salivary glands (Fig. 15 B1, B3, C1, C3; Fig. 16 B1, B3, C1, C3; Fig. 17 B1, B3, C1, C3) and tracheae lumen (Fig. 18 B1, B3, C1, C3; Fig. 19 B1, B3, C1, C3; Fig. 20 B1, B3, C1, C3) of embryos expressing hOATP1B1, hOATP2B1, and hOATP1B3 in their salivary glands or tracheae. Again, the DBF signal and the CLF signal were also detected in the salivary glands (Fig. 15 B4, B6, C4, C6; Fig. 16 B4, B6, C4, C6; Fig. 17 B4, B6, C4, C6) and tracheal lumen (Fig. 18 B4, B6,

C4, C6; Fig. 19 B4, B6, C4, C6; Fig. 20 B4, B6, C4, C6) of control embryos. Based on these results, I conclude that fluorescent hOATP1B1, hOATP2B1, and hOATP1B3 substrates were taken up into the lumen of the salivary glands and tracheae of embryos independently of hOATP1B1, hOATP2B1, and hOATP1B3 activity.

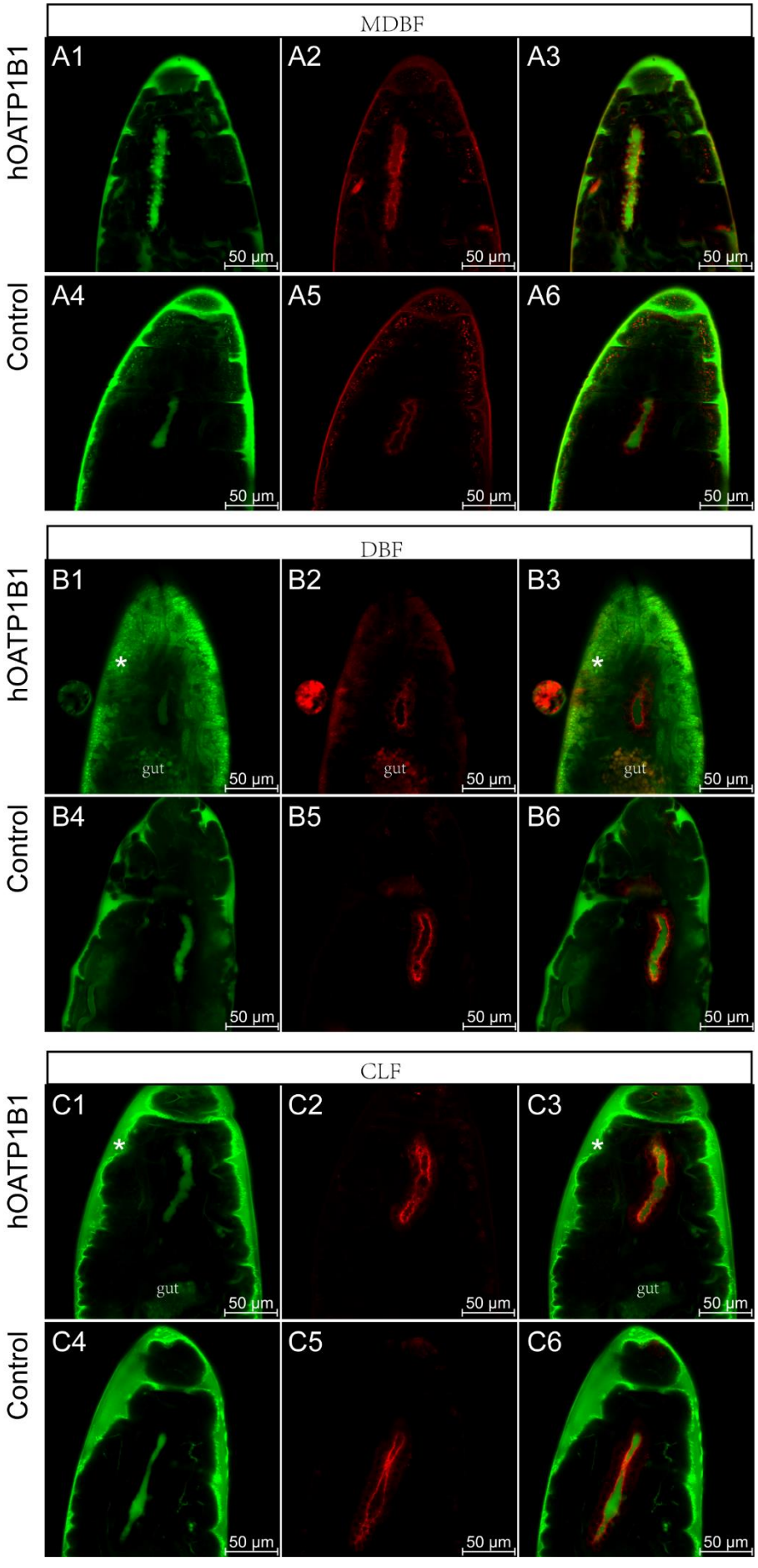
MDBF
hOATP1B1
A1
A2
A3
Control
A4
A5
A6
DBF
hOATP1B1
B1
B2
B3
gut
Control
B4
B5
B6
CLF
hOATP1B1
C1
C2
C3
gut
Control
C4
C5
C6
50 µm

Figure 15. Fluorescent hOATP1B1 substrates penetrated into the lumen of salivary glands independently of hOATP1B1. Four hours after injection, the MDBF signal (A1), the DBF signal (B1), and the CLF signal (C1) were observed in the salivary gland lumen (fkh-GAL4; UAS-CD8-RFP). The salivary glands of embryos were marked by RFP co-expression (A2, A5, B2, B5, C2, C5). In negative control embryos (fkh-GAL4; UAS-CD8-RFP) injected with MDBF (A4), DBF (B4), or CLF (C4), a signal was detected in the salivary gland lumen. A3, A6, B3, B6, C3, and C6 show mergers of the GFP and RFP channels. The white star shows the space between eggshells and embryos. Scale bar = 50 μm.

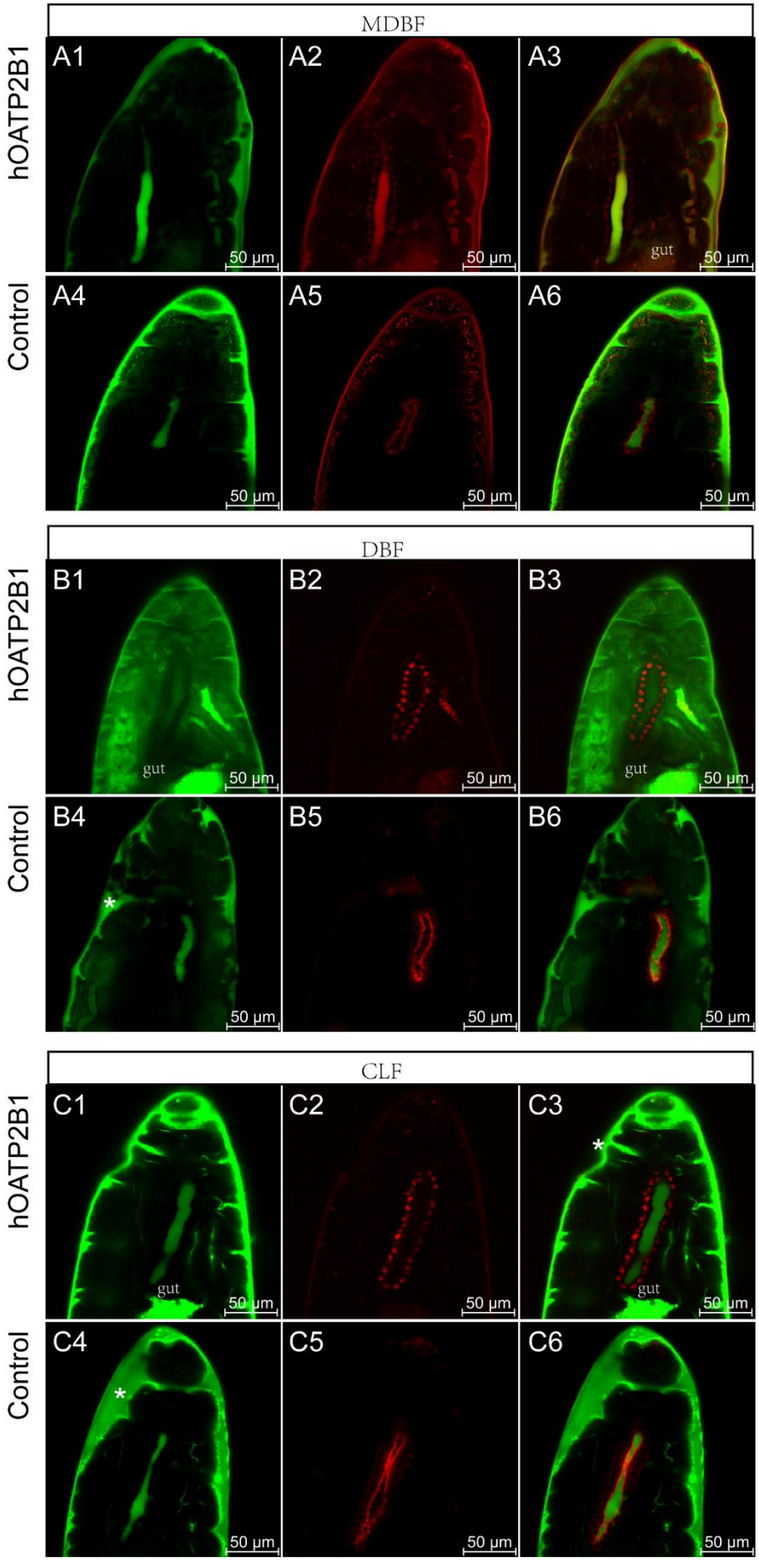
MDBF
hOATP2B1
A1
A2
A3
gut
50 µm
Control
A4
A5
A6
DBF
hOATP2B1
B1
B2
B3
gut
Control
B4
B5
B6
*
CLF
hOATP2B1
C1
C2
C3
*
gut
Control
C4
C5
C6
*

Figure 16. Fluorescent hOATP2B1 substrates were accumulated in the lumen of salivary glands independently of hOATP2B1. Four hours after injection, the MDBF (A1), the DBF (B1), and the CLF signals (C1) were observed in the salivary gland lumen (fkh-GAL4; UAS-CD8-RFPnls). The salivary glands of embryos were visualized through RFPnls co-expression by microscopy (A2, A5, B2, B5, C2, C5). In negative control embryos (fkh-GAL4; UAS-CD8-RFPnls) injected with MDBF (A4), DBF (B4), and CLF (C4), a signal was accumulated in the salivary gland lumen. A3, A6, B3, B6, C3, and C6 show mergers of the GFP and RFP channels. The position of the white star points to the space between the eggshell and the embryo. Scale bar = 50 µm.

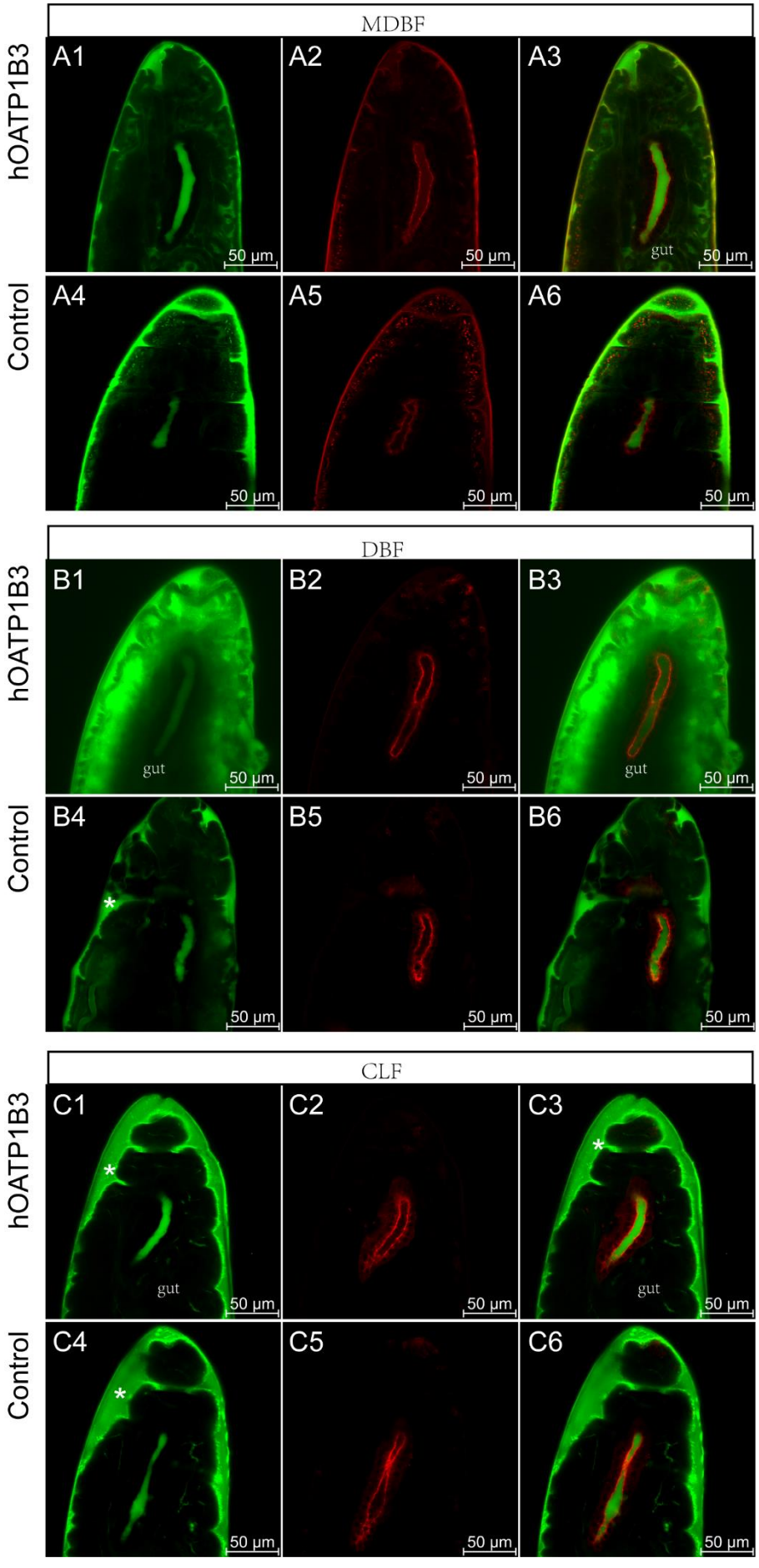
MDBF
hOATP1B3
A1
A2
A3
50 µm
gut
Control
A4
A5
A6
DBF
B1
B2
B3
B4
B5
B6
*
CLF
C1
C2
C3
C4
C5
C6

Figure 17. Fluorescent hOATP1B3 substrates were taken up into the lumen of salivary glands independently of hOATP1B3. Four hours after injection, the salivary gland lumen of these embryos visualized through RFP co-expression (A2, A5, B2, B5, C2, C5) was observed by confocal microscopy. MDBF (A1), DBF (B1), and CLF signals (C1) were detected not only in the salivary gland lumen of these embryos but also in control embryos (fkh-GAL4; UAS-CD8-RFP) (A4), (B4), (C4). A3, A6, B3, B6, C3, and C6 show mergers of the GFP and RFP channels. The white star points to the space between eggshells and embryos. Scale bar = 50 μm.

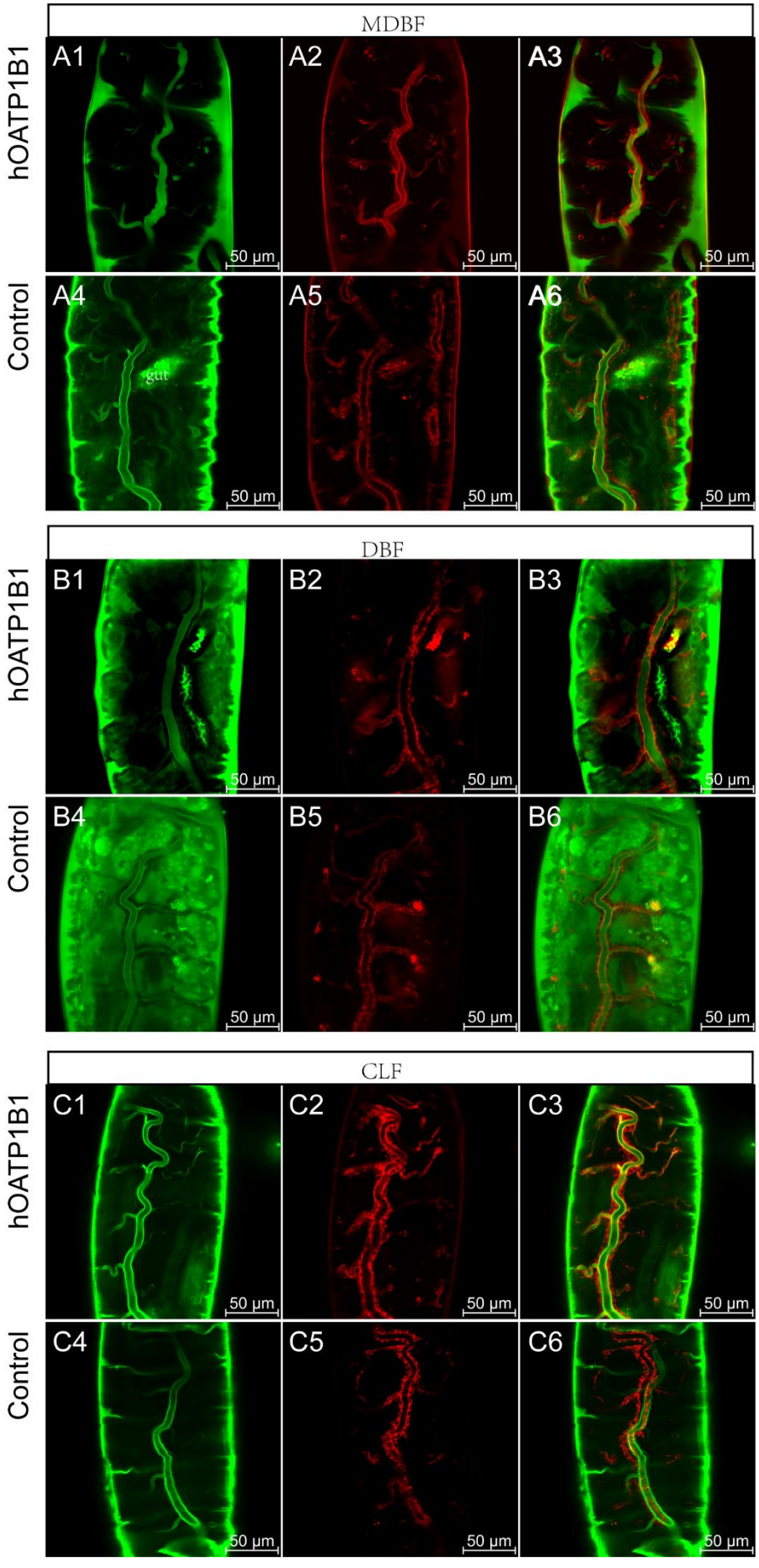
MDBF
hOATP1B1
A1
A2
A3
Control
A4
A5
A6
gut
DBF
hOATP1B1
B1
B2
B3
Control
B4
B5
B6
CLF
hOATP1B1
C1
C2
C3
Control
C4
C5
C6
50 µm

Figure 18. Fluorescent hOATP1B1 substrates accumulated in the lumen of the tracheae independently of hOATP1B1. Four hours after injection MDBF (A1), DBF (B1), and CLF signals (C1) were visualized not only in the tracheae of these embryos but also in control embryos (btl-GAL4; UAS-CD8-RFP) (A4), (B4), (C4). The tracheae of these embryos co-expressed RFP (A2, A5, B2, B5, C2, C5). A3, A6, B3, B6, C3, and C6 show mergers of the GFP and RFP channels. Scale bar = 50 μm.

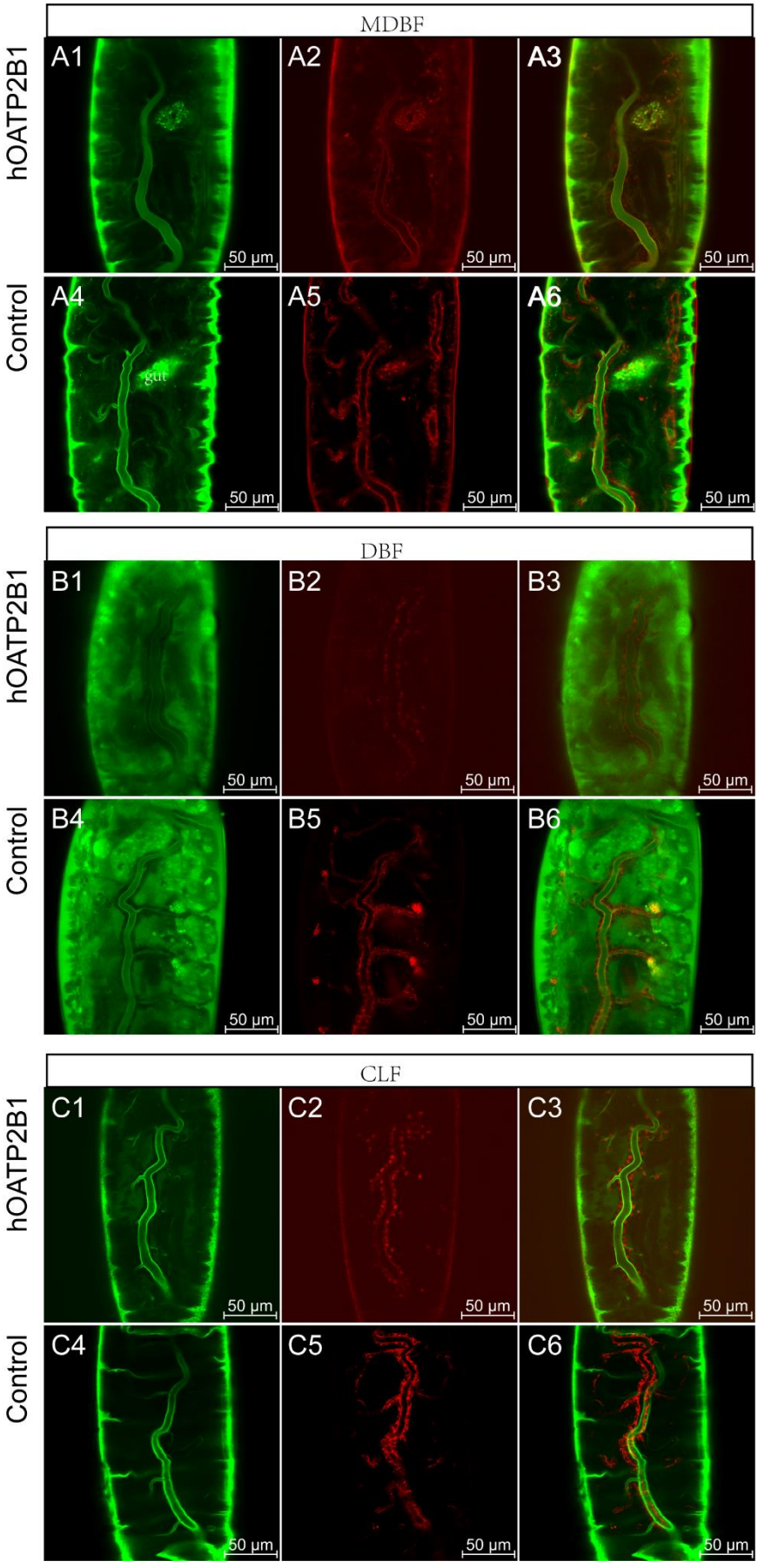
MDBF
hOATP2B1
A1
A2
A3
50 µm
Control
A4
A5
A6
gut
DBF
B1
B2
B3
B4
B5
B6
CLF
C1
C2
C3
C4
C5
C6

Figure 19. Fluorescent hOATP2B1 substrates were accumulated in the tracheae independently of hOATP2B1. Four hours after injection, the tracheae of stage 15-16 embryos were visualized through RFPnls co-expression (A2, A5, B2, B5, C2, C5) by confocal microscopy. The MDBF (A1), DBF (B1), and CLF (C1) signals were observed in the tracheae of embryos expressing hOATP2B1 in their tracheae (btl-GAL4; UAS-hOATP2B1; UAS-CD8-RFPnls). Again, the MDBF (A4), DBF (B4), and CLF signal (C4) were also detected in the tracheae of control embryos (btl-GAL4; UAS-CD8-RFPnls). A3, A6, B3, B6, C3, and C6 show mergers of the GFP and RFPnls signals. Scale bar = 50 μm.

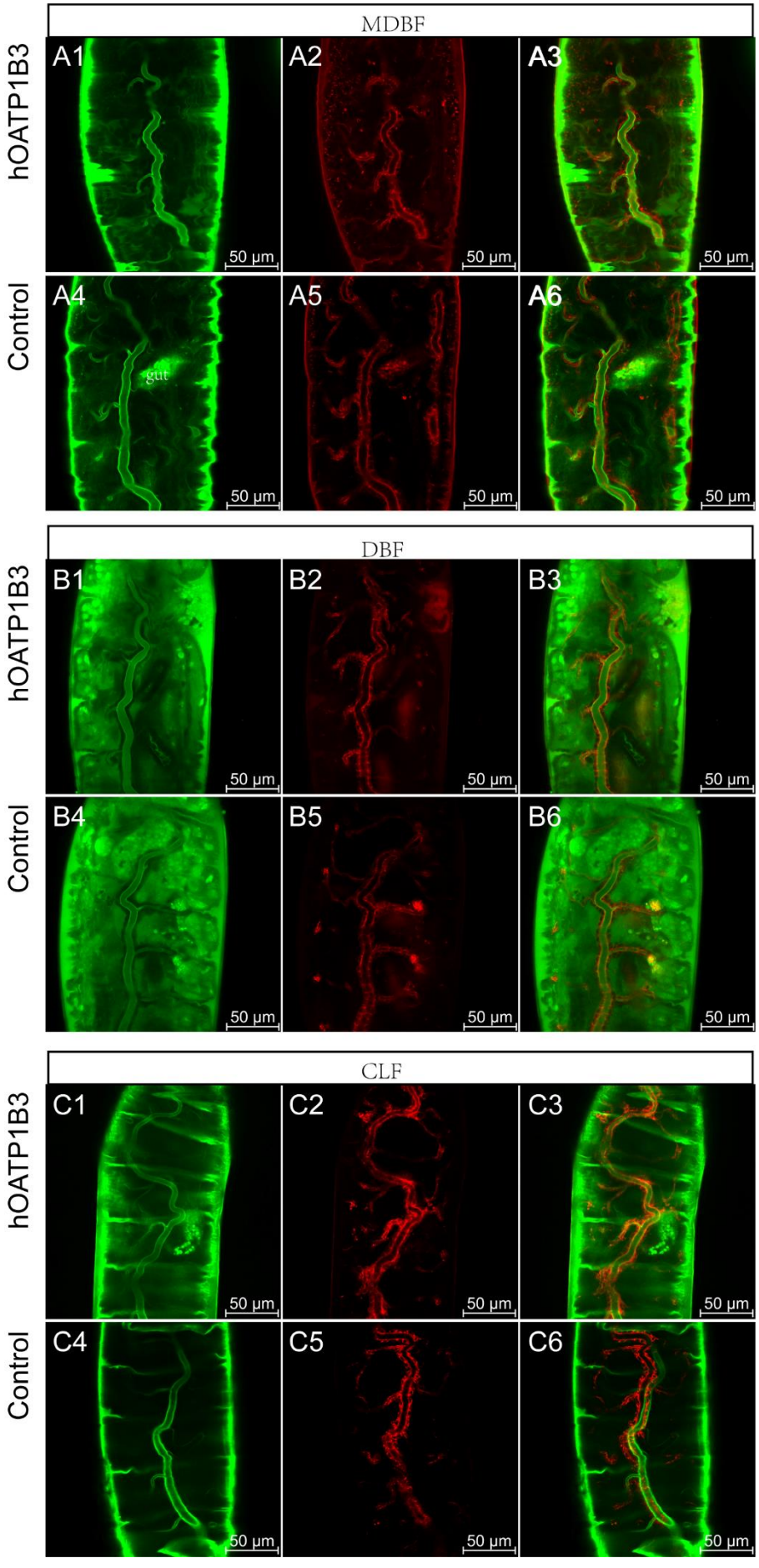
MDBF
hOATP1B3
A1
A2
A3
50 μm
Control
A4
A5
A6
gut
DBF
B1
B2
B3
B4
B5
B6
CLF
C1
C2
C3
C4
C5
C6

Figure 20. Fluorescent hOATP1B3 substrates were taken up into the lumen of tracheae independently of hOATP1B3. Four hours after injection, the tracheae were visualized through RFP co-expression (A2, A5, B2, B5, C2, C5) and the MDBF signal was observed in the tracheae (A1). Also, in negative control embryos (btl-GAL4; UAS-CD8-RFP) injected with MDBF, a signal was detected in the tracheae (btl-GAL4; UAS-CD8-RFP; A4). Similarly, a DBF signal (B1) and a CLF signal (C1) were detected in the tracheae of embryos expressing hOATP1B3 in their tracheae (btl-GAL4; UAS-hOATP1B3; UAS-CD8-RFP). Again, the DBF signal (B4) and the CLF signal (C4) were also detected in the tracheae of control embryos (btl-GAL4; UAS-CD8-RFP). A3, A6, B3, B6, C3, and C6 show mergers of the GFP and RFP signals. Scale bar = 50 µm.

3.1.6.2 Fluorescent hOATP1B, hOATP2B1, and hOATP1B3 substrates did not accumulate in oenocytes by hOATP1B1, hOATP2B1 and hOATP1B3

The function of OATP1B, OATP2B1, and OATP1B3 in the oenocytes (bo-GAL4; UAS-hOATP1B1, UAS-CD8-RFP; UAS-hOATP2B1, UAS-CD8-RFPnls; UAS-hOATP1B3, UAS-CD8-RFP) was studied in parallel dye injection experiments. The oenocytes were marked by the co-expression of RFP (Fig. 21 A2, A5, B2, B5, C2, C5 and Fig. 23 A2, A5, B2, B5, C2, C5) and RFPnls (Fig. 22 A2, A5, B2, B5, C2, C5). Neither MDBF (Fig. 21 A1, A3; Fig. 22 A1, A3; and Fig. 23 A1, A3), nor DBF (Fig. 21 B1, B3; Fig. 22 B1, B3; and 23 B1, B3), nor CLF (Fig. 21 C1, C3; Fig. 22 C1, C3; and Fig. 23 C1, C3) was detected in the oenocytes of these embryos. Similarly, the MDBF (Fig. 21 A4, A6; Fig. 22 A4, A6; and Fig. 23 A4, A6), DBF (Fig. 21 B4, B6; Fig. 22 B4, B6; and Fig. 23 B4, B6), and CLF (Fig. 21 C4, C6; Fig. 22 C4, C6; and Fig. 23 C4, C6) signals were not detected in negative control embryos (bo-GAL4; UAS-CD8-RFP). According to these results, I concluded that fluorescent hOATP1B, hOATP2B1, and hOATP1B3 substrates were not transported into oenocytes by hOATP1B, hOATP2B1, and hOATP1B3.

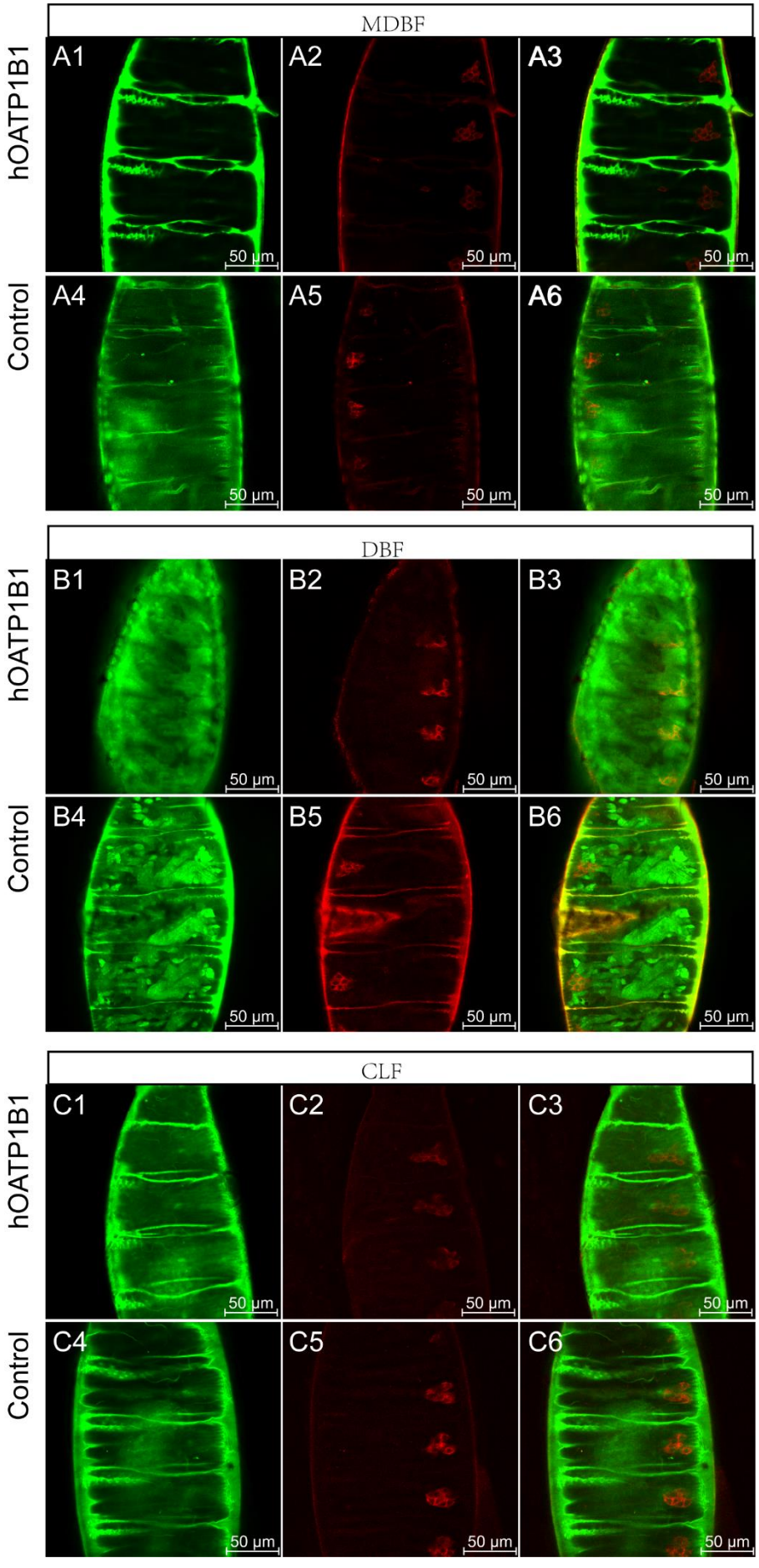
MDBF
hOATP1B1
A1
A2
A3
Control
A4
A5
A6
DBF
hOATP1B1
B1
B2
B3
Control
B4
B5
B6
CLF
hOATP1B1
C1
C2
C3
Control
C4
C5
C6
50 µm

Figure 21. Fluorescent OATP1B1 substrates did not penetrate oenocytes expressing hOATP1B1. Four hours after injection MDBF (A1), DBF (B1), or CLF (C1), no signal was detected in respective embryos (bo-GAL4; UAS-hOATP1B1; UAS-CD8-RFP). Similarly, there was no signal detected in the oenocytes of negative control embryos (bo-GAL4; UAS-CD8-RFP) after injection of MDBF (A4), DBF (B4), or CLF (C4). The tracheae of stage 15-16 embryos were visualized through RFPnls co-expression (A2, A5, B2, B5, C2, C5). A3, A6, B3, B6, C3, and C6 show mergers of the GFP and RFP signals. Scale bar = 50 μm.

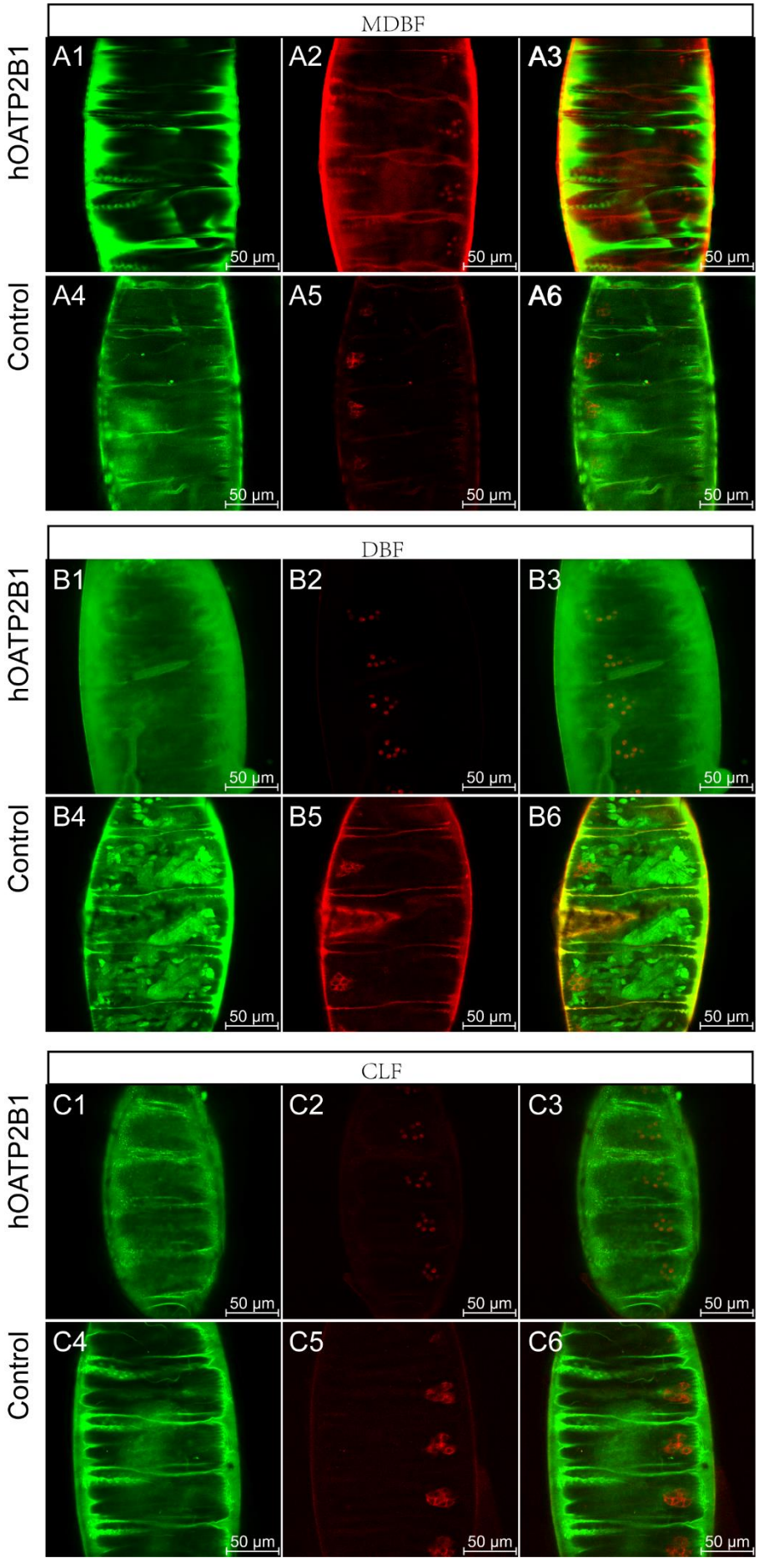
MDBF
hOATP2B1
A1
A2
A3
Control
A4
A5
A6
DBF
hOATP2B1
B1
B2
B3
Control
B4
B5
B6
CLF
hOATP2B1
C1
C2
C3
Control
C4
C5
C6
50 μm

Figure 22. Fluorescent hOATP2B1 substrates were not accumulated in oenocytes expressing hOATP2B1. Four hours after injection into respective embryos (bo-GAL4; UAS-hOATP2B1; UAS-CD8-RFPnls), oenocytes co-expressing RFPnls were observed (A2, A5, B2, B5, C2, C5). Neither MDBF (A1), nor DBF (B1), nor CLF (C1) was detected in the oenocytes of these embryos. Similarly, the MDBF (A4), DBF (B4), and CLF (C4) signals were not detected in the oenocytes of negative control embryos (bo-GAL4; UAS-CD8-RFPnls). A3, A6, B3, B6, C3, and C6 show mergers of the GFP and RFPnls signals. Scale bar = 50 μm.

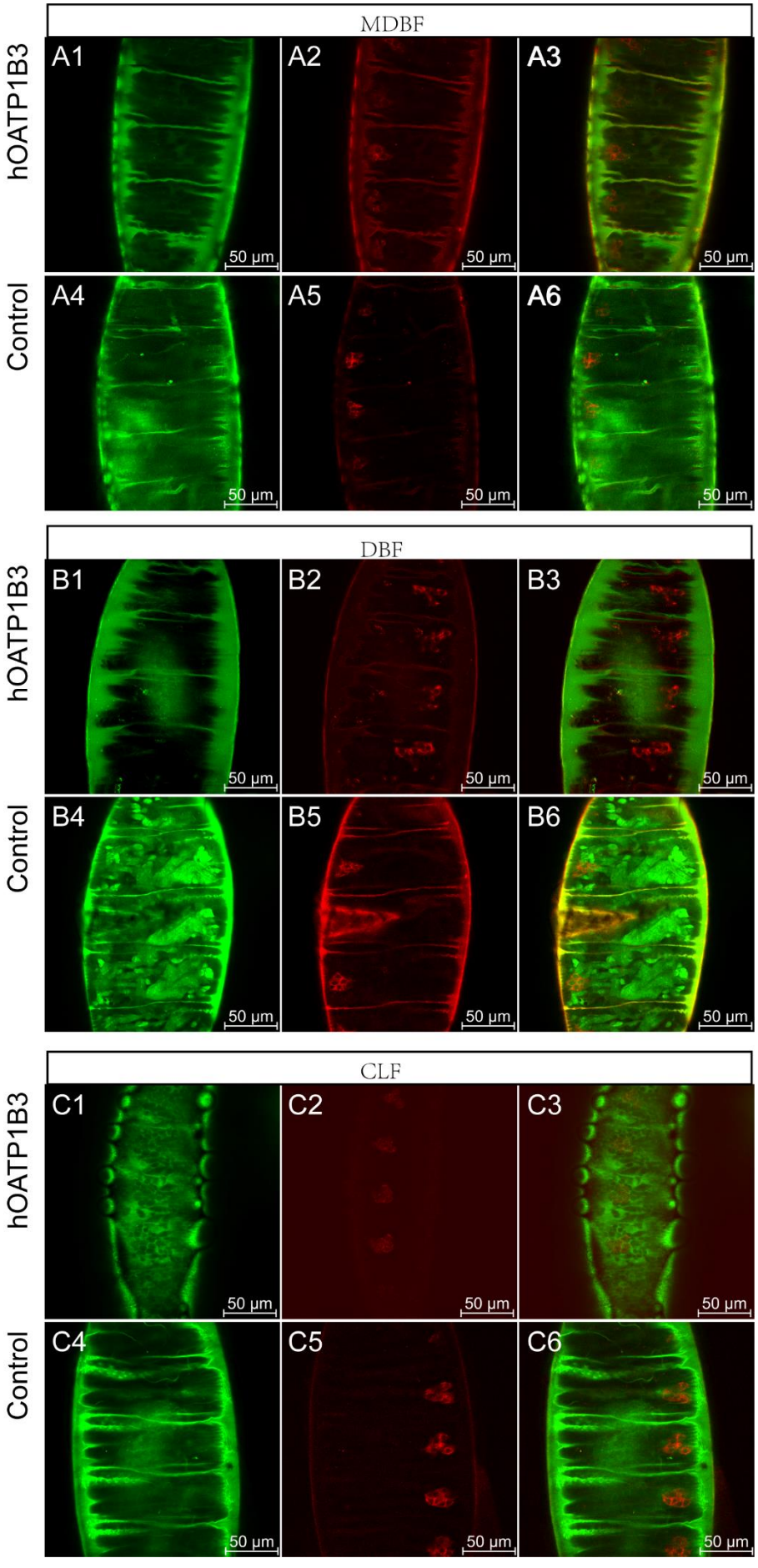
MDBF
hOATP1B3
A1
A2
A3
Control
A4
A5
A6
DBF
hOATP1B3
B1
B2
B3
Control
B4
B5
B6
CLF
hOATP1B3
C1
C2
C3
Control
C4
C5
C6
50 μm

Figure 23. Fluorescent hOATP1B3 substrates were not taken up into the oenocytes by hOATP1B3. Four hours after injection into respective embryos (bo-GAL4; UAS-hOATP1B3; UAS-CD8-RFP), neither MDBF (A1), nor DBF (B1), nor CLF (C1) was detected in the oenocytes of these embryos. Likewise, in negative control embryos (bo-GAL4; UAS-CD8-RFP) no signal was observed in oenocytes after injection of MDBF (A4), DBF (B4), or CLF (C4). The oenocytes were visualized through RFP co-expression (A2, A5, B2, B5, C2, C5). A3, A6, B3, B6, C3, and C6 show mergers of the GFP and RFP signals. Scale bar = 50 µm.

3.1.7 The function of *D. melanogaster* Oatps was evaluated by feeding MDBF into fly *oatp* RNAi larvae

3.1.7.1 MDBF was taken up into the gut and Malpighian tubules of *oatp* RNAi larvae

Since fluorescent hOATP1B1 substrates were taken up into the lumen of the salivary gland and tracheae of transgenic embryos independently of hOATP1B1, hOATP2B1 and hOATP1B3, *D. melanogaster* Oatps were considered to play a role in assisting fluorescent substrate uptake into the lumen of these tissues. In *D. melanogaster*, there are eight genes coding for Oatps (see Figure 24). I used 13 *oatp* RNAi lines targeting the transcript levels of these *oatps* to examine their function. To reduce *oatp* transcript levels, I crossed the UAS-RNAi flies to tub-GAL4 flies that express GAL4 ubiquitously. After feeding MDBF for about 15 h, the first instar larvae were observed by microscopy. Tissue of *oatp* RNAi (tub-GAL4, UAS-oatp^{RNAi}) and control larvae (tub-GAL4, UAS-CD8-RFP) was observed by bright-field microscopy (X 15 magnification) (Fig.24 A1, B1, C1, D1, E1, F1, G1, H1, I1, J1, K1, L1, M1, N1). A strong MDBF signal was detected in the gut and the Malpighian tubules of *oatp* RNAi and control larvae (Fig. 24 A2, B2, C2, D2, E2, F2, G2, H2, I2, J2, K2, L2, M2, N2). A detailed structure of the gut and Malpighian tubule was observed at high magnification (X 40) (Fig. 24 A3, B3, C3, D3, E3, F3, G3, H3, I3, J3, K3, L3, M3, N3). The strong MDBF signal in the gut and the Malpighian tubules was present in *oatp* RNAi and control larvae (Fig. 24 A4, B4, C4, D4, E4, F4, G4, H4, I4, J4, K4, L4, M4, N4). Presence of the signal in control larvae suggested that MDBF might have been taken up into the gut and Malpighian

tubules of *oatp* RNAi larvae independently of fly Oatps.

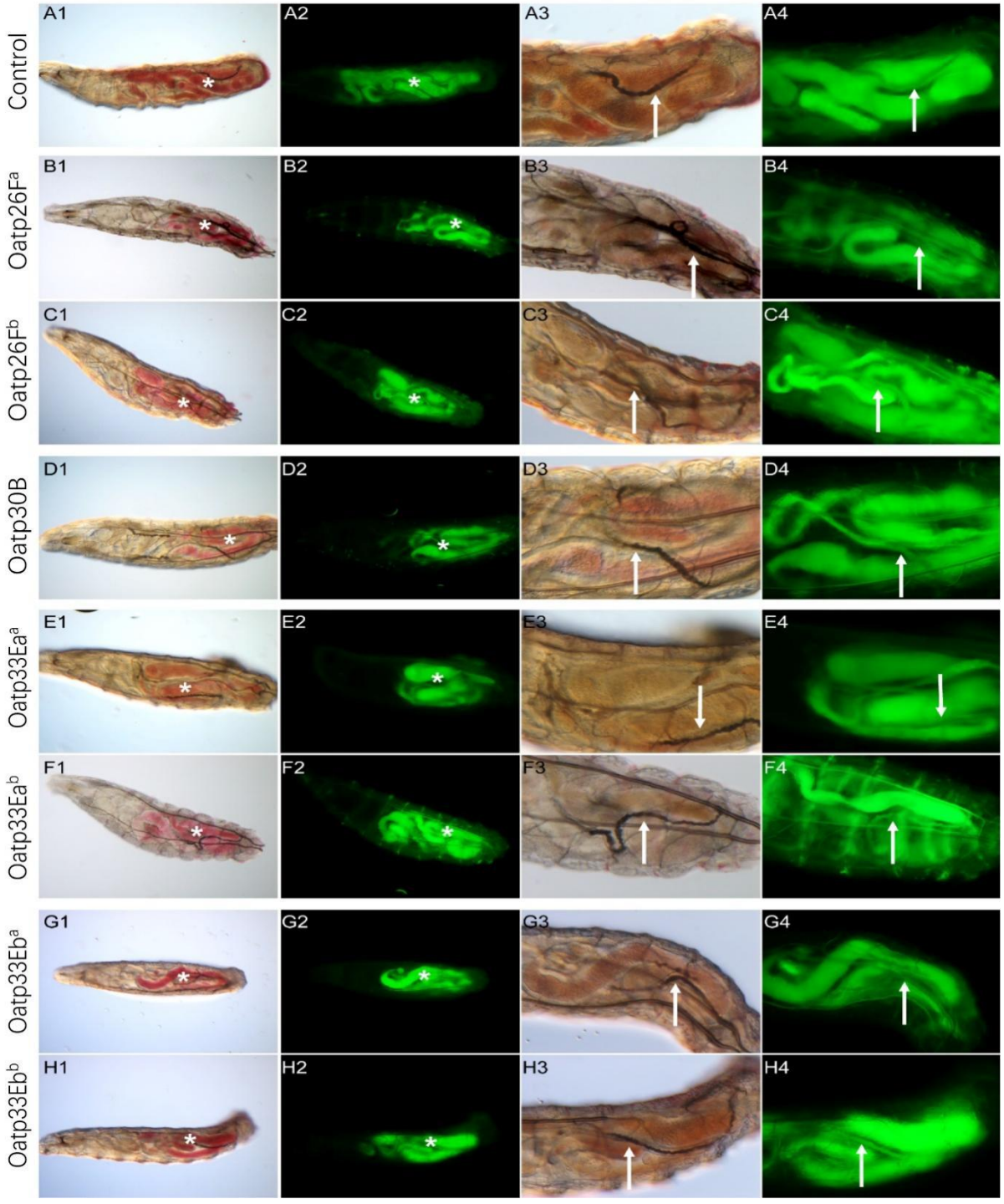

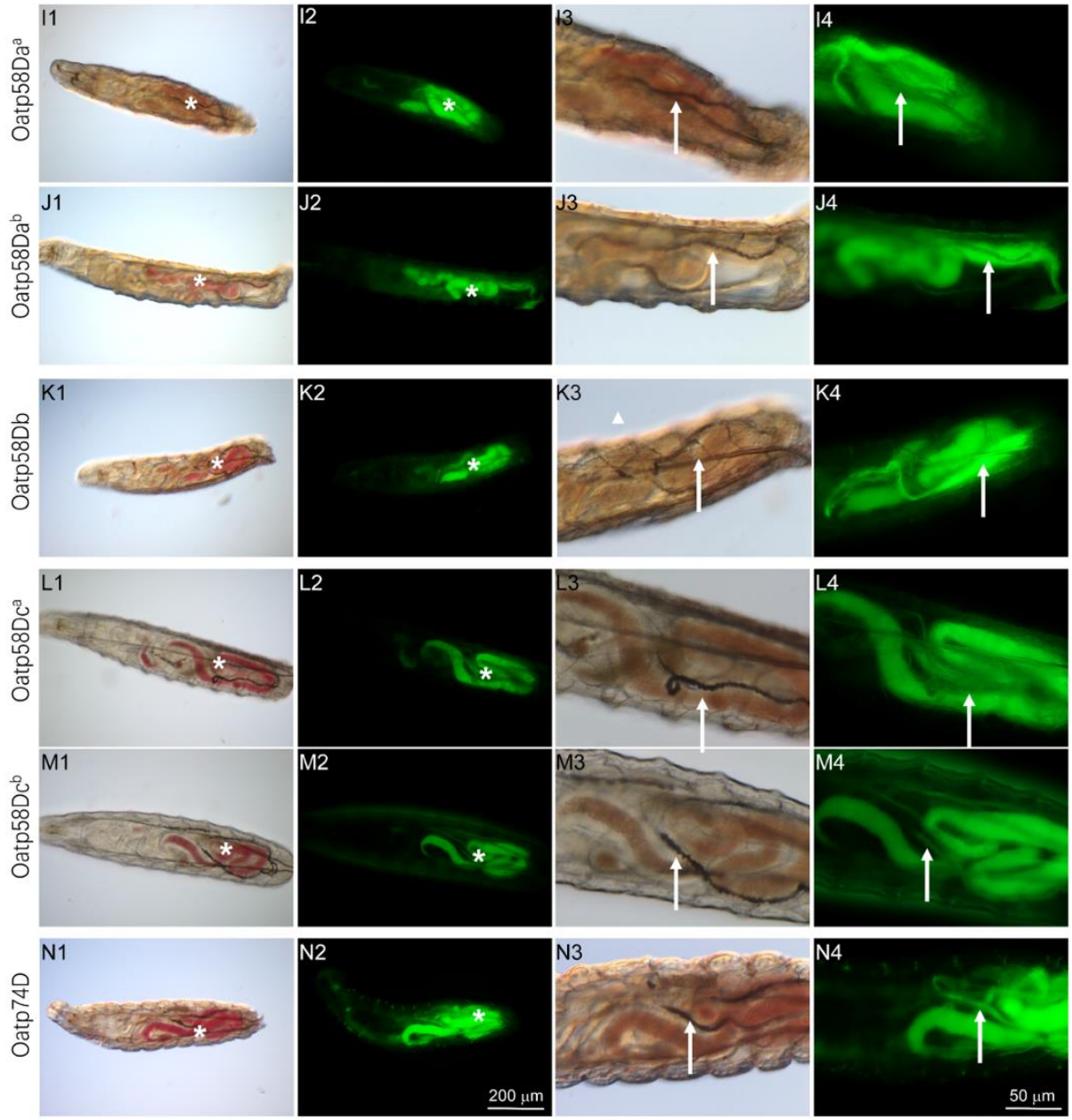

Figure 24. MDBF was taken up into the gut and Malpighian tubules independently of Oatps. *oatp* RNAi (tub-GAL4, UAS-oatp^{RNAi}) and control larvae (tub-GAL4, UAS-CD8-RFP) were observed under the bright-field microscope at low magnification (X 15 magnification) (A1, B1, C1, D1, E1, F1, G1, H1, I1, J1, K1, L1, M1, N1) and at high magnification (X 40 magnification) (A3, B3, C3, D3, E3, F3, G3, H3, I3, J3, K3, L3, M3, N3). A green signal was observed in the gut and Malpighian tubule of *oatp* RNAi larvae and control larvae at low magnification (X 15 magnification) (A2, B2, C2, D2, E2, F2, G2, H2, I2, J2, K2, L2, M2, N2) and at high magnification (X 40 magnification) by fluorescence microscopy (A4, B4, C4, D4, E4, F4, G4, H4, I4, J4, K4, L4, M4, N4). The white star indicates the position of the gut and the white arrow

indicates the position of the Malpighian tubules. Scale bar = 50 μm and 200 μm.

3.1.7.2 Transcript levels of *oatp* genes in *oatp* RNAi larvae was measured by RT-qPCR

The observation that MDBF was taken up into the gut and Malpighian tubules independently of Oatps, may suggest that the RNAi efficiency was low. Therefore, the transcription levels of the *oatp* genes were measured using qPCR. First instar larvae (tub-GAL4, UAS-oatp^{RNAi}) were used for qPCR. The transcript levels were a little higher in *Oatp26F^a, Oatp33Eb^a, Oatp58Da^a,* and *Oatp58Db* RNAi larvae than in control larvae (tub-GAL4, UAS-CD8-RFP), while the transcript levels were decreased in *Oatp26F^b, Oatp30B, Oatp33Ea^a, Oatp33Ea^b, Oatp33Eb^b, Oatp58Da^b, Oatp58Dc^a, Oatp58Dc^b*and *Oatp74D* RNAi larvae compared to control larvae. Transcript reduction was significant only in *Oatp58Da^b* and *Oatp74D* RNAi larvae. These results indicated that most *oatp* genes were not efficiently knocked down in the *oatp* RNAi larvae.

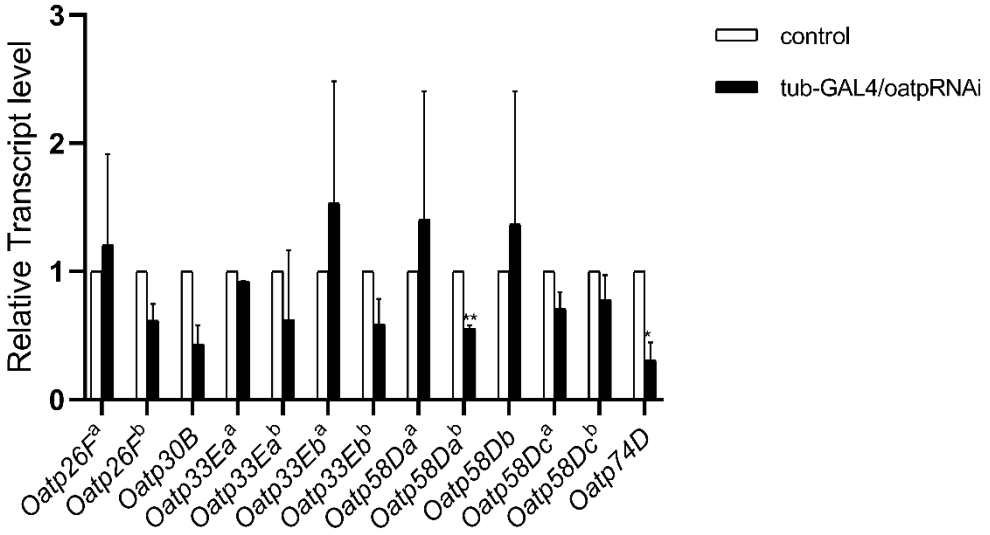

Figure 25. Transcript levels of *oatps* in the *oatp* RNAi larvae was measured by qRT-PCR. The expression of the *oatp* gene in the *oatp* RNAi larvae (tub-GAL4, UAS- Oatp26F^a; tub-GAL4, UAS-Oatp33Eb^a; tub-GAL4, UAS-Oatp58Da^a; tub-GAL4, UAS-Oatp58Db) was higher than in control larvae (tub-GAL4, UAS-CD8-RFP). The expression levels of the *oatp* genes were lower in *Oatp26F^b, Oatp30B, Oatp33Ea^a, Oatp33Ea^b, Oatp33Eb^b, Oatp58Da^b, Oatp58Dc^a, Oatp58Dc^b* and *Oatp74D* RNAi larvae than in control larvae. This effect was especially

significant in *Oatp58Da*^{b} and *Oatp74D* RNAi larvae. (* $p < 0.05$, ** $p < 0.01$). Data shown are mean ±SEM and represent two independent experiments.

3.2 Study of the expression and function of hOCT1 and hABCB1 in embryos

The transport of a substrate from the basal side of an epithelial cell to its apical side requires the concerted activity of one transporter in the basal plasma membrane for substrate uptake and one transporter in the apical plasma membrane for substrate efflux. The basally localized hOCT1 and the apically localized hABCB1 are such a couple of transporters needed for the transport of a number of cations including drugs across epithelia. In a previous work from the group, the function of hOCT1 was established in fruit fly embryos. In my thesis, I sought to analyze the functionality of hABCB1 in order to reconstitute the complete hOCT1/hABCB1 transport system in the *D. melanogaster*.

3.2.1 Generation of *hABCB1* expressing flies

To establish the hOCT1/hABCB1 transport system “humanized” UAS-hABCB1 flies were generated following my standard protocol. To verify that the hABCB1 construct was successfully transferred into flies, the expression levels of *hABCB1* were measured by qRT-PCR after GAL4 induction. Stage 16 - 17 embryos (fkh-GAL4, UAS-hABCB1) were used for qPCR analysis. The expression levels of hABCB1 were significantly higher in hABCB1 transgenic embryos than their background levels in wild-type Dijon embryos (Fig. 26). As the expression detected with the qABCB1-1 primers in the wild-type Dijon embryos was relatively high (but significantly lower than in *hABCB1*-expressing embryos), I designed another, independent pair of primers (qABCB1-2) for qRT-PCR analysis. This measure did not change the result suggesting that *hABCB1* similar sequences are present in *D. melanogaster* that are amplified with the *hABCB1* primers (Fig. 28 B). Together I conclude that the human gene *hABCB1*

has been successfully transferred into *D. melanogaster*.

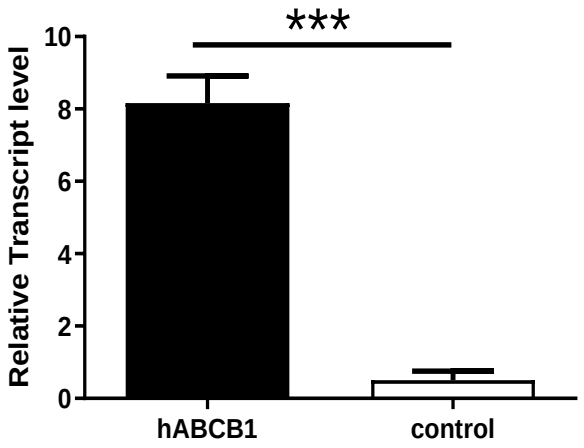

Figure 26. Gene expression of *hABCB1* in the "humanized" embryos was measured by qRT-PCR. The expression of the *hABCB1* gene in the "humanized" hABCB1 embryos (fkh-GAL4, UAS-hABCB1) was significantly higher than in wild-type Dijon embryos (*** $p < 0.001$). Data shown are mean ±SEM and represent two independent experiments.

3.2.2 Immune-detection of hABCB1 in embryos

To examine the localization and distribution of hABCB1 in the "humanized" hABCB1 embryos, an antibody directed against ABCB1 (Anti-P-Glycoprotein Mouse mAb, C219), was used to detect the transporter in embryos expressing hABCB1 in the salivary glands (UAS-hABCB1 driven by fkh-GAL4). Embryo selection and fixation methods were the same as for the hOATP1B1 antibody staining experiments (see Materials & Methods 2.2.3). No signal was detected after anti-hABCB1 application in the salivary glands of embryos expressing hABCB1 (fkh-GAL4, UAS-hABCB1) fixed with formaldehyde or by heat treatment (Fig. 27 A1, A4).

Because no signal was detected with the hABCB1 antibody in the salivary glands, I concluded that the hABCB1 C219-antibody did not successfully recognize the transporter expressed in fruit fly embryos. Therefore, I tried to use another commercially available hABCB1 antibody for detection. A positive immunofluorescence signal of human hABCB1 detected with the anti-ABCB1, # HPA002199 antibody (Sigma-Aldrich) was observed in the salivary glands of embryos

expressing hABCB1 (fkh-GAL4, UAS-hABCB1) fixed with formaldehyde or by heat treatment (Fig. 27 A2, A5). As a negative control, no signal was detected in wild-type Dijon embryos incubated with the same anti-hABCB1 antibody (Fig. 27 A3, A6).

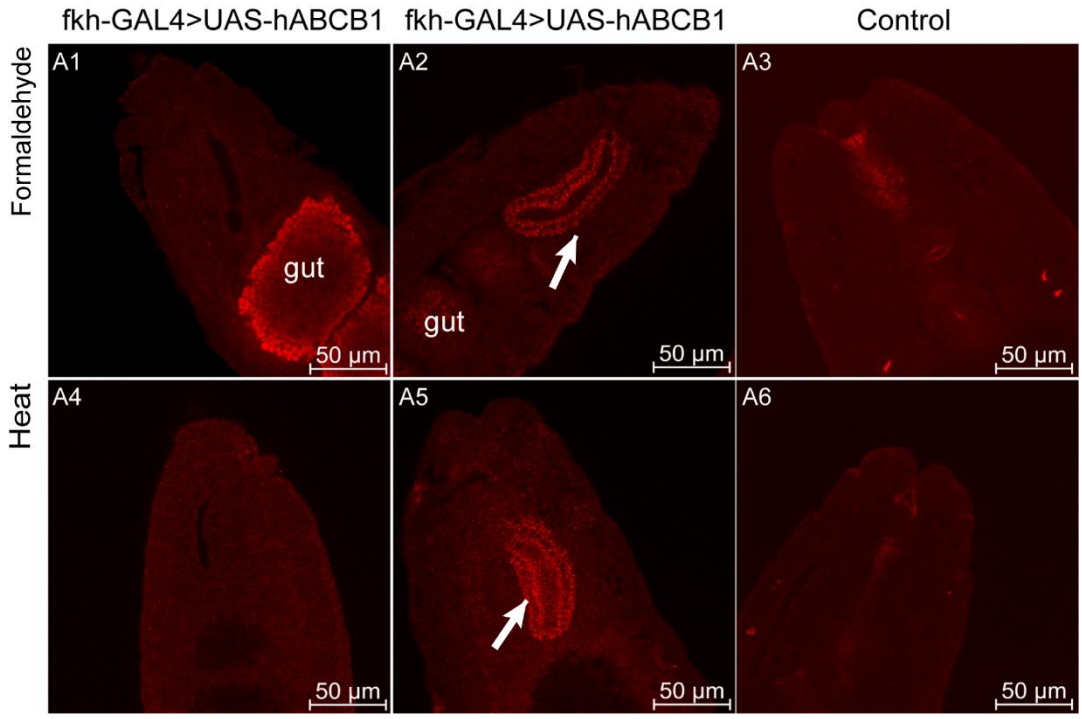

Figure 27. The hABCB1 antibody detects the protein in the *D. melanogaster* embryos. After formaldehyde fixation or heat treatment and detection with the anti-hABCB1 (Anti-P-Glycoprotein Mouse mAb, C219) antibody, no signal was observed in the salivary glands of respective embryos (fkh-GAL4; UAS-hABCB1; A1, A4). With another anti-hABCB1 (Anti-ABCB1, # HPA002199, Sigma) antibody, a signal was observed in the salivary glands of respective embryos (fkh-GAL4; UAS-hABCB1; A2, A5). The staining of wild-type Dijon embryos is shown as the negative control (A3, A6). Scale bar = 50 µm.

3.2.3 Transcription of the *hABCB1* and *hOCT1* genes in transgenic embryos was measured by qRT-PCR

To assay Et^+ transport across epithelial cells in fly embryos, the UAS-hABCB1 insertion was recombined to the UAS-hOCT1, UAS-GFP chromosome to generate double “humanized” flies (UAS-hABCB1, UAS-hOCT1, UAS-GFP). Unfortunately, due to recombination events between UAS-hABCB1, UAS-hOCT1 and UAS-GFP I only

obtained UAS-hABCB1, UAS-hOCT1 flies without UAS-GFP.

To demonstrate that *hABCB1* and *hOCT1* genes are expressed in the respective embryos (UAS-hABCB1, UAS-hOCT1 driven by fkh-GAL4) at the same time, qRT-PCR was applied for gene expression of *hABCB1* and *hOCT1*. Compared to wild-type Dijon embryos, the transcription levels of the *hABCB1* gene (qABCB1-1 primers) in the embryos expressing hABCB1 and hOCT1 was significantly higher (Fig. 28 A). Regarding the *hOCT1* gene, expression in these embryos was significantly higher than in wild-type Dijon with no *hOCT1* transcript signal (Fig. 28 C). These results indicated that the *hABCB1and hOCT1* genes were successfully expressed in the embryos (fkh-GAL4, UAS-hABCB1, UAS-hOCT1).

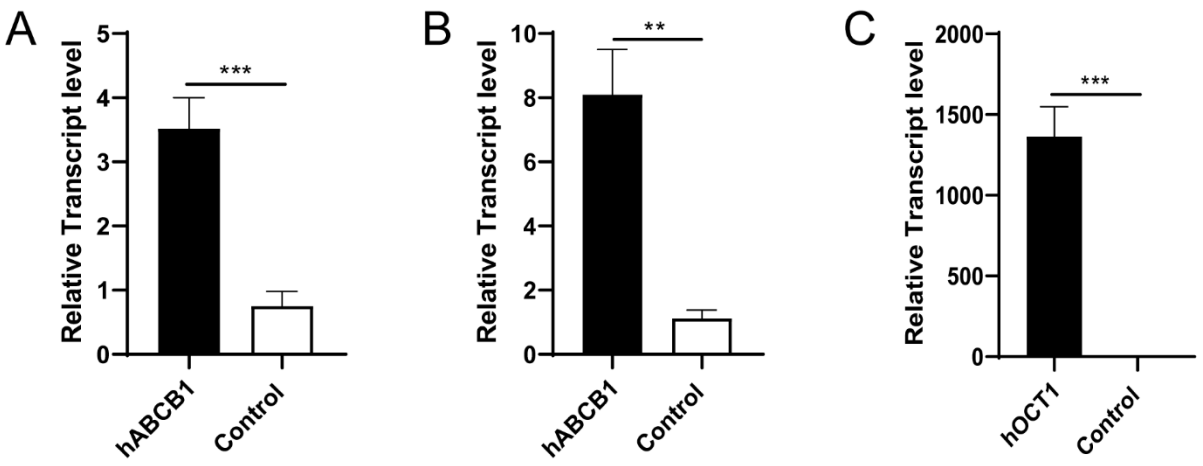

Figure 28. Gene transcription levels were evaluated in the “humanized” embryos by qRT-PCR. The expression of hABCB1 in the “humanized” hABCB1 and hOCT1 embryos (fkh-GAL4, UAS-hABCB1, UAS-hOCT1) was significantly higher than in wild-type Dijon embryos (A, *** $p < 0.001$; B, ** $p < 0.01$); wild-type Dijon embryos expressed traces of transcripts using qABCB1-1 and qABCB1-2 primers suggesting that *hABCB1*-like sequences are present in *D. melanogaster*. Embryos expressing *hABCB1* and *hOCT1* had a much higher transcription level of *hOCT1* compared to wild-type Dijon embryos (C, *** $p < 0.001$). Data shown are mean ±SEM and represent two independent experiments.

3.2.4 Analyses of the function of hOCT1 and hABCB1 in “humanized” transgenic fly embryos using EtBr

To repeat previous results, the hOCT1 line was first tested for its original transporter activity in fruit fly epithelial cells. The eggs from the UAS-hOCT1, UAS-GFP X fkh-GAL4 cage were collected at stage 15 - 16 and visualized through GFP (Fig 29 A1). The Et^+ uptake of salivary gland epithelial cells was analyzed at four hours after injection by confocal microscopy. Indeed, four hours after injection a very strong Et^+ signal was observed in salivary gland cells (Fig 29 A2, A3). This result confirmed that the exogenous transporter hOCT1 was able to transport Et^+ from the hemolymph into the epithelial cells.

The function of hOCT1 and hABCB1 was evaluated by injection of EtBr into the embryos expressing both genes in the salivary glands (fkh-GAL4, UAS-hOCT1, UAS-hABCB1). Et^+ was accumulated within the cells of the salivary glands, but not in the lumen (Fig. 29 B).

To further verify the function of hOCT1 and hABCB1, embryos expressing the transgenes in the tracheal system (btl-GAL4, UAS-hOCT1, UAS-GFP, and btl-GAL4, UAS-hOCT1, UAS-hABCB1) were used for tracer injection and their tracheae were visualized through GFP (Fig. 29 C1). Similarly, Et^+ was only taken up into the cell of the tracheae of embryos expressing hOCT1 and embryos expressing hOCT1 and hABCB1 (Fig. 29 C2, C3, D). These results indicated that expression of hOCT1 mediated Et^+ uptake into the cells of the salivary glands and tracheae, but co-expression of hOCT1 and hABCB1 did not lead to the transport of Et^+ from the cells of the salivary glands or tracheae into the lumen of the respective tissue.

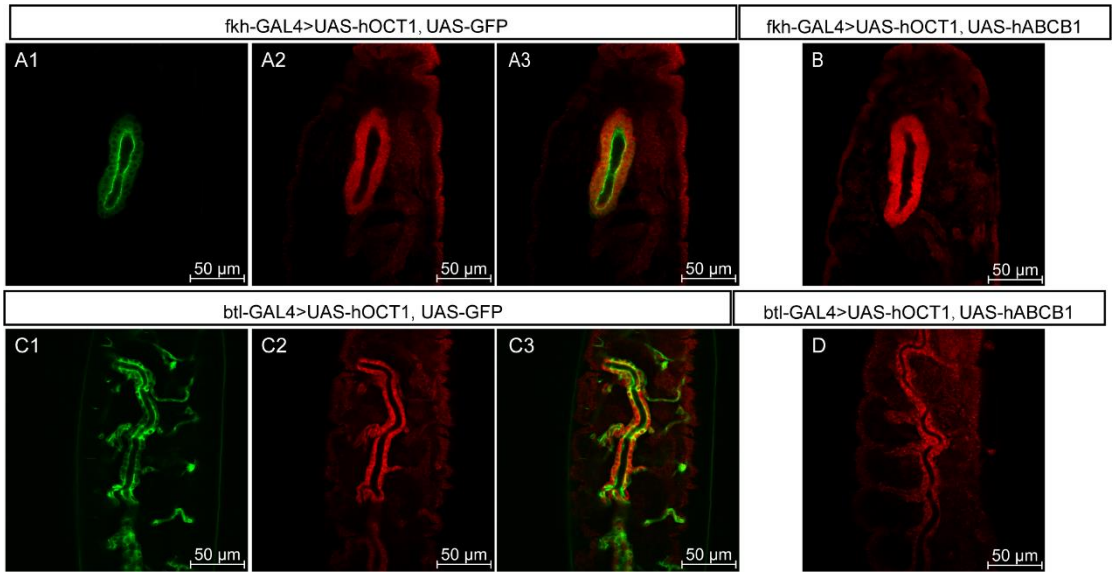

Figure 29. The function of hOCT1 and hABCB1 was studied by injection of the fluorescent substrate Et^+ into the respective embryos. Four hours after injection, the Et^+ signal was observed in the salivary gland cells of embryos expressing hOCT1 (fkh-GAL4, UAS-hOCT1, UAS-GFP, A2, A3). In embryos co-expressing hOCT1 and hABCB1 (fkh-GAL4, UAS-hOCT1, UAS-hABCB1) and injected with EtBr, no signal was detected in the salivary gland lumen (B). Similarly, there was a signal detected in the tracheal cell of embryos expressing hOCT1 in the tracheae (btl-GAL4, UAS-hOCT1, UAS-GFP, C2, C3) after injection with EtBr, but no signal was detected in the tracheal lumen of embryos expressing both transporters (btl-GAL4, UAS-hOCT1, UAS-ABCB1, D). The salivary glands and tracheae of embryos were marked with GFP co-expression in A and C. Scale bar = 50 µm.

3.2.5 The function of hOCT1 and hABCB1 was studied in "humanized" hOCT1 and hABCB1 embryos using rhodamine 123

Obviously hABCB1 was unable to shuffle Et^+ into the lumen of salivary glands. Therefore, I decided to test the transport activity of hOCT1 and hABCB1 in fly embryos for rhodamine 123, which is another established substrate for these transporters (Jouan et al., 2014). This tracer substrate was injected into embryos expressing hOCT1 and hABCB1 in their salivary glands (fkh-GAL4; UAS-hOCT1; UAS-ABCB1). Two concentrations of rhodamine 123 were injected into stage 15 - 16 embryos. In both cases, the dye accumulated in the salivary gland cells but not in the lumen (Fig.

30 A, B). Based on these results, I concluded that Et^+ and rhodamine 123 could not be transported from the salivary gland cells into the lumen when hOCT1 and hABCB1 are expressed in the salivary glands.

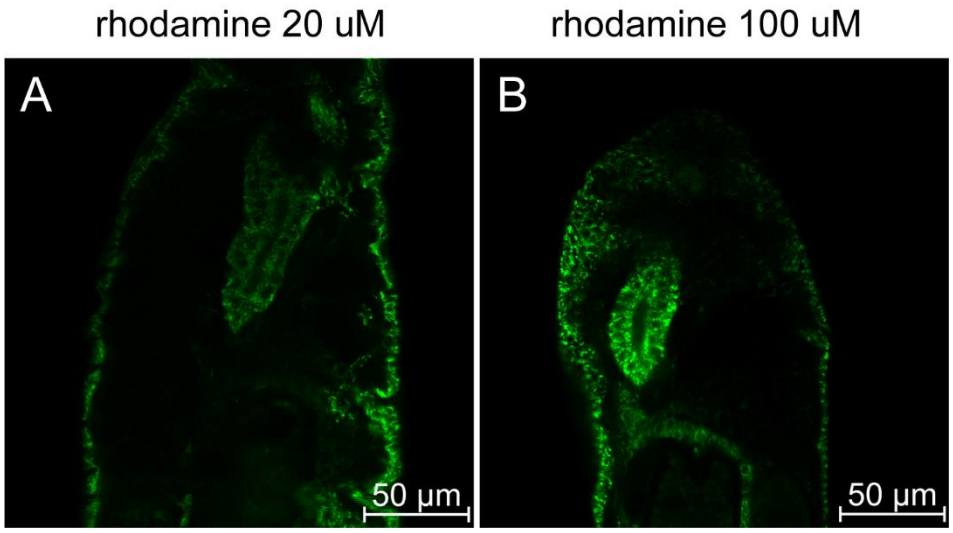

Figure 30. The function of hOCT1 and hABCB1 was studied by injection of the fluorescent substrate rhodamine 123 into embryos. Four hours after injection, the rhodamine 123 signal was observed in the salivary gland cells; the lumen was, however, clear (fkh-GAL4, UAS-hOCT1, UAS-hABCB1, A, B). Scale bar = 50 µm.

3.3 Functional analysis of hOCT1 in embryos by feeding cisplatin and cimetidine

Although Et^+ and rhodamine 123 were not transported into the lumen of salivary glands of embryos expressing hOCT1 and hABCB1 (fkh-GAL4; UAS-hOCT1; UAS-hABCB1), they were transported into the cells of the salivary gland. This confirmed and suggested that hOCT1 retained its function in fly embryos. To further study the function of hOCT1 in embryos, I planned to feed cisplatin, a cytotoxin transported by hOCT1, to hOCT1 transgenic females. Feeding instead of injection would allow fast and high-throughput testing; indeed, our previous results and long-term experience indicated that embryos from females fed with toxins (i.e. insecticides) were affected by the

toxicity (Gangishetti et al., 2009). The goal of this experiment is, hence, to establish a drug-testing system by inducing cisplatin-caused tissue damage and by consequence embryo lethality that would be rescued by co-feeding of hOCT1 inhibitors like cimetidine.

To identify the optimal set up for the experiment, UAS-hOCT1 flies were crossed with different tissue-specific GAL4 drivers (fkh-GAL4 for salivary glands, hh-GAL4 and en-GAL4 for early epidermis, cut-GAL4, elav-GAL4 and pros-GAL4 for nervous system, drm-GAL4 for midgut) to express hOCT1 in these tissues in the embryo and exposed them to cisplatin and cisplatin/cimetidine. In the following, I present the description and the results of the experiments conducted with elav-GAL4, pros-GAL4 and the other GAL4 drivers in respective sub-chapters as the results I obtained were distinctly different. Please also note that because the hOCT1-expressing flies were heterozygous for the insertions (UAS-hOCT1, UAS-GFP / + +) while the GAL4 insertion was homozygous, only half of the selected embryos expressed hOCT1, allowing to use the other half as controls.

Before starting the experiment, I analyzed the effects of cisplatin and cisplatin/cimetidine on wild-type fly embryos (Fig. 31F). From day 1 to day 5, cisplatin slightly affects hatching that is not rescued by the co-feeding of cimetidine. On day 6, by contrast, I observed a strong decline in larval hatching after feeding the mothers with cisplatin; this effect was reversed by co-feeding cimetidine. Thus, continuous feeding of females for at least 6 days is needed to influence hatching behavior in *D. melanogaster*. Cimetidine is able to counteract this effect in my assay.

3.3.1 The effect of cimetidine on the mortality of embryos expressing hOCT1 in different embryonic tissues produced by mothers fed with cisplatin

In principle, compared to wild-type (no expression of hOCT1) embryos, I reckon that cisplatin lethality is probably enhanced in embryos expressing hOCT1. Based on this assumption, I planned to study whether cimetidine can reverse cisplatin toxicity by simultaneously feeding *hOCT1*-flies with cimetidine and cisplatin. I, thus, analyzed two

groups: one group of flies was fed with cisplatin (1 mg/ml) for 7 days, the other group of flies was simultaneously fed with cisplatin (1 mg/ml) and cimetidine (20 mg/ml) for 7 days. After 24 hours, 50 embryos were randomly selected, and embryo hatchability was recorded every day for 6 consecutive days. Moreover, the pupation and eclosion rates of the hatched larvae was assessed. For the drug-interaction assay, flies with the fkh-GAL4, drm-GAL4, en-GAL4, hh-GAL4 or cut-GAL4 driver were crossed with UAS-hOCT1 flies (UAS-hOCT1, UAS-GFP / + +). The hatching rates of the respective group one and group two embryos were similar (Fig. 31 A1, B1, C1, D1, E1). The hatching rate of group one embryo was between 60% - 90%, and it did not improve for group two embryos. Although I observed a trend of hatching rate rescue when cimetidine was co-fed, this difference was not significant. The pupation and eclosion rates of the hatched larvae was not affect by cisplatin or cimetidine (Fig. 31 A2, A3, B2, B3, C2, C3, D2, D3, E2, E3). These results suggest that cimetidine could not rescue the toxin of cisplatin in embryos expressing hOCT1 in the tested tissues.

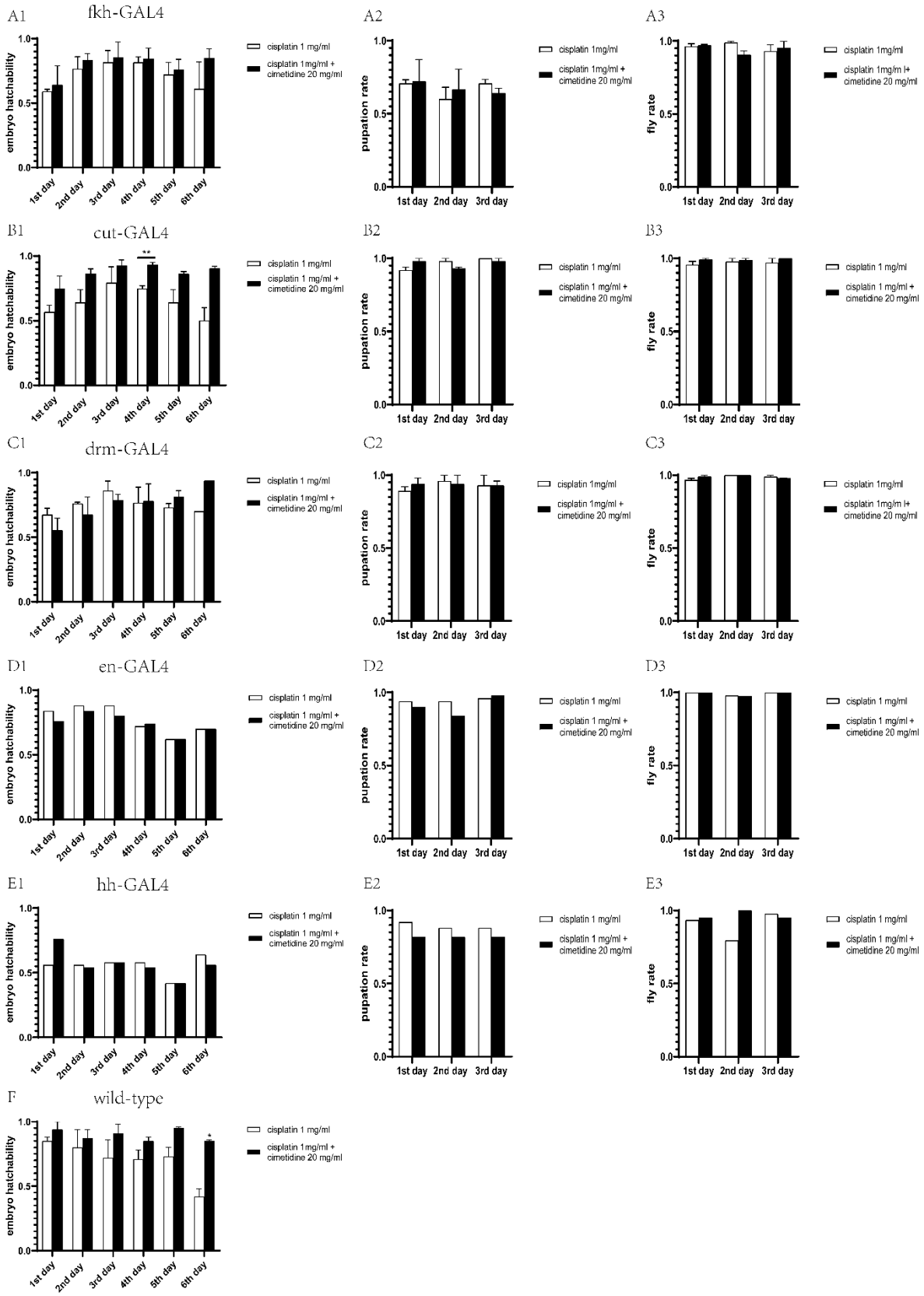
A1
fkh-GAL4
embryo hatchability
1.0
0.5
0.0
1st day
2nd day
3rd day
4th day
5th day
6th day
cisplatin 1 mg/ml
cisplatin 1 mg/ml + cimetidine 20 mg/ml
A2
pupation rate
1st day 2nd day 3rd day
cisplatin 1mg/ml
cisplatin 1mg/ml + cimetidine 20 mg/ml
A3
fly rate
1st day 2nd day 3rd day
cisplatin 1mg/ml
cisplatin 1mg/ml + cimetidine 20 mg/ml
B1
cut-GAL4
**
B2
B3
C1
drm-GAL4
C2
C3
D1
en-GAL4
D2
D3
E1
hh-GAL4
E2
E3
F
wild-type
*

Figure 31. Cimetidine did not rescue the effect of cisplatin on the hatching rate, pupation rate, and eclosion rate of embryos that express hOCT1 in different tissues. Flies were divided into two groups, one group was fed with cisplatin (1 mg/ml), and the other was fed with cisplatin and cimetidine (20 mg/ml). Embryos of both groups had similar hatching rates. N=1-4. The data were statistically analyzed by an independent sample Student's t-test.

3.3.2 The effect of cisplatin and cimetidine on embryo hatchability expressing hOCT1 in the nervous system

The drug-interaction assay was also conducted using the nervous system-specific GAL4 driver elav-GAL4. Females with this GAL4-driver were crossed with "humanized" hOCT1 males (UAS-hOCT1, UAS-GFP / + +). After feeding flies with cisplatin (1 mg/ml), embryo hatchability was less than 10%, only going up to about 25% on the sixth day. But in the cimetidine group, embryo hatchability significantly increased to about 40% - 60% except for the sixth day at which the difference was not significant (Fig. 32 A1).

The strong effect of cisplatin in this experiment suggested a maternal effect. To test this possibility, I repeated this experiment by crossing "humanized" hOCT1 flies (UAS-hOCT1, UAS-GFP / + +) as females with males harboring the elav-GAL4 driver. After feeding cisplatin, embryo hatchability was about 65% - 85%. In the cimetidine group, embryo hatchability had an increasing tendency, especially on the second day and the third day (Fig. 32 A2). To further test whether there was a maternal effect in elav-GAL4 driver females in the cisplatin group, respective females were crossed with UAS-CD8-RFP males as a control. About 40% of embryos hatched in the first three days; the number decreased to 10% from the fourth day on in the cisplatin group. Compared to this, there was an increasing tendency of hatching in the cimetidine group, especially on the fourth day and the fifth day (Fig. 32 B1). When female UAS-CD8-RFP flies were crossed with the elav-GAL4 driver males, about 45% - 75% of embryos hatched in the cisplatin group. After the co-feeding with cimetidine, embryo hatchability increased but this effect was not significant (Fig. 32 B2). These results indicated that cimetidine

counteracted cisplatin toxicity in embryos. However, this effect seems to be independent of hOCT1 expressed in the nervous system under the control of the elav-GAL4 driver. It was nevertheless interesting that elav-GAL4 females apparently were sensitive to cisplatin regarding the hatchability of their progeny.

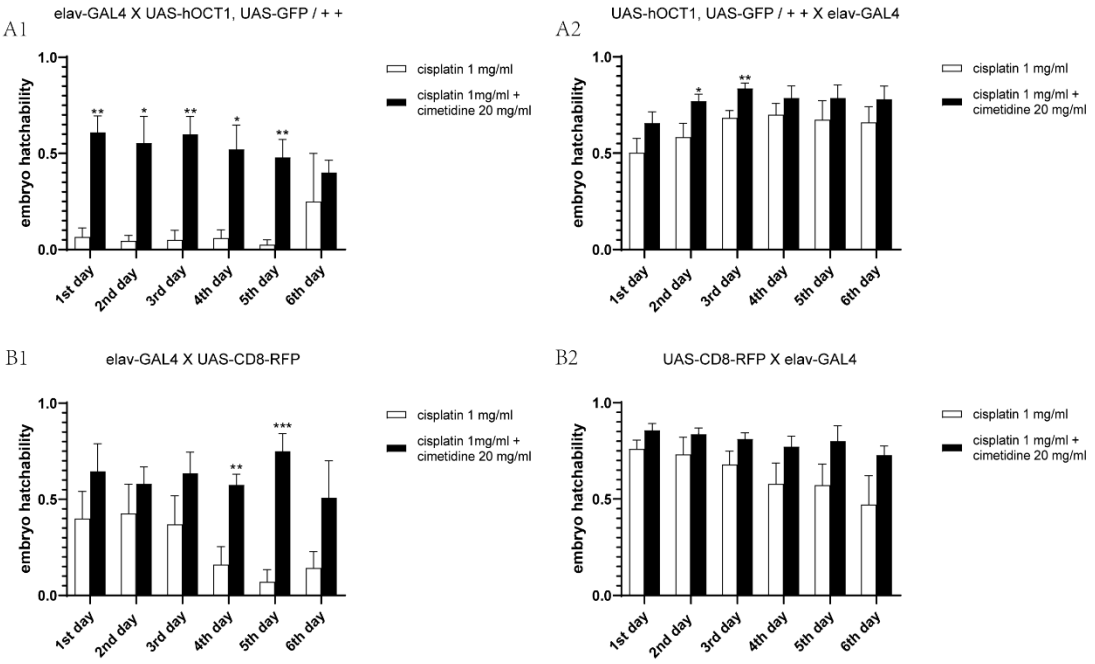

Figure 32. Cimetidine recovered the toxicity of cisplatin on the hatching rate of embryos with hOCT1 expressed in the nervous system under the control of the elav-GAL4 driver. Compared to the cisplatin group, the hatching rate increased significantly for embryos produced by flies with the elav-GAL4 driver as female or male crossed with “humanized” hOCT1 flies (UAS-hOCT1, UAS-GFP / + +) when additionally fed with cimetidine (A1, A2). However, when the elav-GAL4 driver was present in females, produced embryos died by about 90%. Less than 50% of control embryos (cisplatin only) laid by the elav-GAL4 driver as females crossed with UAS-CD8-RFP males hatched. Cimetidine tended to increase embryo hatchability irrespective of the sex of the fly harboring the elav-GAL4 driver (B1, B2). N=6. The data were statistically analyzed by independent sample Student’s t-test, asterisks indicate significant differences (*, $p < 0.05$; **, $p < 0.01$).

3.3.3 Cimetidine rescued the toxicity of cisplatin in embryos expressing hOCT1 in the nervous system under the control of the pros-GAL4 driver

In this chapter, I describe the drug-interaction assay that I performed with the nervous system driver pros-GAL4. In the cisplatin group, when females with the pros-GAL4 driver were crossed with “humanized” hOCT1 males (UAS-hOCT1, UAS-GFP / + +), embryo hatchability was about 50% decreasing to about 35% on the sixth day. Compared to this, cimetidine (20 mg/ml) significantly increased the hatching rate of embryos, especially on the second day, the third day and the sixth day. At a higher concentration of cimetidine (100 mg/ml), embryo hatchability increased significantly, compared to the control group. By contrast, I did not observe a hatchability difference between embryos fed with either higher or lower concentrations of cimetidine together with cisplatin (Fig. 33 A1). In the reciprocal experiment, when “humanized” hOCT1 females (UAS-hOCT1, UAS-GFP / + +) were crossed with the pros-GAL4 driver males, the hatching rate dropped from 75% on the first day to 45% on the sixth day. The lower and the higher concentration of cimetidine again tended to increase embryo hatchability compared to the cisplatin group. However, again, there was no significant difference between the two concentrations (Fig. 33 B1).

With these encouraging results, I extended my drug-interaction assay to another hOCT1 inhibitor, namely metformin, The combined use of metformin and cisplatin has been shown to have contradicting effects. Some evidence suggested that metformin could enhance the anticancer effect of cisplatin, while other studies indicated that metformin could reduce the side effects of cisplatin. After feeding flies with lower concentrations of metformin, 50% - 70% of the embryos produced by pros-GAL4 driver females crossed to “humanized” hOCT1 males (UAS-hOCT1, UAS-GFP / + +) hatched in the first 5 days, dropping to 35% in the sixth day. Compared to feeding flies cisplatin, embryo hatchability tended to increase on the first day, the second day and the fourth day, but not significantly. Feeding flies with higher concentrations of metformin, embryo hatchability tended to decrease (Fig. 33 A2).

In the reciprocal experiment, when “humanized” hOCT1 females (UAS-hOCT1, UAS-

GFP / + +) were crossed with pros-GAL4 driver males, compared to the cisplatin control group, hatchability of produced embryos at lower and higher concentrations of metformin was not different (Fig. 33 B2).

For a complete analysis, I needed to evaluate the effects of cimetidine or metformin alone on “humanized” hOCT1 embryos. When females with the pros-GAL4 driver were crossed with “humanized” hOCT1 males (UAS-hOCT1, UAS-GFP / + +) and fed with metformin or cimetidine, embryo hatchability was not changed compared to the control (Fig. 33 C1, C2). This result indicates that cimetidine and metformin do not have adverse effects on fly embryos.

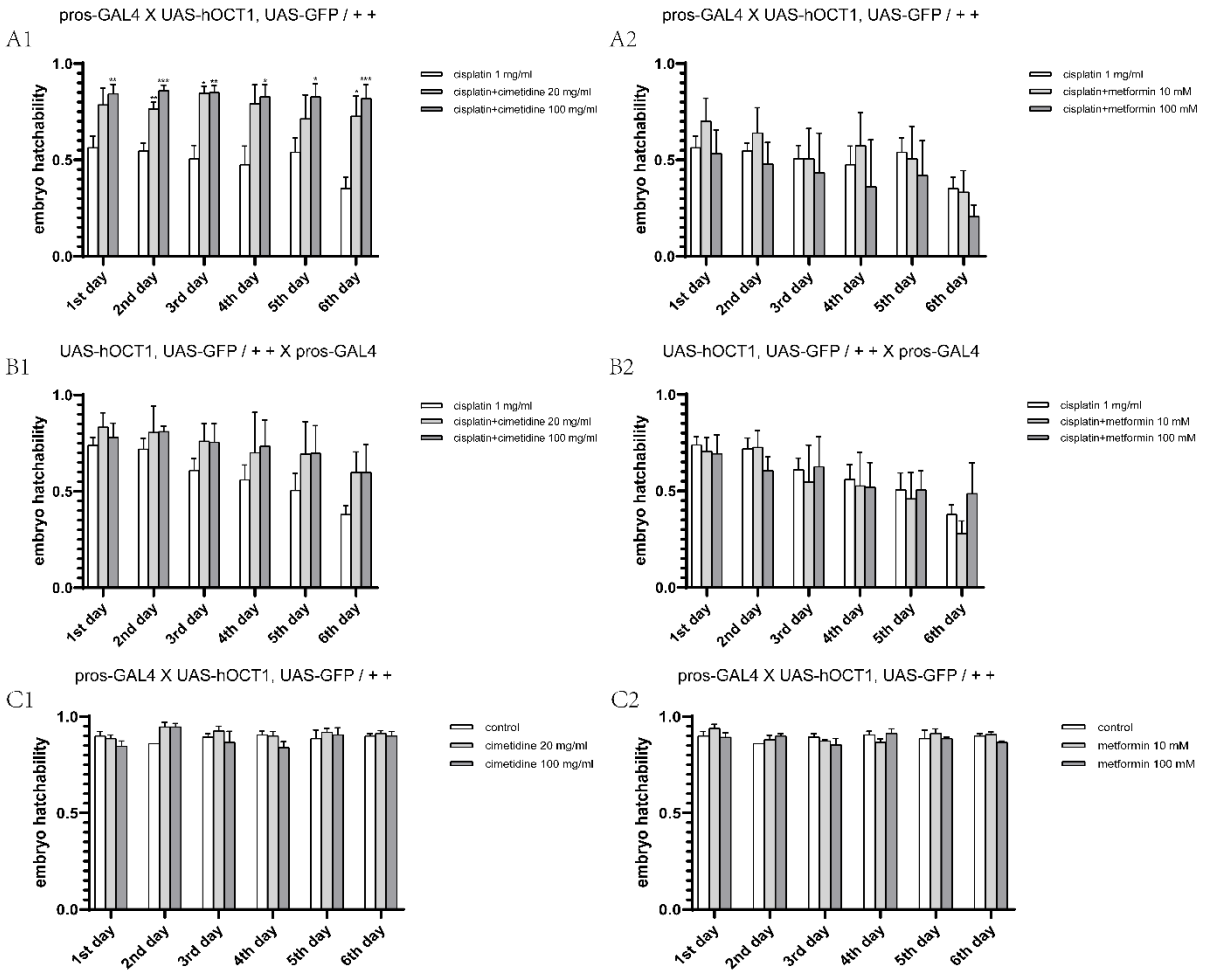

Figure 33. The effect of cimetidine and metformin on the toxicity of cisplatin on the embryonic hatching rate of hOCT1 expressed in the nervous system of the embryo. Compared to the cisplatin group, the lower and higher concentration of cimetidine increased the hatchability of embryos produced by pros-GAL4 flies crossed to “humanized” hOCT1 flies (UAS-hOCT1, UAS-GFP / + +). The effect was only significant when the pros-GAL4 driver was provided by females (A1, B1). Compared to the cisplatin group, after feeding higher or lower concentrations of metformin, embryos produced by flies with the pros-GAL4 driver crossed with “humanized” hOCT1 flies (UAS-hOCT1, UAS-GFP / + +) showed normal hatchability (A2, B2). Compared to the control, higher or lower concentrations of cimetidine or metformin did not affect the hatching of embryos produced by flies with the pros-GAL4 driver provided by females crossed with “humanized” hOCT1 males (UAS-hOCT1, UAS-GFP / + +) (C1, C2). N=4. The data were statistically analyzed by independent sample Student’s t-test, and asterisks indicate significant differences (*, $p < 0.05$; **, $p < 0.01$, ***, $p < 0.001$).

3.3.4 The expression pattern of pros-GAL4 in different stage embryos

The expression pattern of pros-GAL4 is not clearly described in the literature. As the drug-interaction assays using this GAL4-driver are promising, I sought to record the expression pattern of pros-GAL4 during embryogenesis. For this purpose, I crossed pros-GAL4 females to UAS-CD8-RFP males to detect CD8-RFP distribution by fluorescence microscopy. The stages of embryos were verified by bright-field microscopy (Fig. 34 A1, B1, C1, D1). A CD8-RFP signal was not detected in stage 13 - 14 embryos (Fig. 34 A2). However, in stage 15 embryos, a CD8-RFP signal was observed in a subset of cells in the nervous system; the signals became stronger as the embryo developed (Fig. 34 B2, C2, D2).

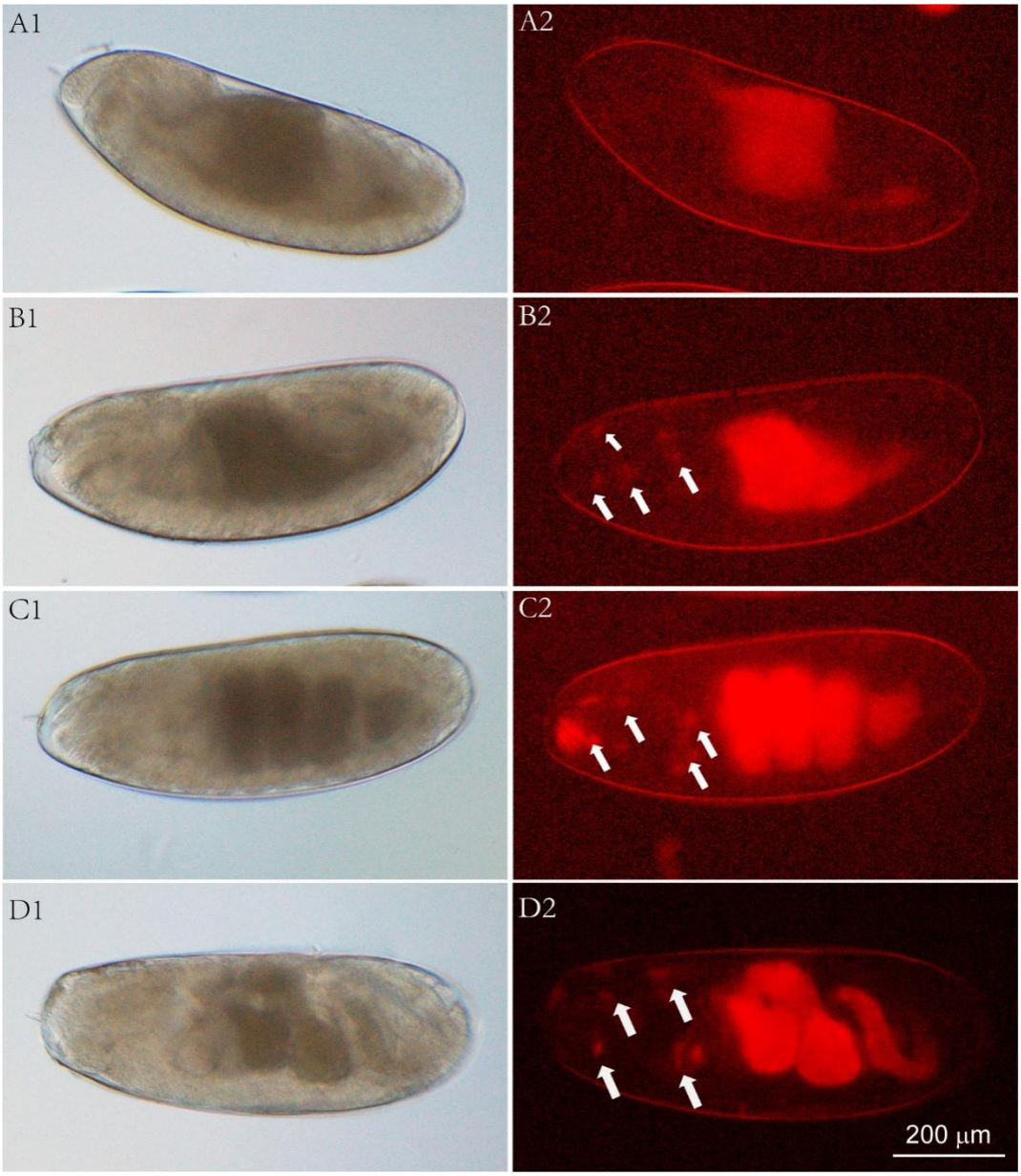

Figure 34. The expression pattern of pros-GAL4 in embryos at different stages. Stage 13-14, 15, 16, and 17 embryos (pros-GAL4, UAS-CD8-RFP) were observed by bright-field microscopy (A1, B1, C1, D1). The white arrow points to the position of CD8-RFP expression in stage 15,16 and 17 embryos (B2, C2, D2). Scale bar = 200 μm.

4 Discussion

My work is composed of three parts: first, I sought to analyze the functions of the human transporters hOATP1B1, hOATP2B1 and hOATP1B3 in fly embryos. Second, I studied the function of hOCT1 and ABCB1 in transporting their substrate ethidium across epithelial cells. Third, I performed preparatory experiments to establish a drug testing system based on hOCT1 in fly embryos.

4.1 hOATP1B1, hOATP2B1, and hOATP1B3 function in fly embryos

4.1.1 Epitope damage might affect the immune-detection of human transporters in the fly embryo

In this work, I generated transgenic flies with the human transporters hOATP1B1, hOATP2B1, and hOATP1B3. To detect their localization in the respective “humanized” transgenic embryos, immune-fluorescence experiments using specific antibodies were carried out. The anti-hOATP1B1 antibody only successfully recognized the transporter expressed in the oenocytes of fruit fly embryos; hOATP1B1 could not be detected in the salivary glands or in the tracheae. Similarly, the anti-hOATP1B3 antibody only successfully recognized the transporter expressed in the tracheae of embryos, hOATP1B3 could not be detected in the oenocytes or in the salivary gland cells. Finally, a signal could be observed in the oenocytes and tracheae after anti-hOATP2B1 antibody staining, but not in the salivary gland. Thus, at the first glance, the transgenic embryos successfully expressed the human transporters. Why is the epitope not detected in all tissues?

In *D. melanogaster* embryos, eggs contain three proteinaceous layers, the vitelline membrane, inner chorionic layer, and outer chorion (Papassideri et al., 1993). It has been reported that for antibody staining in embryos, fixatives were needed to permeate the waxy layer of the vitelline envelope (Papassideri et al., 1993). During embryo development, the follicle cells synthesize and secrete lipid vesicles to form a waxy

layer (Quattropani and Anderson, 1969, Mahowald, 1972, Waring and Mahowald, 1979, Margaritis et al., 1980, Margaritis, 1985). In stage 10 - 12 egg chambers, secreted lipids are assembled on the vitelline membrane, while at stage 13 - 14 egg chambers, because the lipid vesicles are pressed between the vitelline membrane and innermost chorionic layer, this waxy layer became thinner and harder (Papassideri et al., 1993). There are two fixation methods to overcome the complex architecture of the *D. melanogaster* egg: Formaldehyde-Based Fixation (FBF) and Heat-Methanol Fixation (HMF).

For FBF, 0.05% Tween-20 was added to the formaldehyde fixative to increase permeabilization by an improved extraction of cytosolic proteins and membrane lipids. Occasionally, there is an advantage of HMF, in which addition of methanol is thought to better preserve the epitope. However, the tissue structure is poorly preserved; especially following this process, cytosolic antigens will be rather extracted. Papassideri (Papassideri et al., 1993) compared FBF and HMF by applying anti-Neurotactin (NRT), anti-Armadillo (ARM) antibodies, and DAPI for embryos at post gastrulation stages. He found that plasma membranes were preserved better by FBF than by HMF. HMF caused loss of cytoplasmic ARM but detected ARM associated with adhesion junctions. Compared with HMF, the signal was more obvious by FBF. I supposed that according to these observations the localization of hOATP1B1 in the membrane of oenocytes cells was detected in embryos (bo-GAL4, UAS-hOATP1B1) only when they were fixed with formaldehyde.

However, in either method, FBF or HMF, applied for embryo fixation, methanol as fixative penetrates embryos, thereby affecting the antigenicity and the localization of proteins. Because the whole embryo was stained in my experiments, the structure of cells in the organs was not preserved well. In the process of fixation and labeling, the structure of cells was usually destroyed or extracted, especially for proteins in the membrane. So, the localization of antigens of whole embryos might not represent the precise subcellular localization. In summary, epitope damage in hOATP1B1, hOATP2B1, and hOATP1B3 might be a reason for the missing signal in the corresponding organ.

4.1.2 hOATP1B1-, hOATP2B1-, and hOATP1B3-RFP fusion proteins did not localize to their target tissues

Since the detection of hOATP1B1, hOATP2B1, and hOATP1B3 in the salivary glands of embryos expressing the respective genes was unsuccessful, flies were generated that express the hOATP1B1, hOATP2B1, or hOATP1B3 transporters fused to the red fluorescence protein (RFP) to localize hOATP1B1, hOATP2B1, and hOATP1B3 in the embryo. The signal was not detected in the salivary glands of embryos expressing the hOATP1B1-, hOATP2B1-, or hOATP1B3-RFP fusion protein in the salivary glands, while it was observed in the nervous system, the heart, and the anal pads of respective larvae. This finding is surprising as the respective GAL4 drivers are not active in these tissues. Similar results were found when embryos and larvae expressed hOATP1B1-, hOATP2B1-, or hOATP1B3-RFP fusion protein in the tracheae. What could be the reason for these results?

The *D. melanogaster* excretory system consists of nephrocytes and Malpighian tubules, which are responsible for filtration and reabsorption in the body (Denholm and Skaer, 2009). In 1889, Kowalevsky had first called nephrocytes as ‘storage kidneys’ that filter hemolymph before it is pumped into the heart, and store components from the hemolymph (Denholm and Skaer, 2009). The nephrocytes contain two kinds of cell types: pericardial nephrocytes that are positioned around the heart tube, and garland nephrocytes that are surrounding the esophagus (Zhang et al., 2013b). In the late-stage embryos, 120 pericardial cells have been observed around the heart. But only about 40 pericardial cells were detected in the larvae and adults (Sellin et al., 2006, Das et al., 2008).

The highly specialized filtration function of pericardial nephrocytes depends on the structure of the nephrocyte diaphragm, which is similar to glomerular podocytes of mammalians (Weavers et al., 2009, Zhang et al., 2013a). In 2013, Zhang and his colleagues found that secreted green fluorescent protein (GFP) could be taken up into the nephrocytes. Depending on this, they designed an experiment. When the UAS-GFP flies were crossed with tub-GAL4 flies, a GFP signal was detected in all tissue of

larvae. Later, in flies overexpressing GFP fused with the wingless secretion peptide (UAS-secr-GFP) crossed to tub-GAL4 flies, a signal was only found in the nephrocyte, which indicated that secreted GFP had been taken up into nephrocytes from circulating hemolymph. To further confirm this result, they overexpressed secreted GFP in different organs of larvae with six GAL4s. However, a signal was always observed in the nephrocyte suggesting the GFP fusion protein was transported from its original tissue to the nephrocytes. In our project, similar results were found that a signal was found in the heart, probably nephrocytes of larvae expressing hOATP1B1-, hOATP2B1-, or hOATP1B3-RFP fusion protein in the salivary glands and tracheae.

In *D. melanogaster* larvae, anal pads are a pair of symmetrical plates with a thin cuticle layer localized at the ventral side on the last segment and around the anus. They are involved in the process of ion transport and osmoregulation (Jarial, 1987). A role in excretion as for nephrocytes has not been described for this tissue. Further genetic and molecular studies are needed to elucidate the ectopic presence of hOATP1B1-, hOATP2B1-, or hOATP1B3-RFP fusion proteins in anal pads.

In *D. melanogaster*, the BBB consists of glial cells, which is a structure of selectively permeable barrier to regulate the concentration of various chemical components into the nervous system, such as nutrients, ions, toxins, and large molecules (Davis et al., 2019). Theoretically, hOATP1B1-, hOATP2B1-, or hOATP1B3-RFP fusion proteins as large molecules cannot be taken up into the nervous system across BBB. So, it is currently unclear why hOATP1B1-, hOATP2B1-, or hOATP1B3-RFP fusion protein were present in the nervous system of larvae.

Taken together, it is obvious that animals need to maintain the balance of the environment in the body by eliminating metabolic and foreign toxins with their excretory systems. For fly larvae, hOATP1B1-, hOATP2B1-, or hOATP1B3-RFP fusion proteins may have adverse effects that trigger their elimination through the excretory system possibly including unexpected tissues such as the glia cells and the anal pads. To verify this hypothesis, the trajectories of these proteins during excretion need to be analyzed in genetic and molecular experiments.

4.1.3 Fluorescent substrates were taken up into the lumen of salivary glands independently of hOATP1B1, hOATP2B1, and hOATP1B3

To characterize hOATP1B1, hOATP2B1, and hOATP1B3, I expressed the respective genes in the epithelial salivary glands. Four hours after injection of the fluorescent hOATP1B1, hOATP2B1, and hOATP1B3 substrates MDBF, DBF, and CLF into stage 15 - 16 embryos, the MDBF, DBF, and CLF signal was observed in the salivary gland lumen. However, these signals were also detected in the salivary gland lumen of control embryos.

D. melanogaster salivary glands only contain two major epithelial cell types: secretory cells and duct cells (Andrew et al., 2000, Bradley et al., 2001). Secretory cells are polarized columnar epithelial cells and are involved in synthesizing and secreting high levels of protein (Abrams et al., 2003). Polarization of these cells and of human hepatocytes, which express various human transporters, such as OATP1B1, OATP2B1, OATP1B3, ABCB1, and OCT1, is similar (Abrams et al., 2003, Schaeffeler et al., 2011, Nies et al., 2022). Thus, these cells may be equipped with various endogenous transporters. Based on this, I hypothesize that *D. melanogaster* transporters assist uptake of fluorescent substrates into the lumen of the salivary glands. However, there is no evidence that any *hOATP1B1*, *OATP2B1*, *or hOATP1B3* homologous gene or other human anion transporters homologous gene is expressed in the salivary glands of *D. melanogaster* embryos. Interestingly, after injecting MDBF, DBF, and CLF, some dye-containing vesicles in the epithelial cells of the salivary glands were detected. Therefore, alternatively to the transporter hypothesis, I suggest that fluorescent substrates were taken up into the lumen of the salivary glands by transcytosis. This issue merits detailed analyses in the next future.

At this point, I would like to emphasize that *in vitro*, DBF is taken up into the human embryonic kidney 293 cells expressing hOATP1B1, OATP2B1, and hOATP1B3. Especially in hOATP2B1-expressing cells, DBF was taken up 27-fold more than in control cells (Izumi et al., 2016). CLF is a fluorescent bile salt that plays an important role in evaluating liver function *in vivo* (Milkiewicz et al., 2000). Waart (de Waart et al.,

2010) found that CLF was taken up into OATP1B1- and OATP1B3-expressing CHO (Chinese hamster ovary) cells. Until today, however, there is no research showing the function of DBF and CLF in whole animals expressing hOATP1B1, OATP2B1, or hOATP1B3.

4.1.4 Fluorescent substrates were not taken up into the oenocytes by hOATP1B1, hOATP2B1, or hOATP1B3

The salivary gland and tracheal cells are epithelial. It is unlikely but possible that the hOATP localization in fly epithelial cells is compromised but not in non-epithelial cells. To test this hypothesis, I assayed dye uptake by hOATP1B1, hOATP2B1, and hOATP1B3 in non-epithelial oenocytes. Four hours after injection into respective embryos, neither MDBF, nor DBF, nor CLF was observed in the oenocytes of these embryos. Similarly, after injection of MDBF, DBF, and CLF, no signal was detected in negative control embryos.

In *D. melanogaster*, the oenocytes play an important role in lipid metabolism. The oenocytes are assembled into individual groups of cells, which are distributed at a characteristic lateral and subepidermal positions in each hemi-segment in the mature embryos. The cell number of each cell group of oenocytes is about 4 - 9, with an average of 6 (Elstob et al., 2001). Oenocytes are considered as a human liver homolog, encoding at least 22 genes with fat-metabolic function present also in human hepatocytes (Gutierrez et al., 2007). The central question to me is of course: are the oenocytes competent to take up substrates from the haemolymph? Indy (I'm not dead yet) is a sodium dicarboxylate cotransporter that is expressed in the oenocytes but also in the midgut and the fat body, in *D. melanogaster* (Rogina et al., 2000, Knauf et al., 2002). In mammals, sodium dicarboxylate cotransporter SLC13A5 belongs to the SLC13 family, which shows significant homology (34% identity) with Indy (Knauf et al., 2002, Bergeron et al., 2013). Like the mammalian sodium dicarboxylate cotransporter SLC13A5, Indy selectively transports the same substrates. Studies have shown that Indy transports succinate, α-ketoglutarate, fumarate, glutarate, and citrate, but not

pyruvate or lactate (Knauf et al., 2002). To date, no evidence suggests that Indy or mammalian sodium dicarboxylate SLC13A5 have an affinity for MDBF, DBF, or CLF. This is supported by the fact that these fluorescent substrates did not accumulate in the oenocytes.

4.1.5 Fluorescent substrates were taken up into the tracheae independently of hOATP1B1, hOATP2B1, or hOATP1B3

Four hours after injection into respective embryos, MDBF, DBF, and CLF signals were detected not only in the tracheae of these embryos but also in control embryos.

In *D. melanogaster*, the tracheal system is a respiratory organ and consists of a network of epithelial branched tubules, which are involved in transporting oxygen to different specific organs (Affolter and Caussinus, 2008, Schottenfeld et al., 2010). The tracheae begins to develop at stage 10 of the embryos, which has 10 pairs of tracheal placodes, that is one per hemi segment (Hayashi and Kondo, 2018). The tubes of tracheal branches are formed by a monolayer of epithelial cells (Ghabrial et al., 2003). In *D. melanogaster*, Serpentine (Serp) as a chitin deacetylase plays a vital role in maintaining tracheal tube morphogenesis (Luschnig et al., 2006). Both overexpression and reduction of Serp expression in the tracheae induces abnormal morphogenesis of the tracheae (Luschnig et al., 2006, Wang et al., 2006). Dong (Dong et al., 2014) demonstrated that Serp expressed in the fat body was secreted into the haemolymph, and was taken up into the tracheal lumen by the tracheal cells. Their further experiments showed that Serp may cross epithelial barriers into the tracheal lumen by transcytosis. Based on this, I hypothesize that MDBF, DBF, and CLF were taken up into the lumen of the tracheae across epithelial barriers through transcytosis similarly to the situation in salivary glands.

Alternatively, these fluorescent compounds might be transported by endogenous fly transporters.

4.1.6 *Drosophila oatps* have redundant functions in the fly larvae

Since my data suggest that probably *D. melanogaster* Oatps are involved in assisting fluorescent substrate uptake into the lumen of the salivary glands and the tracheal system of embryos, 13 *oatp* RNAi lines directed against eight *oatps* were used to target the expression of these *oatps* to examine their function in this process. After feeding first instar larvae expressing any of the *oatp* RNAi with MDBF for about 15 h, a signal was observed in the gut and the Malpighian tubules that was also found in control larvae.

In *D. melanogaster*, there are eight genes (*Oatp26F, Oatp30B, Oatp33Ea, Oatp33Eb, Oatp58Da, Oatp58Db, Oatp58Dc, Oatp74D*) coding for Oatps, of which four are expressed in the gut (Oatp30B, Oatp33Ea, Oatp33Eb, Oatp74D) and six (Oatp30B, Oatp33Eb, Oatp58Da, Oatp58Db, Oatp58Dc, Oatp74D) in the Malpighian tubules. Therefore, I propose that when one single *Oatp* gene was knocked down, other *Oatp* genes may be present to assist MDBF transport into the gut and Malpighian tubules.

Besides *Oatp* genes, there are other *SLC* genes expressed in the gut and Malpighian tubules of *D. melanogaster*. Salt is the Na+-dependent transporter and is predicted to have moderate homology with human SLC5 members (SLC5A5, SLC5A6, SLC5A8, and SLC5A12), which are involved in the uptake of substrates including biotin, pantothenate, and iodide (Wright, 2013). Prestin, an anion transporter, plays an important role in the transport of monovalent and divalent anions, such as sulfate, chloride, iodide, and formate (Mount and Romero, 2004). It is homologous to the human transporters SLC26A4, SLC26A5, and SLC26A6. In addition to the Oatps, I hypothesize that these SLCs transporters may be involved in transporting MDBF into the gut and Malpighian tubules.

According to these, I concluded that Oatp and other SLC transporters might cooperate to assist MDBF transport into the gut and Malpighian tubules of *oatp* RNAi larvae. Thus, more RNAi experiments with combined knockdowns are needed to clarify this point.

4.2 The function of hOCT1 and hABCB1 in fly embryos

A central aim of this thesis was to establish a transport system across epithelial cells in the fly embryo using human transporters. At first, I repeated our previous work on hOCT1 expressed in the basal plasma membrane of salivary gland epithelial cells. After injection of EtBr into embryos, as expected, Et+ was detected in the cells of the salivary glands. This result, suggesting that human transporters are active in the fly, inspired us to further study the cooperation between hOCT1 and hABCB1, which is the transporter at the apical plasma membrane that is needed for the efflux of substrates taken up by hOCT1. I hypothesized that in this constellation, Et+ would be taken up from the hemolymph into the cells by hOCT1 and delivered to the lumen of the salivary glands by hABCB1. Unfortunately, after Et+ was accumulated within the cells of the salivary glands by hOCT1, it was not exported into the lumen by hABCB1. When rhodamine 123, which is another substrate of hOCT1 and hABCB1 (reference PMID 22913740), was injected into embryos, it was not detected in the salivary gland lumen. Similar results were obtained when instead of the salivary glands the tracheal epithelium was used as a target tissue for hOCT1 and hABCB1 expression.

Obviously, in the *D. melanogaster* embryos, hABCB1 did not exert its function. One reason could be that *hABCB1* gene expression levels were not high in the tested embryos. Transcript levels of the *hABCB1* gene were 4-8 times higher in these embryos compared to wild-type Dijon embryos, while the *hOCT1* mRNA levels were about 1300 times higher than in wild-type Dijon embryos.

Indeed, there is evidence that transcript levels matter. Imatinib, a tyrosine kinase inhibitor, which is not a substrate of hOCT1 (Neul et al., 2016), is an effective drug against chronic myeloid leukemia (Malhotra et al., 2015). After oral intake, it is absorbed into the enterocytes of the intestine and hepatocytes of the liver and secreted depending on efflux transporters such as hABCB1 (Kumar et al., 2022). Results indicated that low expression of ABCB1 mRNA in patients would lead to a significant increase in imatinib levels within peripheral blood mononuclear cells (Rajamani et al., 2020). Therefore, the transcription levels of transporters are essential

for the amount of substrate accumulated in the cell.

Alternatively, hABCB1 in the *D. melanogaster* embryos may be non-functional due to incorrect processing in the rough endoplasmic reticulum (ER) and the Golgi apparatus. Before a translated polypeptide becomes a functional protein, it needs to be further glycosylated and folded. hABCB1 is a polypeptide with 1280 amino acids. As a 150 kDa polypeptide precursor, it is synthesized on the rough ER. In the ER lumen, hABCB1 is correctly folded assisted by calnexin and Hsc70. Next, it is transferred to the Golgi apparatus to further glycosylation (N-glycans) to become a 170 kDa mature protein (Hano et al., 2018). Thus, hABCB1 is a heavily glycosylated protein (Greer and Ivey, 2007). Overall, N-glycosylation is essential during post-translational modifications of proteins in the secretory pathway. This step requires the catalysis of various glycosidases and glycosyltransferases. It begins at the endoplasmic reticulum and ends at the Golgi apparatus (Zhang and Wang, 2016). Therefore, the process of N-glycosylation is complex. If an error occurs during this time, the functionality of hABCB1 may be affected. Although some types of N-glycan structures are conserved between *Drosophila* and humans even though they share some similar substrate specificities, there are only half the number of glycosyltransferases in *Drosophila* compared to humans (Nishihara, 2020). Therefore, when the hABCB1 polypeptide is translated in *Drosophila* embryos, the subsequent N-glycosylation process may show differences from that performed in humans. This may eventually cause hABCB1 not to be active in the fly embryos.

Taken together, hABCB1 expressed in *Drosophila* embryos did not show the expected function. These results indicate that not all human transporters could be studied in *Drosophila*. However, the results of hOCT1 were promising so that I continued to study the function of OCT in drug-drug interaction assays.

4.3 Drug interaction assays in hOCT1 expressing embryos

Cisplatin has been demonstrated to be the first metal-based chemotherapeutic drug that was widely used against various cancers, such as cervical cancer, melanoma,

lymphomas, testicular, ovarian, lung, and other cancers (Dasari and Tchounwou, 2014, Ho et al., 2016). It binds to DNA to induce DNA lesions and arrest DNA replication, which activate some signal transduction pathways that trigger apoptosis (Jordan and Carmo-Fonseca, 2000, Aryal et al., 2010). Cisplatin are suitable substrates for hOCT1 and hOCT2 (Yonezawa et al., 2006). Lin (Lin et al., 2013) found that apoptosis induced by cisplatin of esophageal cancer cells was affected when hOCT1 was silenced. The effects of cisplatin may be counteracted by a group of drugs including cimetidine and metformin. Cimetidine is considered as an additive of chemotherapeutic drugs because it decreases the side effects of cisplatin by an interaction on the molecular level (Ciarimboli et al., 2010, Katsuda et al., 2010, Brauckmann et al., 2013). Ding (Ding et al., 2011) found, for instance, that cimetidine reduced hair cell loss mediated by cisplatin. Metformin is described as a drug against type 2 diabetes, but there is increasing evidence suggesting an effect of metformin as an anti-cancer drug (Emami Riedmaier et al., 2013).The uptake of metformin into the cell relies on membrane transporters including hOCT1 (Nies et al., 2022). Studying the molecular mechanisms of metformin activity is complicated because it shows different effects when it is combined with other anti-cancer drugs (Peng et al., 2017). A study showed that metformin alleviates genotoxicity and apoptosis in cells of rat bone marrow after using cisplatin (Cheki et al., 2021). However, other data indicated that metformin enhance apoptosis in tumors after cisplatin treatment (Moro et al., 2018).

Here, to establish a drug interaction system based on hOCT1 function, I used seven GAL4s to express hOCT1 in different organs including the salivary glands, oenocytes, tracheae, fat body, nervous system, and the gut in order to analyze cisplatin toxicity in dependence of hOCT1 in *D. melanogaster*. After feeding flies cisplatin, as expected, about half of the respective embryos (harboring GAL4 and hOCT1) that were produced by “humanized” hOCT1 flies crossed with different GAL4 (except elav-GAL4) flies hatched. This result suggested that cisplatin was taken up into the cell of embryos expressing hOCT1, thereby exerting its lethal effects. When crossing “humanized” hOCT1 flies with the different GAL4 (fkh-, cut-, drm-, en-, hh-, elav-, pros-GAL4) flies fed with cisplatin and cimetidine simultaneously, cimetidine significantly increased the

hatching rate of embryos only under the control of elav-GAL4 and pros-GAL4 drivers. In other words, cimetidine rescued the toxicity of cisplatin in embryos expressing hOCT1 in the nervous system under the control of the elav-GAL4 and pros-GAL4 driver. Metformin failed to have a clear effect. In fact, in my work, different concentrations of metformin showed a tendency of enhanced or attenuated cisplatin-induced embryo lethality. Based on these results, I hypothesize that in the fly, metformin activity is concentration dependent. Elucidation of this effect requires further studies. These results allowed two important conclusions: 1) *D. melanogaster* embryos produced by females fed with cisplatin are sensitive to cisplatin; 2) Compared to the other tissues, the nervous system (as represented by elav- and pros-GAL4 expression) seems to be sensitive to the effects of cimetidine on cisplatin toxicity. Based on my data, I hypothesize that cimetidine is efficiently taken up by some cells of the nervous system, while uptake into other types of tissues is less efficient.

What are these cells in the nervous system that are cisplatin- and cimetidine-sensitive? The gene *elav* is expressed in neurons during neural development. It plays an important role in neuronal differentiation and the maintenance of the nervous system in adults (Robinow and White, 1988, Robinow and White, 1991, Yao et al., 1993). Prospero (Pros) is localized in a subset of neuroblasts and ganglion mother cells (GMCs), but not in neurons *per se* (Chu-Lagraff et al., 1991). It regulates the different fates of neuroblast cell lineages and the specification of GMCs during development (Karcavich, 2005). Cells expressing elav- or pros-GAL4 need to be characterized and more in detail.

In summary, my data indicate that cisplatin could be taken up into the embryos by hOCT1 and that it was embryonic lethal, a phenotype that could be rescued by the addition of cimetidine. Although the exact molecular mechanisms remain unclear and require further experiments, this test system provides a good model to study drug-drug interactions and the molecular mechanism of drug function. Because using *D. melanogaster* is ethically unproblematic and cheap compared to conventional assays this test system might be helpful in the future to monitor potential hOCT1 inhibitors alleviating or enhancing cisplatin toxicity.

5. References

ABRAMS, E. W., VINING, M. S. & ANDREW, D. J. 2003. Constructing an organ: the Drosophila salivary gland as a model for tube formation. *Trends Cell Biol,* 13**,** 247-54.

AFFOLTER, M. & CAUSSINUS, E. 2008. Tracheal branching morphogenesis in Drosophila: new insights into cell behaviour and organ architecture. *Development,* 135**,** 2055-64.

AHLIN, G., KARLSSON, J., PEDERSEN, J. M., GUSTAVSSON, L., LARSSON, R., MATSSON, P., NORINDER, U., BERGSTRöM, C. A. & ARTURSSON, P. 2008. Structural requirements for drug inhibition of the liver specific human organic cation transport protein 1. *J Med Chem,* 51**,** 5932-42.

AMBUDKAR, S. V., KIM, I. W. & SAUNA, Z. E. 2006. The power of the pump: mechanisms of action of P-glycoprotein (ABCB1). *Eur J Pharm Sci,* 27**,** 392-400.

ANDREEV, E., BROSSEAU, N., CARMONA, E., MES-MASSON, A. M. & RAMOTAR, D. 2016. The human organic cation transporter OCT1 mediates high affinity uptake of the anticancer drug daunorubicin. *Sci Rep,* 6**,** 20508.

ANDREW, D. J., HENDERSON, K. D. & SESHAIAH, P. 2000. Salivary gland development in Drosophila melanogaster. *Mech Dev,* 92**,** 5-17.

ARIMANY-NARDI, C., KOEPSELL, H. & PASTOR-ANGLADA, M. 2015. Role of SLC22A1 polymorphic variants in drug disposition, therapeutic responses, and drug-drug interactions. *Pharmacogenomics J,* 15**,** 473-87.

ARYAL, S., HU, C. M. & ZHANG, L. 2010. Polymer--cisplatin conjugate nanoparticles for acid-responsive drug delivery. *ACS Nano,* 4**,** 251-8.

BECKER, M. L., VISSER, L. E., VAN SCHAIK, R. H., HOFMAN, A., UITTERLINDEN, A. G. & STRICKER, B. H. 2011. OCT1 polymorphism is associated with response and survival time in anti-Parkinsonian drug users. *Neurogenetics,* 12**,** 79-82.

BERGERON, M. J., CLéMENçON, B., HEDIGER, M. A. & MARKOVICH, D. 2013. SLC13 family of Na^+-coupled di- and tri-carboxylate/sulfate transporters. *Mol Aspects Med,* 34**,** 299-312.

BISCHOF, J., MAEDA, R. K., HEDIGER, M., KARCH, F. & BASLER, K. 2007. An optimized transgenesis system for Drosophila using germ-line-specific phiC31 integrases. *Proc Natl Acad Sci U S A,* 104**,** 3312-7.

BOXBERGER, K. H., HAGENBUCH, B. & LAMPE, J. N. 2014. Common drugs inhibit human organic cation transporter 1 (OCT1)-mediated neurotransmitter uptake. *Drug Metab Dispos,* 42**,** 990-5.

BRADLEY, P. L., HABERMAN, A. S. & ANDREW, D. J. 2001. Organ formation in Drosophila: specification and morphogenesis of the salivary gland. *Bioessays,* 23**,** 901-11.

BRAND, A. H. & PERRIMON, N. 1993. Targeted gene expression as a means of altering cell fates and generating dominant phenotypes. *Development,* 118**,** 401-15.

BRAUCKMANN, C., FABER, H., LANVERS-KAMINSKY, C., SPERLING, M. & KARST, U. 2013. Influence of cimetidine and its metabolites on Cisplatin--investigation of adduct formation by means of electrochemistry/liquid chromatography/electrospray mass spectrometry. *J Chromatogr A,* 1279**,** 49-57.

BREIDERT, T., SPITZENBERGER, F., GRüNDEMANN, D. & SCHöMIG, E. 1998. Catecholamine transport by the organic cation transporter type 1 (OCT1). *Br J Pharmacol,* 125**,** 218-24.

BRIZ, O., ROMERO, M. R., MARTINEZ-BECERRA, P., MACIAS, R. I., PEREZ, M. J., JIMENEZ, F., SAN MARTIN, F. G. & MARIN, J. J. 2006. OATP8/1B3-mediated cotransport of bile acids and glutathione: an export pathway for organic anions from hepatocytes? *J Biol Chem,* 281**,** 30326-35.

BRIZ, O., SERRANO, M. A., MACIAS, R. I., GONZALEZ-GALLEGO, J. & MARIN, J. J. 2003. Role of organic

anion-transporting polypeptides, OATP-A, OATP-C and OATP-8, in the human placenta-maternal liver tandem excretory pathway for foetal bilirubin. *Biochem J,* 371**,** 897-905.

BRUHN, O. & CASCORBI, I. 2014. Polymorphisms of the drug transporters ABCB1, ABCG2, ABCC2 and ABCC3 and their impact on drug bioavailability and clinical relevance. *Expert Opin Drug Metab Toxicol,* 10**,** 1337-54.

CASCORBI, I. 2011. P-glycoprotein: tissue distribution, substrates, and functional consequences of genetic variations. *Handb Exp Pharmacol***,** 261-83.

CASTRO, J. P. & CARARETO, C. M. 2004. Drosophila melanogaster P transposable elements: mechanisms of transposition and regulation. *Genetica,* 121**,** 107-18.

CHAE, Y. J., LEE, K. R., LEE, J. H., LEE, W., KIM, D. D., CHUNG, S. J. & MAENG, H. J. 2017. Feasibility of the functional expression of the human organic anion transporting polypeptide 1B1 (OATP1B1) and its genetic variant 521T/C in the mouse liver. *Eur J Pharm Sci,* 96**,** 28-36.

CHEKI, M., GHASEMI, M. S., REZAEI RASHNOUDI, A. & ERFANI MAJD, N. 2021. Metformin attenuates cisplatin-induced genotoxicity and apoptosis in rat bone marrow cells. *Drug Chem Toxicol,* 44**,** 386-393.

CHEN, L., PAWLIKOWSKI, B., SCHLESSINGER, A., MORE, S. S., STRYKE, D., JOHNS, S. J., PORTMAN, M. A., CHEN, E., FERRIN, T. E., SALI, A. & GIACOMINI, K. M. 2010. Role of organic cation transporter 3 (SLC22A3) and its missense variants in the pharmacologic action of metformin. *Pharmacogenet Genomics,* 20**,** 687-99.

CHEN, L., SHU, Y., LIANG, X., CHEN, E. C., YEE, S. W., ZUR, A. A., LI, S., XU, L., KESHARI, K. R., LIN, M. J., CHIEN, H. C., ZHANG, Y., MORRISSEY, K. M., LIU, J., OSTREM, J., YOUNGER, N. S., KURHANEWICZ, J., SHOKAT, K. M., ASHRAFI, K. & GIACOMINI, K. M. 2014. OCT1 is a high-capacity thiamine transporter that regulates hepatic steatosis and is a target of metformin. *Proc Natl Acad Sci U S A,* 111**,** 9983-8.

CHIEN, S., REITER, L. T., BIER, E. & GRIBSKOV, M. 2002. Homophila: human disease gene cognates in Drosophila. *Nucleic Acids Res,* 30**,** 149-51.

CHINTAPALLI, V. R., WANG, J. & DOW, J. A. 2007. Using FlyAtlas to identify better Drosophila melanogaster models of human disease. *Nat Genet,* 39**,** 715-20.

CHU-LAGRAFF, Q., WRIGHT, D. M., MCNEIL, L. K. & DOE, C. Q. 1991. The prospero gene encodes a divergent homeodomain protein that controls neuronal identity in Drosophila. *Dev Suppl,* Suppl 2**,** 79-85.

CHU, X., PHILIP, G. & EVERS, R. 2012. Comments on Mougey et al. (2009): Absorption of montelukast is transporter mediated: a common variant of OATP2B1 is associated with reduced plasma concentrations and poor response. Pharmacogenet Genomics 19: 129-138. *Pharmacogenet Genomics,* 22**,** 319-22.

CIARIMBOLI, G., DEUSTER, D., KNIEF, A., SPERLING, M., HOLTKAMP, M., EDEMIR, B., PAVENSTäDT, H., LANVERS-KAMINSKY, C., AM ZEHNHOFF-DINNESEN, A., SCHINKEL, A. H., KOEPSELL, H., JüRGENS, H. & SCHLATTER, E. 2010. Organic cation transporter 2 mediates cisplatin-induced oto- and nephrotoxicity and is a target for protective interventions. *Am J Pathol,* 176**,** 1169-80.

CORDóN-CARDO, C., CASALS MARULL, D. & GUIX PERICAS, M. 1989. [Antigenic determinants in blood groups: past, present and future]. *Med Clin (Barc),* 93**,** 64-7.

CREWS, S. T. 2010. Axon-glial interactions at the Drosophila CNS midline. *Cell Adh Migr,* 4**,** 67-71.

DAS, D., ARADHYA, R., ASHOKA, D. & INAMDAR, M. 2008. Post-embryonic pericardial cells of Drosophila are required for overcoming toxic stress but not for cardiac function or adult development. *Cell*

Tissue Res, 331**,** 565-70.

DASARI, S. & TCHOUNWOU, P. B. 2014. Cisplatin in cancer therapy: molecular mechanisms of action. *Eur J Pharmacol,* 740**,** 364-78.

DAVIS, M. J., TALBOT, D. & JEMC, J. 2019. Assay for Blood-brain Barrier Integrity in Drosophila melanogaster. *J Vis Exp*.

DE GOOIJER, M. C., KEMPER, E. M., BUIL, L. C. M., CITIRIKKAYA, C. H., BUCKLE, T., BEIJNEN, J. H. & VAN TELLINGEN, O. 2021. ATP-binding cassette transporters restrict drug delivery and efficacy against brain tumors even when blood-brain barrier integrity is lost. *Cell Rep Med,* 2**,** 100184.

DE WAART, D. R., HäUSLER, S., VLAMING, M. L., KUNNE, C., HäNGGI, E., GRUSS, H. J., OUDE ELFERINK, R. P. & STIEGER, B. 2010. Hepatic transport mechanisms of cholyl-L-lysyl-fluorescein. *J Pharmacol Exp Ther,* 334**,** 78-86.

DEAN, M., RZHETSKY, A. & ALLIKMETS, R. 2001. The human ATP-binding cassette (ABC) transporter superfamily. *Genome Res,* 11**,** 1156-66.

DEGORTER, M. K., HO, R. H., LEAKE, B. F., TIRONA, R. G. & KIM, R. B. 2012. Interaction of three regiospecific amino acid residues is required for OATP1B1 gain of OATP1B3 substrate specificity. *Mol Pharm,* 9**,** 986-95.

DENHOLM, B. & SKAER, H. 2009. Bringing together components of the fly renal system. *Curr Opin Genet Dev,* 19**,** 526-32.

DEWANJEE, S., DUA, T. K., BHATTACHARJEE, N., DAS, A., GANGOPADHYAY, M., KHANRA, R., JOARDAR, S., RIAZ, M., FEO, V. & ZIA-UL-HAQ, M. 2017. Natural Products as Alternative Choices for P-Glycoprotein (P-gp) Inhibition. *Molecules,* 22.

DIETZL, G., CHEN, D., SCHNORRER, F., SU, K. C., BARINOVA, Y., FELLNER, M., GASSER, B., KINSEY, K., OPPEL, S., SCHEIBLAUER, S., COUTO, A., MARRA, V., KELEMAN, K. & DICKSON, B. J. 2007. A genome-wide transgenic RNAi library for conditional gene inactivation in Drosophila. *Nature,* 448**,** 151-6.

DING, D., HE, J., ALLMAN, B. L., YU, D., JIANG, H., SEIGEL, G. M. & SALVI, R. J. 2011. Cisplatin ototoxicity in rat cochlear organotypic cultures. *Hear Res,* 282**,** 196-203.

DONG, B., MIAO, G. & HAYASHI, S. 2014. A fat body-derived apical extracellular matrix enzyme is transported to the tracheal lumen and is required for tube morphogenesis in Drosophila. *Development,* 141**,** 4104-9.

DUFFY, J. B. 2002. GAL4 system in Drosophila: a fly geneticist's Swiss army knife. *Genesis,* 34**,** 1-15.

ELSTOB, P. R., BRODU, V. & GOULD, A. P. 2001. spalt-dependent switching between two cell fates that are induced by the Drosophila EGF receptor. *Development,* 128**,** 723-32.

EMAMI RIEDMAIER, A., FISEL, P., NIES, A. T., SCHAEFFELER, E. & SCHWAB, M. 2013. Metformin and cancer: from the old medicine cabinet to pharmacological pitfalls and prospects. *Trends Pharmacol Sci,* 34**,** 126-35.

FAN, X., BAI, J., HU, M., XU, Y., ZHAO, S., SUN, Y., WANG, B., HU, J. & LI, Y. 2020. Drug interaction study of flavonoids toward OATP1B1 and their 3D structure activity relationship analysis for predicting hepatoprotective effects. *Toxicology,* 437**,** 152445.

FISCHER, J. A., GINIGER, E., MANIATIS, T. & PTASHNE, M. 1988. GAL4 activates transcription in Drosophila. *Nature,* 332**,** 853-6.

FISH, M. P., GROTH, A. C., CALOS, M. P. & NUSSE, R. 2007. Creating transgenic Drosophila by microinjecting the site-specific phiC31 integrase mRNA and a transgene-containing donor plasmid. *Nat Protoc,* 2**,** 2325-31.

FOHNER, A. E., BRACKMAN, D. J., GIACOMINI, K. M., ALTMAN, R. B. & KLEIN, T. E. 2017. PharmGKB

summary: very important pharmacogene information for ABCG2. *Pharmacogenet Genomics,* 27**,** 420-427.

FULKERSON, E. & ESTES, P. A. 2011. Common motifs shared by conserved enhancers of Drosophila midline glial genes. *J Exp Zool B Mol Dev Evol,* 316**,** 61-75.

FUNK, C. 2008. The role of hepatic transporters in drug elimination. *Expert Opin Drug Metab Toxicol,* 4**,** 363-79.

GANGISHETTI, U., BREITENBACH, S., ZANDER, M., SAHEB, S. K., MüLLER, U., SCHWARZ, H. & MOUSSIAN, B. 2009. Effects of benzoylphenylurea on chitin synthesis and orientation in the cuticle of the Drosophila larva. *Eur J Cell Biol,* 88**,** 167-80.

GAO, B., VAVRICKA, S. R., MEIER, P. J. & STIEGER, B. 2015. Differential cellular expression of organic anion transporting peptides OATP1A2 and OATP2B1 in the human retina and brain: implications for carrier-mediated transport of neuropeptides and neurosteriods in the CNS. *Pflugers Arch,* 467**,** 1481-1493.

GHABRIAL, A., LUSCHNIG, S., METZSTEIN, M. M. & KRASNOW, M. A. 2003. Branching morphogenesis of the Drosophila tracheal system. *Annu Rev Cell Dev Biol,* 19**,** 623-47.

GIACOMINI, K. M., HUANG, S. M., TWEEDIE, D. J., BENET, L. Z., BROUWER, K. L., CHU, X., DAHLIN, A., EVERS, R., FISCHER, V., HILLGREN, K. M., HOFFMASTER, K. A., ISHIKAWA, T., KEPPLER, D., KIM, R. B., LEE, C. A., NIEMI, M., POLLI, J. W., SUGIYAMA, Y., SWAAN, P. W., WARE, J. A., WRIGHT, S. H., YEE, S. W., ZAMEK-GLISZCZYNSKI, M. J. & ZHANG, L. 2010. Membrane transporters in drug development. *Nat Rev Drug Discov,* 9**,** 215-36.

GILLIGAN, L. C., GONDAL, A., TANG, V., HUSSAIN, M. T., ARVANITI, A., HEWITT, A. M. & FOSTER, P. A. 2017. Estrone Sulfate Transport and Steroid Sulfatase Activity in Colorectal Cancer: Implications for Hormone Replacement Therapy. *Front Pharmacol,* 8**,** 103.

GINIGER, E., VARNUM, S. M. & PTASHNE, M. 1985. Specific DNA binding of GAL4, a positive regulatory protein of yeast. *Cell,* 40**,** 767-74.

GLAESER, H., BAILEY, D. G., DRESSER, G. K., GREGOR, J. C., SCHWARZ, U. I., MCGRATH, J. S., JOLICOEUR, E., LEE, W., LEAKE, B. F., TIRONA, R. G. & KIM, R. B. 2007. Intestinal drug transporter expression and the impact of grapefruit juice in humans. *Clin Pharmacol Ther,* 81**,** 362-70.

GONG, I. Y. & KIM, R. B. 2013. Impact of genetic variation in OATP transporters to drug disposition and response. *Drug Metab Pharmacokinet,* 28**,** 4-18.

GORBOULEV, V., ULZHEIMER, J. C., AKHOUNDOVA, A., ULZHEIMER-TEUBER, I., KARBACH, U., QUESTER, S., BAUMANN, C., LANG, F., BUSCH, A. E. & KOEPSELL, H. 1997. Cloning and characterization of two human polyspecific organic cation transporters. *DNA Cell Biol,* 16**,** 871-81.

GREER, D. A. & IVEY, S. 2007. Distinct N-glycan glycosylation of P-glycoprotein isolated from the human uterine sarcoma cell line MES-SA/Dx5. *Biochim Biophys Acta,* 1770**,** 1275-82.

GROTH, A. C., FISH, M., NUSSE, R. & CALOS, M. P. 2004. Construction of transgenic Drosophila by using the site-specific integrase from phage phiC31. *Genetics,* 166**,** 1775-82.

GRUBE, M., KöCK, K., KARNER, S., REUTHER, S., RITTER, C. A., JEDLITSCHKY, G. & KROEMER, H. K. 2006. Modification of OATP2B1-mediated transport by steroid hormones. *Mol Pharmacol,* 70**,** 1735-41.

GRüNDEMANN, D., GORBOULEV, V., GAMBARYAN, S., VEYHL, M. & KOEPSELL, H. 1994. Drug excretion mediated by a new prototype of polyspecific transporter. *Nature,* 372**,** 549-52.

GRüNDEMANN, D., LIEBICH, G., KIEFER, N., KöSTER, S. & SCHöMIG, E. 1999. Selective substrates for non-neuronal monoamine transporters. *Mol Pharmacol,* 56**,** 1-10.

GUTIERREZ, E., WIGGINS, D., FIELDING, B. & GOULD, A. P. 2007. Specialized hepatocyte-like cells regulate

Drosophila lipid metabolism. *Nature,* 445**,** 275-80.

HAGENBUCH, B. 2007. Cellular entry of thyroid hormones by organic anion transporting polypeptides. *Best Pract Res Clin Endocrinol Metab,* 21**,** 209-21.

HAGENBUCH, B. & MEIER, P. J. 2003. The superfamily of organic anion transporting polypeptides. *Biochim Biophys Acta,* 1609**,** 1-18.

HAGENBUCH, B. & MEIER, P. J. 2004. Organic anion transporting polypeptides of the OATP/ SLC21 family: phylogenetic classification as OATP/ SLCO superfamily, new nomenclature and molecular/functional properties. *Pflugers Arch,* 447**,** 653-65.

HAGENBUCH, B. & STIEGER, B. 2013. The SLCO (former SLC21) superfamily of transporters. *Mol Aspects Med,* 34**,** 396-412.

HANO, M., TOMASOVA, L., SERES, M., PAVLIKOVA, L., BREIER, A. & SULOVA, Z. 2018. Interplay between P-Glycoprotein Expression and Resistance to Endoplasmic Reticulum Stressors. *Molecules,* 23.

HAYASHI, S. & KONDO, T. 2018. Development and Function of the Drosophila Tracheal System. *Genetics,* 209**,** 367-380.

HAYER-ZILLGEN, M., BRüSS, M. & BöNISCH, H. 2002. Expression and pharmacological profile of the human organic cation transporters hOCT1, hOCT2 and hOCT3. *Br J Pharmacol,* 136**,** 829-36.

HEDIGER, M. A., CLEMENCON, B., BURRIER, R. E. & BRUFORD, E. A. 2013. The ABCs of membrane transporters in health and disease (SLC series): introduction. *Mol Aspects Med,* 34**,** 95-107.

HEISE, M., LAUTEM, A., KNAPSTEIN, J., SCHATTENBERG, J. M., HOPPE-LOTICHIUS, M., FOLTYS, D., WEILER, N., ZIMMERMANN, A., SCHAD, A., GRüNDEMANN, D., OTTO, G., GALLE, P. R., SCHUCHMANN, M. & ZIMMERMANN, T. 2012. Downregulation of organic cation transporters OCT1 (SLC22A1) and OCT3 (SLC22A3) in human hepatocellular carcinoma and their prognostic significance. *BMC Cancer,* 12**,** 109.

HENDRICKX, R., JOHANSSON, J. G., LOHMANN, C., JENVERT, R. M., BLOMGREN, A., BöRJESSON, L. & GUSTAVSSON, L. 2013. Identification of novel substrates and structure-activity relationship of cellular uptake mediated by human organic cation transporters 1 and 2. *J Med Chem,* 56**,** 7232-42.

HIRANO, M., MAEDA, K., SHITARA, Y. & SUGIYAMA, Y. 2004. Contribution of OATP2 (OATP1B1) and OATP8 (OATP1B3) to the hepatic uptake of pitavastatin in humans. *J Pharmacol Exp Ther,* 311**,** 139-46.

HO, G. Y., WOODWARD, N. & COWARD, J. I. 2016. Cisplatin versus carboplatin: comparative review of therapeutic management in solid malignancies. *Crit Rev Oncol Hematol,* 102**,** 37-46.

HöGLUND, P. J., NORDSTRöM, K. J., SCHIöTH, H. B. & FREDRIKSSON, R. 2011. The solute carrier families have a remarkably long evolutionary history with the majority of the human families present before divergence of Bilaterian species. *Mol Biol Evol,* 28**,** 1531-41.

HUBER, R. D., GAO, B., SIDLER PFäNDLER, M. A., ZHANG-FU, W., LEUTHOLD, S., HAGENBUCH, B., FOLKERS, G., MEIER, P. J. & STIEGER, B. 2007. Characterization of two splice variants of human organic anion transporting polypeptide 3A1 isolated from human brain. *Am J Physiol Cell Physiol,* 292**,** C795-806.

IZUMI, S., NOZAKI, Y., KOMORI, T., TAKENAKA, O., MAEDA, K., KUSUHARA, H. & SUGIYAMA, Y. 2016. Investigation of Fluorescein Derivatives as Substrates of Organic Anion Transporting Polypeptide (OATP) 1B1 To Develop Sensitive Fluorescence-Based OATP1B1 Inhibition Assays. *Mol Pharm,* 13**,** 438-48.

JACOBS, J. R. 2000. The midline glia of Drosophila: a molecular genetic model for the developmental functions of glia. *Prog Neurobiol,* 62**,** 475-508.

JARIAL, M. S. 1987. Ultrastructure of the anal organ of Drosophila larva with reference to ion transport. *Tissue Cell,* 19**,** 559-75.

JONKER, J. W. & SCHINKEL, A. H. 2004. Pharmacological and physiological functions of the polyspecific organic cation transporters: OCT1, 2, and 3 (SLC22A1-3). *J Pharmacol Exp Ther,* 308**,** 2-9.

JORDAN, P. & CARMO-FONSECA, M. 2000. Molecular mechanisms involved in cisplatin cytotoxicity. *Cell Mol Life Sci,* 57**,** 1229-35.

JOUAN, E., LE VEE, M., DENIZOT, C., DA VIOLANTE, G. & FARDEL, O. 2014. The mitochondrial fluorescent dye rhodamine 123 is a high-affinity substrate for organic cation transporters (OCTs) 1 and 2. *Fundam Clin Pharmacol,* 28**,** 65-77.

JULIANO, R. L. & LING, V. 1976. A surface glycoprotein modulating drug permeability in Chinese hamster ovary cell mutants. *Biochim Biophys Acta,* 455**,** 152-62.

JUNG, N., LEHMANN, C., RUBBERT, A., KNISPEL, M., HARTMANN, P., VAN LUNZEN, J., STELLBRINK, H. J., FAETKENHEUER, G. & TAUBERT, D. 2008. Relevance of the organic cation transporters 1 and 2 for antiretroviral drug therapy in human immunodeficiency virus infection. *Drug Metab Dispos,* 36**,** 1616-23.

KALLIOKOSKI, A. & NIEMI, M. 2009. Impact of OATP transporters on pharmacokinetics. *Br J Pharmacol,* 158**,** 693-705.

KARCAVICH, R. E. 2005. Generating neuronal diversity in the Drosophila central nervous system: a view from the ganglion mother cells. *Dev Dyn,* 232**,** 609-16.

KARLGREN, M., VILDHEDE, A., NORINDER, U., WISNIEWSKI, J. R., KIMOTO, E., LAI, Y., HAGLUND, U. & ARTURSSON, P. 2012. Classification of inhibitors of hepatic organic anion transporting polypeptides (OATPs): influence of protein expression on drug-drug interactions. *J Med Chem,* 55**,** 4740-63.

KATSUDA, H., YAMASHITA, M., KATSURA, H., YU, J., WAKI, Y., NAGATA, N., SAI, Y. & MIYAMOTO, K. 2010. Protecting cisplatin-induced nephrotoxicity with cimetidine does not affect antitumor activity. *Biol Pharm Bull,* 33**,** 1867-71.

KELL, D. B., DOBSON, P. D. & OLIVER, S. G. 2011. Pharmaceutical drug transport: the issues and the implications that it is essentially carrier-mediated only. *Drug Discov Today,* 16**,** 704-14.

KELL, D. B. & OLIVER, S. G. 2014. How drugs get into cells: tested and testable predictions to help discriminate between transporter-mediated uptake and lipoidal bilayer diffusion. *Front Pharmacol,* 5**,** 231.

KIM, K. A., JOO, H. J., LEE, H. M. & PARK, J. Y. 2013. SLCO2B1 genetic polymorphisms in a Korean population: pyrosequencing analyses and comprehensive comparison with other populations. *Mol Biol Rep,* 40**,** 4211-7.

KINDLA, J., RAU, T. T., JUNG, R., FASCHING, P. A., STRICK, R., STOEHR, R., HARTMANN, A., FROMM, M. F. & KöNIG, J. 2011. Expression and localization of the uptake transporters OATP2B1, OATP3A1 and OATP5A1 in non-malignant and malignant breast tissue. *Cancer Biol Ther,* 11**,** 584-91.

KINZI, J., GRUBE, M. & MEYER ZU SCHWABEDISSEN, H. E. 2021. OATP2B1 - The underrated member of the organic anion transporting polypeptide family of drug transporters? *Biochem Pharmacol,* 188**,** 114534.

KIRBY, B. J. & UNADKAT, J. D. 2007. Grapefruit juice, a glass full of drug interactions? *Clin Pharmacol Ther,* 81**,** 631-3.

KLäMBT, C., GLAZER, L. & SHILO, B. Z. 1992. breathless, a Drosophila FGF receptor homolog, is essential for migration of tracheal and specific midline glial cells. *Genes Dev,* 6**,** 1668-78.

KLATT, S., FROMM, M. F. & KöNIG, J. 2013. The influence of oral antidiabetic drugs on cellular drug uptake mediated by hepatic OATP family members. *Basic Clin Pharmacol Toxicol,* 112**,** 244-50.

KLEBERG, K., JENSEN, G. M., CHRISTENSEN, D. P., LUNDH, M., GRUNNET, L. G., KNUHTSEN, S., POULSEN, S. S., HANSEN, M. B. & BINDSLEV, N. 2012. Transporter function and cyclic AMP turnover in normal colonic mucosa from patients with and without colorectal neoplasia. *BMC Gastroenterol,* 12**,** 78.

KLEMENZ, R., WEBER, U. & GEHRING, W. J. 1987. The white gene as a marker in a new P-element vector for gene transfer in Drosophila. *Nucleic Acids Res,* 15**,** 3947-59.

KNAUF, F., ROGINA, B., JIANG, Z., ARONSON, P. S. & HELFAND, S. L. 2002. Functional characterization and immunolocalization of the transporter encoded by the life-extending gene Indy. *Proc Natl Acad Sci U S A,* 99**,** 14315-9.

KOBAYASHI, D., NOZAWA, T., IMAI, K., NEZU, J., TSUJI, A. & TAMAI, I. 2003. Involvement of human organic anion transporting polypeptide OATP-B (SLC21A9) in pH-dependent transport across intestinal apical membrane. *J Pharmacol Exp Ther,* 306**,** 703-8.

KOEPSELL, H. 2015. Role of organic cation transporters in drug-drug interaction. *Expert Opin Drug Metab Toxicol,* 11**,** 1619-33.

KOEPSELL, H., LIPS, K. & VOLK, C. 2007. Polyspecific organic cation transporters: structure, function, physiological roles, and biopharmaceutical implications. *Pharm Res,* 24**,** 1227-51.

KONIG, J., CUI, Y., NIES, A. T. & KEPPLER, D. 2000. Localization and genomic organization of a new hepatocellular organic anion transporting polypeptide. *J Biol Chem,* 275**,** 23161-8.

KöNIG, J., CUI, Y., NIES, A. T. & KEPPLER, D. 2000. A novel human organic anion transporting polypeptide localized to the basolateral hepatocyte membrane. *Am J Physiol Gastrointest Liver Physiol,* 278**,** G156-64.

KONIG, J., SEITHEL, A., GRADHAND, U. & FROMM, M. F. 2006. Pharmacogenomics of human OATP transporters. *Naunyn Schmiedebergs Arch Pharmacol,* 372**,** 432-43.

KOPPLOW, K., LETSCHERT, K., KöNIG, J., WALTER, B. & KEPPLER, D. 2005. Human hepatobiliary transport of organic anions analyzed by quadruple-transfected cells. *Mol Pharmacol,* 68**,** 1031-8.

KOTSAMPASAKOU, E., BRENNER, S., JäGER, W. & ECKER, G. F. 2015. Identification of Novel Inhibitors of Organic Anion Transporting Polypeptides 1B1 and 1B3 (OATP1B1 and OATP1B3) Using a Consensus Vote of Six Classification Models. *Mol Pharm,* 12**,** 4395-404.

KRAFT, M. E., GLAESER, H., MANDERY, K., KöNIG, J., AUGE, D., FROMM, M. F., SCHLöTZER-SCHREHARDT, U., WELGE-LüSSEN, U., KRUSE, F. E. & ZOLK, O. 2010. The prostaglandin transporter OATP2A1 is expressed in human ocular tissues and transports the antiglaucoma prostanoid latanoprost. *Invest Ophthalmol Vis Sci,* 51**,** 2504-11.

KULLAK-UBLICK, G. A., ISMAIR, M. G., STIEGER, B., LANDMANN, L., HUBER, R., PIZZAGALLI, F., FATTINGER, K., MEIER, P. J. & HAGENBUCH, B. 2001. Organic anion-transporting polypeptide B (OATP-B) and its functional comparison with three other OATPs of human liver. *Gastroenterology,* 120**,** 525-33.

KUMAR, V., SINGH, P., GUPTA, S. K., ALI, V. & VERMA, M. 2022. Transport and metabolism of tyrosine kinase inhibitors associated with chronic myeloid leukemia therapy: a review. *Mol Cell Biochem,* 477**,** 1261-1279.

LAI, R. E., JAY, C. E. & SWEET, D. H. 2018. Organic solute carrier 22 (SLC22) family: Potential for interactions with food, herbal/dietary supplements, endogenous compounds, and drugs. *J Food Drug Anal,* 26**,** S45-s60.

LAUGHON, A. & GESTELAND, R. F. 1984. Primary structure of the Saccharomyces cerevisiae GAL4 gene. *Mol Cell Biol,* 4**,** 260-7.

LIEDAUER, R., SVOBODA, M., WLCEK, K., ARRICH, F., Jä, W., TOMA, C. & THALHAMMER, T. 2009. Different expression patterns of organic anion transporting polypeptides in osteosarcomas, bone metastases and aneurysmal bone cysts. *Oncol Rep,* 22**,** 1485-92.

LIN, C. J., TAI, Y., HUANG, M. T., TSAI, Y. F., HSU, H. J., TZEN, K. Y. & LIOU, H. H. 2010. Cellular localization of the organic cation transporters, OCT1 and OCT2, in brain microvessel endothelial cells and its implication for MPTP transport across the blood-brain barrier and MPTP-induced dopaminergic toxicity in rodents. *J Neurochem,* 114**,** 717-27.

LIN, R., LI, X., LI, J., ZHANG, L., XU, F., CHU, Y. & LI, J. 2013. Long-term cisplatin exposure promotes methylation of the OCT1 gene in human esophageal cancer cells. *Dig Dis Sci,* 58**,** 694-8.

LIPS, K. S., LüHRMANN, A., TSCHERNIG, T., STOEGER, T., ALESSANDRINI, F., GRAU, V., HABERBERGER, R. V., KOEPSELL, H., PABST, R. & KUMMER, W. 2007. Down-regulation of the non-neuronal acetylcholine synthesis and release machinery in acute allergic airway inflammation of rat and mouse. *Life Sci,* 80**,** 2263-9.

LITMAN, T., ZEUTHEN, T., SKOVSGAARD, T. & STEIN, W. D. 1997. Competitive, non-competitive and cooperative interactions between substrates of P-glycoprotein as measured by its ATPase activity. *Biochim Biophys Acta,* 1361**,** 169-76.

LIU, X. 2019. ABC Family Transporters. *Adv Exp Med Biol,* 1141**,** 13-100.

LOZANO, E., HERRAEZ, E., BRIZ, O., ROBLEDO, V. S., HERNANDEZ-IGLESIAS, J., GONZALEZ-HERNANDEZ, A. & MARIN, J. J. 2013. Role of the plasma membrane transporter of organic cations OCT1 and its genetic variants in modern liver pharmacology. *Biomed Res Int,* 2013**,** 692071.

LUSCHNIG, S., BäTZ, T., ARMBRUSTER, K. & KRASNOW, M. A. 2006. serpentine and vermiform encode matrix proteins with chitin binding and deacetylation domains that limit tracheal tube length in Drosophila. *Curr Biol,* 16**,** 186-94.

LUTZ, K. A., CORNEILLE, S., AZHAGIRI, A. K., SVAB, Z. & MALIGA, P. 2004. A novel approach to plastid transformation utilizes the phiC31 phage integrase. *Plant J,* 37**,** 906-13.

MAHOWALD, A. P. 1972. Ultrastructural observations on oogenesis in Drosophila. *J Morphol,* 137**,** 29-48.

MALAGNINO, V., HUSSNER, J., SEIBERT, I., STOLZENBURG, A., SAGER, C. P. & MEYER ZU SCHWABEDISSEN, H. E. 2018. LST-3TM12 is a member of the OATP1B family and a functional transporter. *Biochem Pharmacol,* 148**,** 75-87.

MALHOTRA, H., SHARMA, P., MALHOTRA, B., BHARGAVA, S., JASUJA, S. & KUMAR, M. 2015. Molecular response to imatinib & its correlation with mRNA expression levels of imatinib influx & efflux transporters in patients with chronic myeloid leukaemia in chronic phase. *Indian J Med Res,* 142**,** 175-82.

MARGARITIS, L. H. 1985. The egg-shell of Drosophila melanogaster III. Covalent crosslinking of the chorion proteins involves endogenous hydrogen peroxide. *Tissue Cell,* 17**,** 553-9.

MARGARITIS, L. H., KAFATOS, F. C. & PETRI, W. H. 1980. The eggshell of Drosophila melanogaster. I. Fine structure of the layers and regions of the wild-type eggshell. *J Cell Sci,* 43**,** 1-35.

MATSUMOTO, J., ARIYOSHI, N., SAKAKIBARA, M., NAKANISHI, T., OKUBO, Y., SHIINA, N., FUJISAKI, K., NAGASHIMA, T., NAKATANI, Y., TAMAI, I., YAMADA, H., TAKEDA, H. & ISHII, I. 2015. Organic anion transporting polypeptide 2B1 expression correlates with uptake of estrone-3-sulfate and cell proliferation in estrogen receptor-positive breast cancer cells. *Drug Metab Pharmacokinet,* 30**,** 133-41.

MAYERL, S., MüLLER, J., BAUER, R., RICHERT, S., KASSMANN, C. M., DARRAS, V. M., BUDER, K., BOELEN, A., VISSER, T. J. & HEUER, H. 2014. Transporters MCT8 and OATP1C1 maintain murine brain thyroid

hormone homeostasis. *J Clin Invest,* 124**,** 1987-99.

MEDWID, S., LI, M. M. J., KNAUER, M. J., LIN, K., MANSELL, S. E., SCHMERK, C. L., ZHU, C., GRIFFIN, K. E., YOUSIF, M. D., DRESSER, G. K., SCHWARZ, U. I., KIM, R. B. & TIRONA, R. G. 2019. Fexofenadine and Rosuvastatin Pharmacokinetics in Mice with Targeted Disruption of Organic Anion Transporting Polypeptide 2B1. *Drug Metab Dispos,* 47**,** 832-842.

MEDWID, S., PRICE, H. R., TAYLOR, D. P., MAILLOUX, J., SCHWARZ, U. I., KIM, R. B. & TIRONA, R. G. 2021. Organic Anion Transporting Polypeptide 2B1 (OATP2B1) Genetic Variants: In Vitro Functional Characterization and Association With Circulating Concentrations of Endogenous Substrates. *Front Pharmacol,* 12**,** 713567.

MEYER, S., SCHMIDT, I. & KLäMBT, C. 2014. Glia ECM interactions are required to shape the Drosophila nervous system. *Mech Dev,* 133**,** 105-16.

MEYER ZU SCHWABEDISSEN, H. E., BOETTCHER, K., STEINER, T., SCHWARZ, U. I., KEISER, M., KROEMER, H. K. & SIEGMUND, W. 2014. OATP1B3 is expressed in pancreatic β-islet cells and enhances the insulinotropic effect of the sulfonylurea derivative glibenclamide. *Diabetes,* 63**,** 775-84.

MIKKAICHI, T., SUZUKI, T., TANEMOTO, M., ITO, S. & ABE, T. 2004. The organic anion transporter (OATP) family. *Drug Metab Pharmacokinet,* 19**,** 171-9.

MILKIEWICZ, P., SAKSENA, S., CARDENAS, T., MILLS, C. O. & ELIAS, E. 2000. Plasma elimination of cholyl-lysyl-fluorescein (CLF): a pilot study in patients with liver cirrhosis. *Liver,* 20**,** 330-4.

MIURA, M., KAGAYA, H., SATOH, S., INOUE, K., SAITO, M., HABUCHI, T. & SUZUKI, T. 2008. Influence of drug transporters and UGT polymorphisms on pharmacokinetics of phenolic glucuronide metabolite of mycophenolic acid in Japanese renal transplant recipients. *Ther Drug Monit,* 30**,** 559-64.

MONKS, N. R., LIU, S., XU, Y., YU, H., BENDELOW, A. S. & MOSCOW, J. A. 2007. Potent cytotoxicity of the phosphatase inhibitor microcystin LR and microcystin analogues in OATP1B1- and OATP1B3-expressing HeLa cells. *Mol Cancer Ther,* 6**,** 587-98.

MORO, M., CAIOLA, E., GANZINELLI, M., ZULATO, E., RULLI, E., MARABESE, M., CENTONZE, G., BUSICO, A., PASTORINO, U., DE BRAUD, F. G., VERNIERI, C., SIMBOLO, M., BRIA, E., SCARPA, A., INDRACCOLO, S., BROGGINI, M., SOZZI, G. & GARASSINO, M. C. 2018. Metformin Enhances Cisplatin-Induced Apoptosis and Prevents Resistance to Cisplatin in Co-mutated KRAS/LKB1 NSCLC. *J Thorac Oncol,* 13**,** 1692-1704.

MOTOHASHI, H. & INUI, K. 2013. Organic cation transporter OCTs (SLC22) and MATEs (SLC47) in the human kidney. *Aaps j,* 15**,** 581-8.

MOUGEY, E. B., LANG, J. E., WEN, X. & LIMA, J. J. 2011. Effect of citrus juice and SLCO2B1 genotype on the pharmacokinetics of montelukast. *J Clin Pharmacol,* 51**,** 751-60.

MOUNT, D. B. & ROMERO, M. F. 2004. The SLC26 gene family of multifunctional anion exchangers. *Pflugers Arch,* 447**,** 710-21.

MUQIT, M. M. & FEANY, M. B. 2002. Modelling neurodegenerative diseases in Drosophila: a fruitful approach? *Nat Rev Neurosci,* 3**,** 237-43.

NAGY, A., SZALAI, R., MAGYARI, L., BENE, J., TOTH, K. & MELEGH, B. 2015. Extreme differences in SLCO1B3 functional polymorphisms in Roma and Hungarian populations. *Environ Toxicol Pharmacol,* 39**,** 1246-51.

NAKANISHI, T. & TAMAI, I. 2017. Roles of Organic Anion Transporting Polypeptide 2A1 (OATP2A1/SLCO2A1) in Regulating the Pathophysiological Actions of Prostaglandins. *Aaps j,* 20**,** 13.

NEUL, C., SCHAEFFELER, E., SPARREBOOM, A., LAUFER, S., SCHWAB, M. & NIES, A. T. 2016. Impact of Membrane Drug Transporters on Resistance to Small-Molecule Tyrosine Kinase Inhibitors. *Trends Pharmacol Sci,* 37**,** 904-932.

NIEMI, M. 2007. Role of OATP transporters in the disposition of drugs. *Pharmacogenomics,* 8**,** 787-802.

NIEMI, M., PASANEN, M. K. & NEUVONEN, P. J. 2011. Organic anion transporting polypeptide 1B1: a genetically polymorphic transporter of major importance for hepatic drug uptake. *Pharmacol Rev,* 63**,** 157-81.

NIES, A. T., KOEPSELL, H., WINTER, S., BURK, O., KLEIN, K., KERB, R., ZANGER, U. M., KEPPLER, D., SCHWAB, M. & SCHAEFFELER, E. 2009. Expression of organic cation transporters OCT1 (SLC22A1) and OCT3 (SLC22A3) is affected by genetic factors and cholestasis in human liver. *Hepatology,* 50**,** 1227-40.

NIES, A. T., SCHAEFFELER, E. & SCHWAB, M. 2022. Hepatic solute carrier transporters and drug therapy: Regulation of expression and impact of genetic variation. *Pharmacol Ther,* 238**,** 108268.

NIGAM, S. K. 2015. What do drug transporters really do? *Nat Rev Drug Discov,* 14**,** 29-44.

NIGAM, S. K. 2018. The SLC22 Transporter Family: A Paradigm for the Impact of Drug Transporters on Metabolic Pathways, Signaling, and Disease. *Annu Rev Pharmacol Toxicol,* 58**,** 663-687.

NISHIHARA, S. 2020. Functional analysis of glycosylation using Drosophila melanogaster. *Glycoconj J,* 37**,** 1-14.

NISHIZATO, Y., IEIRI, I., SUZUKI, H., KIMURA, M., KAWABATA, K., HIROTA, T., TAKANE, H., IRIE, S., KUSUHARA, H., URASAKI, Y., URAE, A., HIGUCHI, S., OTSUBO, K. & SUGIYAMA, Y. 2003. Polymorphisms of OATP-C (SLC21A6) and OAT3 (SLC22A8) genes: consequences for pravastatin pharmacokinetics. *Clin Pharmacol Ther,* 73**,** 554-65.

NOZAWA, T., MINAMI, H., SUGIURA, S., TSUJI, A. & TAMAI, I. 2005. Role of organic anion transporter OATP1B1 (OATP-C) in hepatic uptake of irinotecan and its active metabolite, 7-ethyl-10-hydroxycamptothecin: in vitro evidence and effect of single nucleotide polymorphisms. *Drug Metab Dispos,* 33**,** 434-9.

NOZAWA, T., NAKAJIMA, M., TAMAI, I., NODA, K., NEZU, J., SAI, Y., TSUJI, A. & YOKOI, T. 2002. Genetic polymorphisms of human organic anion transporters OATP-C (SLC21A6) and OATP-B (SLC21A9): allele frequencies in the Japanese population and functional analysis. *J Pharmacol Exp Ther,* 302**,** 804-13.

OLSZEWSKI-HAMILTON, U., SVOBODA, M., THALHAMMER, T., BUXHOFER-AUSCH, V., GEISSLER, K. & HAMILTON, G. 2011. Organic Anion Transporting Polypeptide 5A1 (OATP5A1) in Small Cell Lung Cancer (SCLC) Cells: Possible Involvement in Chemoresistance to Satraplatin. *Biomark Cancer,* 3**,** 31-40.

PANDEY, U. B. & NICHOLS, C. D. 2011. Human disease models in Drosophila melanogaster and the role of the fly in therapeutic drug discovery. *Pharmacol Rev,* 63**,** 411-36.

PAPASSIDERI, I. S., MARGARITIS, L. H. & GULIK-KRZYWICKI, T. 1993. The eggshell of Drosophila melanogaster. VIII. Morphogenesis of the wax layer during oogenesis. *Tissue Cell,* 25**,** 929-36.

PARDRIDGE, W. M. 1997. Drug delivery to the brain. *J Cereb Blood Flow Metab,* 17**,** 713-31.

PASANEN, M. K., NEUVONEN, M., NEUVONEN, P. J. & NIEMI, M. 2006. SLCO1B1 polymorphism markedly affects the pharmacokinetics of simvastatin acid. *Pharmacogenet Genomics,* 16**,** 873-9.

PASANEN, M. K., NEUVONEN, P. J. & NIEMI, M. 2008. Global analysis of genetic variation in SLCO1B1. *Pharmacogenomics,* 9**,** 19-33.

PENG, M., DARKO, K. O., TAO, T., HUANG, Y., SU, Q., HE, C., YIN, T., LIU, Z. & YANG, X. 2017. Combination of metformin with chemotherapeutic drugs via different molecular mechanisms. *Cancer Treat Rev,*

54, 24-33.
PICARD, N., YEE, S. W., WOILLARD, J. B., LEBRANCHU, Y., LE MEUR, Y., GIACOMINI, K. M. & MARQUET, P. 2010. The role of organic anion-transporting polypeptides and their common genetic variants in mycophenolic acid pharmacokinetics. *Clin Pharmacol Ther,* 87, 100-8.
PIZZAGALLI, M. D., BENSIMON, A. & SUPERTI-FURGA, G. 2021. A guide to plasma membrane solute carrier proteins. *FEBS J,* 288, 2784-2835.
QUATTROPANI, S. L. & ANDERSON, E. 1969. The origin and structure of the secondary coat of the egg of Drosophila melanogaster. *Z Zellforsch Mikrosk Anat,* 95, 495-510.
RAJAMANI, B. M., BENJAMIN, E. S. B., ABRAHAM, A., GANESAN, S., LAKSHMI, K. M., ANANDAN, S., KARATHEDATH, S., VARATHARAJAN, S., MOHANAN, E., JANET, N. B., SRIVASTAVA, V. M., RAMACHANDRAN VELAYUDHAN, S., KULKARNI, U. P., DEVASIA, A. J., FOUZIA, N. A., KORULA, A., GEORGE, B., SRIVASTAVA, A., MATHEWS, V. & BALASUBRAMANIAN, P. 2020. Plasma imatinib levels and ABCB1 polymorphism influences early molecular response and failure-free survival in newly diagnosed chronic phase CML patients. *Sci Rep,* 10, 20640.
ROBINOW, S. & WHITE, K. 1988. The locus elav of Drosophila melanogaster is expressed in neurons at all developmental stages. *Dev Biol,* 126, 294-303.
ROBINOW, S. & WHITE, K. 1991. Characterization and spatial distribution of the ELAV protein during Drosophila melanogaster development. *J Neurobiol,* 22, 443-61.
ROGINA, B., REENAN, R. A., NILSEN, S. P. & HELFAND, S. L. 2000. Extended life-span conferred by cotransporter gene mutations in Drosophila. *Science,* 290, 2137-40.
ROTH, M., OBAIDAT, A. & HAGENBUCH, B. 2012. OATPs, OATs and OCTs: the organic anion and cation transporters of the SLCO and SLC22A gene superfamilies. *Br J Pharmacol,* 165, 1260-87.
SAIDIJAM, M., KARIMI DERMANI, F., SOHRABI, S. & PATCHING, S. G. 2018. Efflux proteins at the blood-brain barrier: review and bioinformatics analysis. *Xenobiotica,* 48, 506-532.
SALA-RABANAL, M., LI, D. C., DAKE, G. R., KURATA, H. T., INYUSHIN, M., SKATCHKOV, S. N. & NICHOLS, C. G. 2013. Polyamine transport by the polyspecific organic cation transporters OCT1, OCT2, and OCT3. *Mol Pharm,* 10, 1450-8.
SANTABáRBARA-RUIZ, P. & LéOPOLD, P. 2021. An Oatp transporter-mediated steroid sink promotes tumor-induced cachexia in Drosophila. *Dev Cell,* 56, 2741-2751.e7.
SATO, T., MISHIMA, E., MANO, N., ABE, T. & YAMAGUCHI, H. 2017. Potential Drug Interactions Mediated by Renal Organic Anion Transporter OATP4C1. *J Pharmacol Exp Ther,* 362, 271-277.
SCHAEFFELER, E., HELLERBRAND, C., NIES, A. T., WINTER, S., KRUCK, S., HOFMANN, U., VAN DER KUIP, H., ZANGER, U. M., KOEPSELL, H. & SCHWAB, M. 2011. DNA methylation is associated with downregulation of the organic cation transporter OCT1 (SLC22A1) in human hepatocellular carcinoma. *Genome Med,* 3, 82.
SCHERRMANN, J. M. 2005. Expression and function of multidrug resistance transporters at the blood-brain barriers. *Expert Opin Drug Metab Toxicol,* 1, 233-46.
SCHINKEL, A. H. & JONKER, J. W. 2003. Mammalian drug efflux transporters of the ATP binding cassette (ABC) family: an overview. *Adv Drug Deliv Rev,* 55, 3-29.
SCHNECK, D. W., BIRMINGHAM, B. K., ZALIKOWSKI, J. A., MITCHELL, P. D., WANG, Y., MARTIN, P. D., LASSETER, K. C., BROWN, C. D., WINDASS, A. S. & RAZA, A. 2004. The effect of gemfibrozil on the pharmacokinetics of rosuvastatin. *Clin Pharmacol Ther,* 75, 455-63.
SCHNEPF, R. & ZOLK, O. 2013. Effect of the ATP-binding cassette transporter ABCG2 on pharmacokinetics: experimental findings and clinical implications. *Expert Opin Drug Metab Toxicol,* 9, 287-306.

SCHOTTENFELD, J., SONG, Y. & GHABRIAL, A. S. 2010. Tube continued: morphogenesis of the Drosophila tracheal system. *Curr Opin Cell Biol,* 22**,** 633-9.

SCHWARZ, U. I., MEYER ZU SCHWABEDISSEN, H. E., TIRONA, R. G., SUZUKI, A., LEAKE, B. F., MOKRAB, Y., MIZUGUCHI, K., HO, R. H. & KIM, R. B. 2011. Identification of novel functional organic anion-transporting polypeptide 1B3 polymorphisms and assessment of substrate specificity. *Pharmacogenet Genomics,* 21**,** 103-14.

SEABROOKE, S. & O'DONNELL, M. J. 2013. Oatp58Dc contributes to blood-brain barrier function by excluding organic anions from the Drosophila brain. *Am J Physiol Cell Physiol,* 305**,** C558-67.

SEBASTIAN, K., DETRO-DASSEN, S., RINIS, N., FAHRENKAMP, D., MüLLER-NEWEN, G., MERK, H. F., SCHMALZING, G., ZWADLO-KLARWASSER, G. & BARON, J. M. 2013. Characterization of SLCO5A1/OATP5A1, a solute carrier transport protein with non-classical function. *PLoS One,* 8**,** e83257.

SEITZ, T., STALMANN, R., DALILA, N., CHEN, J., POJAR, S., DOS SANTOS PEREIRA, J. N., KRäTZNER, R., BROCKMöLLER, J. & TZVETKOV, M. V. 2015. Global genetic analyses reveal strong inter-ethnic variability in the loss of activity of the organic cation transporter OCT1. *Genome Med,* 7**,** 56.

SELLIN, J., ALBRECHT, S., KöLSCH, V. & PAULULAT, A. 2006. Dynamics of heart differentiation, visualized utilizing heart enhancer elements of the Drosophila melanogaster bHLH transcription factor Hand. *Gene Expr Patterns,* 6**,** 360-75.

SHIRASAKA, Y., SAGER, J. E., LUTZ, J. D., DAVIS, C. & ISOHERRANEN, N. 2013. Inhibition of CYP2C19 and CYP3A4 by omeprazole metabolites and their contribution to drug-drug interactions. *Drug Metab Dispos,* 41**,** 1414-24.

SHITARA, Y. 2011. Clinical importance of OATP1B1 and OATP1B3 in drug-drug interactions. *Drug Metab Pharmacokinet,* 26**,** 220-7.

SHITARA, Y., ITOH, T., SATO, H., LI, A. P. & SUGIYAMA, Y. 2003. Inhibition of transporter-mediated hepatic uptake as a mechanism for drug-drug interaction between cerivastatin and cyclosporin A. *J Pharmacol Exp Ther,* 304**,** 610-6.

SHITARA, Y., MAEDA, K., IKEJIRI, K., YOSHIDA, K., HORIE, T. & SUGIYAMA, Y. 2013. Clinical significance of organic anion transporting polypeptides (OATPs) in drug disposition: their roles in hepatic clearance and intestinal absorption. *Biopharm Drug Dispos,* 34**,** 45-78.

SLOT, A. J., MOLINSKI, S. V. & COLE, S. P. 2011. Mammalian multidrug-resistance proteins (MRPs). *Essays Biochem,* 50**,** 179-207.

SMEIJER, J. D., KOOMEN, J. V., KOHAN, D. E., MCMURRAY, J. J. V., BAKRIS, G. L., CORREA-ROTTER, R., HOU, F. F., KITZMAN, D. W., MAKINO, H., MAYER, G., NOWICKI, M., PERKOVIC, V., ROSSING, P., TOBE, S., PARVING, H. H., DE ZEEUW, D. & HEERSPINK, H. J. L. 2022. Organic Anion Transporter Gene Variants Associated with Plasma Exposure and Long-Term Response to Atrasentan in Patients With Diabetic Kidney Disease. *Clin Pharmacol Ther*.

SMITH, N. F., FIGG, W. D. & SPARREBOOM, A. 2005. Role of the liver-specific transporters OATP1B1 and OATP1B3 in governing drug elimination. *Expert Opin Drug Metab Toxicol,* 1**,** 429-45.

SOLAZZO, M., FANTAPPIè, O., LASAGNA, N., SASSOLI, C., NOSI, D. & MAZZANTI, R. 2006. P-gp localization in mitochondria and its functional characterization in multiple drug-resistant cell lines. *Exp Cell Res,* 312**,** 4070-8.

SPRADLING, A. C. & RUBIN, G. M. 1982. Transposition of cloned P elements into Drosophila germ line chromosomes. *Science,* 218**,** 341-7.

STEFANKO, E., RYBKA, J., JAŹWIEC, B., HAUS, O., STĄPOR, S., KULICZKOWSKI, K. & WRóBEL, T. 2017.

Significance of OCT1 Expression in Acute Myeloid Leukemia. *Pathol Oncol Res,* 23**,** 665-671.

SU, J., XU, J., LI, X., ZHANG, H., HU, J., FANG, R. & CHEN, X. 2012. ABCB1 C3435T polymorphism and response to clopidogrel treatment in coronary artery disease (CAD) patients: a meta-analysis. *PLoS One,* 7**,** e46366.

SUGA, T., YAMAGUCHI, H., SATO, T., MAEKAWA, M., GOTO, J. & MANO, N. 2017. Preference of Conjugated Bile Acids over Unconjugated Bile Acids as Substrates for OATP1B1 and OATP1B3. *PLoS One,* 12**,** e0169719.

SUGIURA, T., KATO, Y. & TSUJI, A. 2006. Role of SLC xenobiotic transporters and their regulatory mechanisms PDZ proteins in drug delivery and disposition. *J Control Release,* 116**,** 238-46.

TAMAI, I. 2012. Oral drug delivery utilizing intestinal OATP transporters. *Adv Drug Deliv Rev,* 64**,** 508-14.

TAUB, M. E., MEASE, K., SANE, R. S., WATSON, C. A., CHEN, L., ELLENS, H., HIRAKAWA, B., REYNER, E. L., JANI, M. & LEE, C. A. 2011. Digoxin is not a substrate for organic anion-transporting polypeptide transporters OATP1A2, OATP1B1, OATP1B3, and OATP2B1 but is a substrate for a sodium-dependent transporter expressed in HEK293 cells. *Drug Metab Dispos,* 39**,** 2093-102.

THAKKAR, N., KIM, K., JANG, E. R., HAN, S., KIM, K., KIM, D., MERCHANT, N., LOCKHART, A. C. & LEE, W. 2013. A cancer-specific variant of the SLCO1B3 gene encodes a novel human organic anion transporting polypeptide 1B3 (OATP1B3) localized mainly in the cytoplasm of colon and pancreatic cancer cells. *Mol Pharm,* 10**,** 406-16.

THAKKAR, N., LOCKHART, A. C. & LEE, W. 2015. Role of Organic Anion-Transporting Polypeptides (OATPs) in Cancer Therapy. *Aaps j,* 17**,** 535-45.

TIRONA, R. G., LEAKE, B. F., MERINO, G. & KIM, R. B. 2001. Polymorphisms in OATP-C: identification of multiple allelic variants associated with altered transport activity among European- and African-Americans. *J Biol Chem,* 276**,** 35669-75.

TORRIE, L. S., RADFORD, J. C., SOUTHALL, T. D., KEAN, L., DINSMORE, A. J., DAVIES, S. A. & DOW, J. A. 2004. Resolution of the insect ouabain paradox. *Proc Natl Acad Sci U S A,* 101**,** 13689-93.

TREIBER, A., SCHNEITER, R., HAUSLER, S. & STIEGER, B. 2007. Bosentan is a substrate of human OATP1B1 and OATP1B3: inhibition of hepatic uptake as the common mechanism of its interactions with cyclosporin A, rifampicin, and sildenafil. *Drug Metab Dispos,* 35**,** 1400-7.

TSURUOKA, S., SUGIMOTO, K. I., FUJIMURA, A., IMAI, M., ASANO, Y. & MUTO, S. 2001. P-glycoprotein-mediated drug secretion in mouse proximal tubule perfused in vitro. *J Am Soc Nephrol,* 12**,** 177-181.

TZVETKOV, M. V., VORMFELDE, S. V., BALEN, D., MEINEKE, I., SCHMIDT, T., SEHRT, D., SABOLIC, I., KOEPSELL, H. & BROCKMOLLER, J. 2009a. The effects of genetic polymorphisms in the organic cation transporters OCT1, OCT2, and OCT3 on the renal clearance of metformin. *Clin Pharmacol Ther,* 86**,** 299-306.

TZVETKOV, M. V., VORMFELDE, S. V., BALEN, D., MEINEKE, I., SCHMIDT, T., SEHRT, D., SABOLIĆ, I., KOEPSELL, H. & BROCKMöLLER, J. 2009b. The effects of genetic polymorphisms in the organic cation transporters OCT1, OCT2, and OCT3 on the renal clearance of metformin. *Clin Pharmacol Ther,* 86**,** 299-306.

UCHIYAMA, H., TSUJIMOTO, M., KIMURA, A., YUKI, E., SAIKI, T., YOSHIDA, T., FURUKUBO, T., IZUMI, S., YAMAKAWA, T., TACHIKI, H., MINEGAKI, T. & NISHIGUCHI, K. 2019. Effects of Uremic Serum Residue on OATP1B1- and OATP1B3-Mediated Pravastatin Uptake in OATP-Expressing HEK293 Cells and Human Hepatocytes. *Ther Apher Dial,* 23**,** 126-132.

UGUR, B., CHEN, K. & BELLEN, H. J. 2016. Drosophila tools and assays for the study of human diseases. *Dis*

Model Mech, 9**,** 235-44.

UMEHARA, K. I., IWATSUBO, T., NOGUCHI, K. & KAMIMURA, H. 2007. Functional involvement of organic cation transporter1 (OCT1/Oct1) in the hepatic uptake of organic cations in humans and rats. *Xenobiotica,* 37**,** 818-31.

UNGER, M. S., MUDUNURU, J., SCHWAB, M., HOPF, C., DREWES, G., NIES, A. T., ZAMEK-GLISZCZYNSKI, M. J. & REINHARD, F. B. M. 2020. Clinically Relevant OATP2B1 Inhibitors in Marketed Drug Space. *Mol Pharm,* 17**,** 488-498.

VAN DE STEEG, E., STRáNECKý, V., HARTMANNOVá, H., NOSKOVá, L., HŘEBíČEK, M., WAGENAAR, E., VAN ESCH, A., DE WAART, D. R., OUDE ELFERINK, R. P., KENWORTHY, K. E., STICOVá, E., AL-EDREESI, M., KNISELY, A. S., KMOCH, S., JIRSA, M. & SCHINKEL, A. H. 2012. Complete OATP1B1 and OATP1B3 deficiency causes human Rotor syndrome by interrupting conjugated bilirubin reuptake into the liver. *J Clin Invest,* 122**,** 519-28.

VAN DER DEURE, W. M., PEETERS, R. P. & VISSER, T. J. 2010. Molecular aspects of thyroid hormone transporters, including MCT8, MCT10, and OATPs, and the effects of genetic variation in these transporters. *J Mol Endocrinol,* 44**,** 1-11.

WANG, D. S., KUSUHARA, H., KATO, Y., JONKER, J. W., SCHINKEL, A. H. & SUGIYAMA, Y. 2003. Involvement of organic cation transporter 1 in the lactic acidosis caused by metformin. *Mol Pharmacol,* 63**,** 844-8.

WANG, S., JAYARAM, S. A., HEMPHäLä, J., SENTI, K. A., TSAROUHAS, V., JIN, H. & SAMAKOVLIS, C. 2006. Septate-junction-dependent luminal deposition of chitin deacetylases restricts tube elongation in the Drosophila trachea. *Curr Biol,* 16**,** 180-5.

WANG, Y., MOUSSIAN, B., SCHAEFFELER, E., SCHWAB, M. & NIES, A. T. 2018. The fruit fly Drosophila melanogaster as an innovative preclinical ADME model for solute carrier membrane transporters, with consequences for pharmacology and drug therapy. *Drug Discov Today,* 23**,** 1746-1760.

WARING, G. L. & MAHOWALD, A. P. 1979. Identification and time of synthesis of chorion proteins in Drosophila melanogaster. *Cell,* 16**,** 599-607.

WEAVERS, H., PRIETO-SáNCHEZ, S., GRAWE, F., GARCIA-LóPEZ, A., ARTERO, R., WILSCH-BRäUNINGER, M., RUIZ-GóMEZ, M., SKAER, H. & DENHOLM, B. 2009. The insect nephrocyte is a podocyte-like cell with a filtration slit diaphragm. *Nature,* 457**,** 322-6.

WENG, H. J. & TSAI, T. F. 2021. ABCB1 in dermatology: roles in skin diseases and their treatment. *J Mol Med (Berl),* 99**,** 1527-1538.

WLCEK, K., SVOBODA, M., RIHA, J., ZAKARIA, S., OLSZEWSKI, U., DVORAK, Z., SELLNER, F., ELLINGER, I., JäGER, W. & THALHAMMER, T. 2011. The analysis of organic anion transporting polypeptide (OATP) mRNA and protein patterns in primary and metastatic liver cancer. *Cancer Biol Ther,* 11**,** 801-11.

WOLKING, S., SCHAEFFELER, E., LERCHE, H., SCHWAB, M. & NIES, A. T. 2015. Impact of Genetic Polymorphisms of ABCB1 (MDR1, P-Glycoprotein) on Drug Disposition and Potential Clinical Implications: Update of the Literature. *Clin Pharmacokinet,* 54**,** 709-35.

WRIGHT, E. M. 2013. Glucose transport families SLC5 and SLC50. *Mol Aspects Med,* 34**,** 183-96.

YAMADA, A., MAEDA, K., ISHIGURO, N., TSUDA, Y., IGARASHI, T., EBNER, T., ROTH, W., IKUSHIRO, S. & SUGIYAMA, Y. 2011. The impact of pharmacogenetics of metabolic enzymes and transporters on the pharmacokinetics of telmisartan in healthy volunteers. *Pharmacogenet Genomics,* 21**,** 523-30.

YAMAMOTO, S., JAISWAL, M., CHARNG, W. L., GAMBIN, T., KARACA, E., MIRZAA, G., WISZNIEWSKI, W., SANDOVAL, H., HAELTERMAN, N. A., XIONG, B., ZHANG, K., BAYAT, V., DAVID, G., LI, T., CHEN, K.,

GALA, U., HAREL, T., PEHLIVAN, D., PENNEY, S., VISSERS, L., DE LIGT, J., JHANGIANI, S. N., XIE, Y., TSANG, S. H., PARMAN, Y., SIVACI, M., BATTALOGLU, E., MUZNY, D., WAN, Y. W., LIU, Z., LIN-MOORE, A. T., CLARK, R. D., CURRY, C. J., LINK, N., SCHULZE, K. L., BOERWINKLE, E., DOBYNS, W. B., ALLIKMETS, R., GIBBS, R. A., CHEN, R., LUPSKI, J. R., WANGLER, M. F. & BELLEN, H. J. 2014. A drosophila genetic resource of mutants to study mechanisms underlying human genetic diseases. *Cell,* 159**,** 200-214.

YAO, K. M., SAMSON, M. L., REEVES, R. & WHITE, K. 1993. Gene elav of Drosophila melanogaster: a prototype for neuronal-specific RNA binding protein gene family that is conserved in flies and humans. *J Neurobiol,* 24**,** 723-39.

YEE, S. W., BRACKMAN, D. J., ENNIS, E. A., SUGIYAMA, Y., KAMDEM, L. K., BLANCHARD, R., GALETIN, A., ZHANG, L. & GIACOMINI, K. M. 2018. Influence of Transporter Polymorphisms on Drug Disposition and Response: A Perspective From the International Transporter Consortium. *Clin Pharmacol Ther,* 104**,** 803-817.

YONEZAWA, A., MASUDA, S., YOKOO, S., KATSURA, T. & INUI, K. 2006. Cisplatin and oxaliplatin, but not carboplatin and nedaplatin, are substrates for human organic cation transporters (SLC22A1-3 and multidrug and toxin extrusion family). *J Pharmacol Exp Ther,* 319**,** 879-86.

ZHANG, F., ZHAO, Y., CHAO, Y., MUIR, K. & HAN, Z. 2013a. Cubilin and amnionless mediate protein reabsorption in Drosophila nephrocytes. *J Am Soc Nephrol,* 24**,** 209-16.

ZHANG, F., ZHAO, Y. & HAN, Z. 2013b. An in vivo functional analysis system for renal gene discovery in Drosophila pericardial nephrocytes. *J Am Soc Nephrol,* 24**,** 191-7.

ZHANG, S., LOVEJOY, K. S., SHIMA, J. E., LAGPACAN, L. L., SHU, Y., LAPUK, A., CHEN, Y., KOMORI, T., GRAY, J. W., CHEN, X., LIPPARD, S. J. & GIACOMINI, K. M. 2006. Organic cation transporters are determinants of oxaliplatin cytotoxicity. *Cancer Res,* 66**,** 8847-57.

ZHANG, X. & WANG, Y. 2016. Glycosylation Quality Control by the Golgi Structure. *J Mol Biol,* 428**,** 3183-3193.

6. Acknowledgements

First, I would like to express my gratitude to my supervisor Prof. Dr. Bernard Moussian for giving me a chance to study this interesting project. I am grateful to him for providing much guidance and support during my Ph.D. study. He respects my ideas in the project and often discusses them with me, which promotes the improvement of thought for scientific study. I treasure this opportunity to study with him.

I would like to express my appreciation to Prof. Dr. Matthias Schwab and Prof. Dr. Anne Nies for their helpful advice, constructive feedback, and discussions. Because of their professional guidance and kinds of literature, I have gained deeper knowledge in the field of pharmacy.

I would like to thank the technician Nicole Gehring for giving me helps during my study. She teaches me how to use some experimental equipment. She also helped me do a lot of work for keeping fruit flies. Because of her help, my work became organized.

I would like to thank Dr. Justin Flaven-Pouchon for bearing my questions about fly genetics and always patiently explaining to me. He also discussed my thesis with me and gave me a lot of advice. I benefited a lot from working with him. I would also like to thank my colleagues Yang Yang for various discussions and wonderful ideas in the project.

I am very grateful to my parents for supporting and looking after me. Their encouragement gave me a lot of confidence and motivation to keep on pursuing my dreams.

I am very thankful to my friends Ruizhi Geng and Bo Li for all the memories in Tübingen. Although we study in different fields, they often inspire me unexpectedly.

Last, I appreciate the financial support from the IZEPHA funding for my Ph.D. project.